Monte Carlo Simulations of ABC Stacked Kagome Lattice Thin Films

by

© Hennadii Yerzhakov

A thesis submitted to the

School of Graduate Studies

in partial fulfilment of the

requirements for the degree of

Master of Science

Department of Physics and Physical Oceanography

Memorial University of Newfoundland

October 2015

St. John's Newfoundland

Abstract

In this thesis properties of thin films of the frustrated antiferromagnet $IrMn_3$ (chemically ordered phase) are examined using Metropolis Monte Carlo simulations, which is a step towards a better understanding of the exchange bias phenomenon in heterostructures with this material. This fcc compound has an unusual magnetic structure composed of ABC stacked (along cubic $\langle 111 \rangle$ axes) kagome layers of magnetic Mn ions. The kagome lattice is known to exhibit a high degree of frustration for antiferromagnetically coupled spins. A classical spin Heisenberg Hamiltonian is utilized, where symmetry breaking at the surfaces is modeled by introducing a local easy axis anisotropy perpendicular to the film. The impact of having an easy-axis anisotropy on the surface layers and cubic anisotropy in the middle layers is explored. The spin structure at the surface is shown to be different from that of the bulk 3D system, where spins tend to align along the surface [111] normal axis. This alignment tendency then propagates to the middle layers through exchange coupling. Results are shown for the specific heat, magnetization and sub-lattice order parameters for both surface and middle spins in three and six layer films as a function of increasing axial anisotropy. Preliminary results of simulations of the thin films with surface magnetic vacancies, which usually is present in real films, are also shown.

Key Words: Heisenberg model, Monte Carlo simulations, geometrical frustration, thin film, anisotropy, exchange bias

Acknowledgements

I am grateful to my supervisors Dr. Martin Plumer and Dr. John Whitehead for their guidance in the research, their patience, and kind support in an academia related life. I appreciate Martin LeBlanc for several discussions related to my project. I also appreciate School of Graduate Studies, Department of Physics & Physical Oceanography, and my supervisors for financial support, and ACENET for computer facilities provided.

Contents

List of Tables

List of Figures

Chapter 1

Introduction

Current spin valve technology used in magnetic recording transducers is based on the exchange bias phenomenon, an effect for which there does not currently exist a complete theoretical description. The most popular material for the antiferromagnet layer in spin valves is $IrMn_3$, partially because of its high ordering temperature. Due to its fcc stacked kagome magnetic structure, this material belongs to the group of so called geometrically frustrated antiferromagnets. Frustrated magnetism leads to a variety of physical effects (such as non-zero entropy [1]) which have been the subject of active study over the last two decades. Frustrated magnetism is also believed to be important for exchange bias. This thesis is focused on the study of thin films of $IrMn_3$, which is a preliminary step for studying heterostructures like spin valves. In thin films, edge effects are significant and arise because of the reduced number of nearest neighbors and changing the symmetry at surfaces, leading to the easy (or hard) axis normal to the film. This work is a continuation of the study of the bulk $IrMn_3$ system carried out previously [2], [3].

In this chapter, the origins of magnetism in condensed matter, phase transitions and the phenomenon of exchange bias are briefly reviewed as well as a justification of the chosen model for the system studied. A description of the computational method used, namely the Metropolis Monte Carlo algorithm, is also given.

1.1 Magnetism in Condensed Matter

1.1.1 Magnetic moments of isolated atoms and ions

The key notion in magnetism is the magnetic moment. In classical physics it is associated with the current flowing across a closed loop, and for an infinitesimal small loop is given by the formula

$$\mathbf{d}\mu = I\mathbf{dS}, \tag{1.1}$$

where $\mathbf{d}\mu$ is the magnetic moment, I is the current flowing through the loop, and $\mathbf{dS}$ is the vector with a magnitude equal to the area of the loop and directed normal to the surface containing the loop. From the classical point of view, each atom in a solid possesses some magnetic moment due to its electrons orbital motion around the nucleus. Since current is associated with mass transfer, there is also a strong relation between magnetic and orbital moments

$$\mu = \gamma\mathbf{L}, \tag{1.2}$$

where $\mathbf{L}$ is the orbital moment and γ is the gyromagnetic ratio. For an electron $\gamma = -e/2m_e$, where m_e is the electron mass.

However, the Bohr-van Leeuwen theorem [4] states that there is no net magnetization at thermal equilibrium in classical systems. Thus, classical physics fails

to explain magnetic phenomena in condensed matter such as ferromagnetism, antiferromagnetism, ferrimagnetsim, paramagnetism, diamagnetism, etc. Magnetism in condensed matter is essentially due to quantum mechanical effects.

From a quantum mechanical point of view, the energy eigenstates of electrons in the free atom or ion are approximately described by four quantum numbers: energy level n, orbital momentum l, projection of orbital momentum on some fixed axis l_z, and spin projection s_z. The magnitude and projection of magnetic moment associated with orbital momentum are given by $g_l\sqrt{l(l+1)}\mu_B$ and $-g_l l_z \mu_B$, respectively, where g_l is the Lande factor for orbital momentum and equals 1, and $\mu_B = \frac{e\hbar}{2m_e}$ is the Bohr magneton (magnetic moment of the spinless 'electron' orbiting the nucleus with orbital quantum number $l = 1$). The modulus and projection of a magnetic moment associated with intrinsic spin angular momentum are given by $g_s\sqrt{s(s+1)}\mu_B$ and $-g_s s_z \mu_B$, respectively, where the electron Lande factor is $g_s \approx 2$. The total angular momentum of an atom has both orbital and spin components and can be written as $\mu_B(g_s\hat{\mathbf{S}} + g_l\hat{\mathbf{L}})$. However, for heavy atoms the projection of total angular momentum l_z and spin s_z are not good quantum numbers due to spin-orbit interactions, but the projection of the full angular momentum $\hat{\mathbf{J}} = \hat{\mathbf{L}} + \hat{\mathbf{S}}$ is always a good quantum number, since the total angular momentum must be conserved. Thus, an atom or ion can be better described with a set of quantum numbers J, L, S, J_z, where L and S are the modulus of the total orbital momentum and total spin of the atom or the ion. Since J and J_z are conserved, then the component of atomic magnetic moment which can be measured simultaneously with energy is a projection on J_z, and the

corresponding operator can be written as $\mu_B g_J \hat{J}_z$, where

$$g_J = g_L \frac{J(J+1) - S(S+1) + L(L+1)}{2J(J+1)} + g_S \frac{J(J+1) + S(S+1) - L(L+1)}{2J(J+1)}. \tag{1.3}$$

is the Lande g-factor for the atom with quantum numbers J, L and S.

Having some specific number of electrons in the outer shell, these can be characterized by orbital numbers l_i and can be distributed in a number of ways which give different energies. In order to find a ground state of a free ion one can utilize Hund's rules [5]. These rules in the order of importance are as follows:

1. Distribute electrons in such a way that total spin S is maximum.

2. Then keeping this S, choose such configuration at which total orbital momentum L is maximum.

3. If the number of electrons $n \leq 2l + 1$ then $J =\mid L - S \mid$, otherwise $J = L + S$.

The first two rules are explained by reducing Coulomb interaction between electrons, and fulfilling of the third rule minimizes the spin-orbit interaction.

1.1.2 Heisenberg Model

In condensed matter, a system's constituent atoms are interacting and the system should be described by the full Hamiltonian (with nuclear spin and position neglected) involving all the electrons

$$H = \sum_j \frac{1}{2m} \left(-i\hbar\nabla_j + \frac{e}{c}\mathbf{A}(r_j) \right)^2 + \frac{1}{2} \sum_{j \neq k} \frac{e^2}{\mid \mathbf{r_j} - \mathbf{r_k} \mid} - \sum_{j,k} \frac{Z_k e^2}{\mid \mathbf{r_j} - \mathbf{R_k} \mid}$$
$$+ other\ magnetic\ terms, \tag{1.4}$$

where *other magnetic terms* involve interactions between atomic magnetic moments such as dipole and spin-orbit coupling terms, $\mathbf{A}(r_j)$ is the vector potential for the applied magnetic field, c is the speed of light, Z_k is the atomic number in the periodic table of elements of the k^{th} atom, and $\mathbf{r_j}$ and $\mathbf{R_j}$ are the position vectors of the j^{th} electron and nucleus. This is hardly a solvable problem. Instead, in different situations different approximations are useful. In the cases of ionic and molecular crystals, constituent ions can be considered as slightly deformed free ions, and the theory of free (non-interacting) atomic magnetic moments in combination with statistical mechanics gives quite good results. Here, it is important to mention that an external magnetic field applied in experiments leads to small shift in energy with comparison to the energy gap between levels in a free ion [5], so the part of Hamiltonian due to applied magnetic field can be treated with perturbation theory.

In magnetic dielectrics where ions are significantly deformed, it is not so useful to model the system as free ions, and another approach is used. Let us imagine a system of N ions with angular momentum J located at the nodes of some lattice with big enough lattice spacing so the ions can be considered free. Now, shrink the lattice spacing, so the ions begin to feel the field of each other and start to deform. Because of the inter-ion interactions the magnetic moments of the ions will differ from those determined by Hund's rule as the strength of the crystal field becomes comparable to, or exceeds, the strength of the spin-orbit interaction. For example, in the case of the $3d$ ions this can result in the phenomenon of orbital quenching. In this type of system, the crystal field influence is much larger than spin-orbit coupling[1] which

[1]For hydrogen-like atoms spin-orbit energy proportional to Z^4, where Z is an atomic number in the periodic table. For neutral atoms the dependence on Z is close to Z^2 [4].

results in orbital momentum to be about zero and a $[2(J+1)]^N$ degeneracy of the energy levels (not taking into account the hyperfine structure).

For heavier ions, spin-orbit effects cannot be neglected and lift the degeneracy of the quenched state. Typically, it turns out that the gap between the lowest group of energies and next group of energies becomes quite large so that even for high temperatures it is highly improbable that these upper levels will be occupied. In this case the exact Hamiltonian (1.4) can be substituted with an effective, so called, spin or Heisenberg Hamiltonian [5]

$$H = H_{ex} + H_{dip} + H_{mca} + H_{zee}, \tag{1.5}$$

where

$$H_{ex} = -\sum_{i \neq j} J_{ij} \mathbf{S}_i \cdot \mathbf{S}_j \tag{1.6}$$

$$H_{dip} = \sum_{i \neq j} \frac{\mu_0 \gamma_i \gamma_j \hbar^2}{4\pi r_{ij}^3} \left(\mathbf{S_i} \cdot \mathbf{S_j} - 3(\mathbf{S_i} \cdot \hat{\mathbf{r_{ij}}})(\mathbf{S_j} \cdot \hat{\mathbf{r_{ij}}}) \right) \tag{1.7}$$

$$H_{zee} = \sum_i g_{J_i} \mu_0 \mu_B \mathbf{S}_i \cdot \mathbf{H}. \tag{1.8}$$

Here $\mathbf{r_{ij}}$ is a vector connecting spins $\mathbf{S}_i$ and $\mathbf{S}_j$, $\hat{\mathbf{r_{ij}}} = \mathbf{r_{ij}}/r_{ij}$, μ_0 is the magnetic constant, and γ_i is a gyromagnetic ratio for the spin $\mathbf{S}_i$. The first term H_{ex} is called exchange interaction and arises due to combination of the electrostatic interaction with the Pauli exclusion principle. J_{ij} is called the exchange constant. The summation in this term is over all pairs of spins but decays quickly with distance in most cases. The second term is the dipole-dipole interaction which is usually very much weaker than exchange, but is long ranged. H_{zee} is Zeeman energy due to the external field $\mathbf{H}$. H_{mca} is magnetocrystalline anisotropy (MCA) term. Microscopically it arises

from spin-orbit interactions and reflects the tendency of spins to point along certain preferred directions that reflect the symmetry of the spin's crystal environment. The form of this term can be derived from symmetry considerations [6]. A Landau-type free energy can be constructed as Taylor series of spin components which should have only even power terms because of time-reversal symmetry. Further, the terms of this series should be invariants under the symmetry group of the crystal system. Usually, it is sufficient to keep the lowest order terms. In the simplest case of an easy (or hard) axis the lowest order MCA term can be written in the form

$$H_{mca} = -K \sum_i (\mathbf{S_i} \cdot \mathbf{n})^2, \tag{1.9}$$

where $\mathbf{n}$ is a unit vector along easy (or hard) axis and K is called the anisotropy constant. This type of magnetocrystalline anisotropy occurs in many crystal systems, for example those for which point group symmetries are C_3 and C_4. In the case of cubic symmetry, the only invariant at second order is $x^2 + y^2 + z^2$ which is isotropic, so anisotropy for cubic systems starts at fourth order.

If $K \to -\infty$ spins tend to lie in the plane perpendicular to the vector $\mathbf{n}$. In this case Heisenberg model reduces to the XY model. If $K \to \infty$ spins tends to point out along the vector $\mathbf{n}$, thus the Heisenberg model reduces to Ising Model.

The dipole-dipole interaction is also a source of anisotropy in magnetic systems. Anisotropy due to dipole interactions is divided into two types [7]: connected with geometrical shape of a specimen - shape anisotropy, and connected with crystalline axes - crystalline anisotropy. As a rule, the smaller the symmetry of the system the larger the total magnetocrystalline anisotropy (sum of terms with spin-orbital coupling and dipole interaction). Even though J_{ij} and K are called constants, they are

actually functions of temperature, and this dependence can be quite strong [4]. This dependence is mostly attributed to the temperature expansion of lattice spacing [8].

The most significant term in Eq. (1.5) is the exchange interaction term, and fundamentally magnetism in condensed matter emanates from the electrostatic interaction and Pauli exclusion principle, which leads to the exchange term. Usually, the dipole-dipole interaction energy is two or three orders of magnitude smaller than exchange, and in many calculations it can be neglected. This is especially true in antiferromagnetic (AF) systems where the net magnetic moment is small. However, the dipole interaction can result in interesting effects, for example, it is responsible for domain wall formation in ferromagnets (FM) due to its long range, as well as spin ice phenomena in pyrochlore lattices [9].

1.2 Phase Transitions

Thermodynamical systems may show different physical properties depending on the value of the parameters, such as temperature, pressure, or external fields that characterize their environment. These states, which differ from each other by measurable properties, are called phases. Consider the case of varying temperature. If we start with a system in thermal equilibrium at some high temperature and gradually reduce the temperature it may switch to a new phase at some temperature T_c. This is referred to as a phase transition and T_c the transition temperature and is accompanied by a change in the symmetry of the system. Further decreasing of temperature may cause additional symmetry changes and phase transitions. Well known examples of phase transitions are the liquid-gas and the paramagnet-ferromagnet transforma-

tions. Phases can be characterized by one- or multi- component quantities called order parameters, which are zero in a disordered phase and non-zero in an ordered phase.

Phase transitions can be divided into two groups [10]: first order and continuous. This division is based on the behavior of order parameters and the free energy F of a system. In the case of first order transitions, the change in the order parameter is discontinuous at the transition and the first derivative of F with respect to macroscopic parameters of the system has a singularity at the transition temperature T_c. For a continuous phase transition, the order parameter is continuous at the transition and physical quantities which are given by the second derivative of F with respect to macroscopic parameters of the system (for example, specific heat and magnetic susceptibility) are singular at T_c. The behavior of these quantities in the vicinity of a critical point usually is described by power laws (but may be also logarithmic), with exponents that are called critical exponents. In the case of the specific heat and susceptibility, these can be written as

$$C \propto (T - T_c)^{-\alpha}, \quad \chi \propto (T - T_c)^{-\gamma}, \tag{1.10}$$

where α and γ are the critical exponents. These and others critical exponents depend only on certain very basic properties of a system such as the dimensionality, symmetry, and range of the forces acting in the system (i.e. short or long range). This property is referred to as universality. Unlike a continuous phase transitions, first order phase transitions are accompanied by heat transfer and allow coexistence of phases [10].

Well known transitions in magnetism are paramagnet-ferromagnet and paramagnet-antiferromagnet transitions. In these cases the transition temperature is called the

Curie temperature and Néel temperature, respectively. In the paramagnetic phase, all magnetic moments are disordered at zero external magnetic field and the susceptibility is positive, while in the ferromagnet phase, even at $H = 0$, magnetic moments tend to be aligned in one direction, so the total magnetization is non-zero. In an antiferromagnet, magnetic moments have spin order such that the magnetization is zero, forming interpenetrating ferromagnetic sublattices. Obviously, a good order parameter for the paramagnet-ferromagnet transition is the absolute value of the magnetization itself, while for paramagnet-antiferromagnet transition it is given by the sum of the absolute values of the sublattice magnetizations.

1.3 Exchange Bias

Spin valves are a critical component in the read heads used in current magnetic hard drives. Spin valves are composed of stacked antiferromagnetic, ferromagnetic, non-magnetic and ferromagnetic layers and are based on the phenomenon of giant

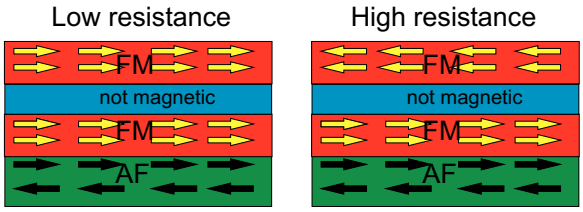

Figure 1.1: Spin valve structure.

magnetoresistance discovered in 1988, which manifests in thin film structures as a strong dependence of resistance on an angle between magnetization directions of ferromagnetic layers. When magnetizations are parallel resistance is low, while when

they are antiparallel resistance is high (Fig. 1.1).

The ability of spin valves to switch from the low resistance, parallel state to the high resistance, antiparallel state relies on the phenomena of exchange bias (EB), discovered by Meiklejohn and Bean in 1956 [11] while studying systems of fine ferromagnet particles of Co covered with antiferromagnet CoO coating. EB is observed in many systems with AF\FM interfaces when cooled in the presence of an external magnetic field, starting from a high temperature $T_N < T < T_C$, where T_N and T_C are Néel and Curie temperatures, respectively. Exchange bias has many features, one of the most significant of which is a shift of the hysteresis loop of the FM layer. It can be understood with a simple physical picture (see Fig. 1.2). By applying magnetic field $\mathbf{H}$ at $T_N < T < T_C$ spins in the FM are aligned along $\mathbf{H}$ while spins in the AF are still random. Cooling the system down below T_N, with the assumption of ferromagnetic exchange interaction across the interface, causes interfacial AF spins to align with FM spins at the interface (and with the assumption of an uncompensated[2] AF surface). Reversing the magnetic field causes the FM spins to rotate, however, if the anisotropy of the AF is strong enough, AF spins at the interface remain unchanged. This increases the field required to reverse the direction of the spins in the FM layer while lowering the field required to restore them to their initial orientation giving rise to a unidirection anisotropy. However, this model of EB is not universal. For example, in systems with a compensated AF interface layer EB are also observed [12]. The microscopic origin of this unidirection anisotropy is not well understood completely and this is partly the motivation for the research described in this thesis.

[2]Surface is called uncompensated if its magnetization is non-zero, otherwise it is called compensated.

In spin valves the AF layer is placed next to one of ferromagnet layers. Applying an external magnetic field only slightly affects the configuration of the AF layer, so that the interfacial spins in FM layer, which are exchange coupled to spins in AF layer, are pinned in one direction. The field thus changes the direction of the magnetization of the unpinned layer while keeping the direction of the pinned one fixed.

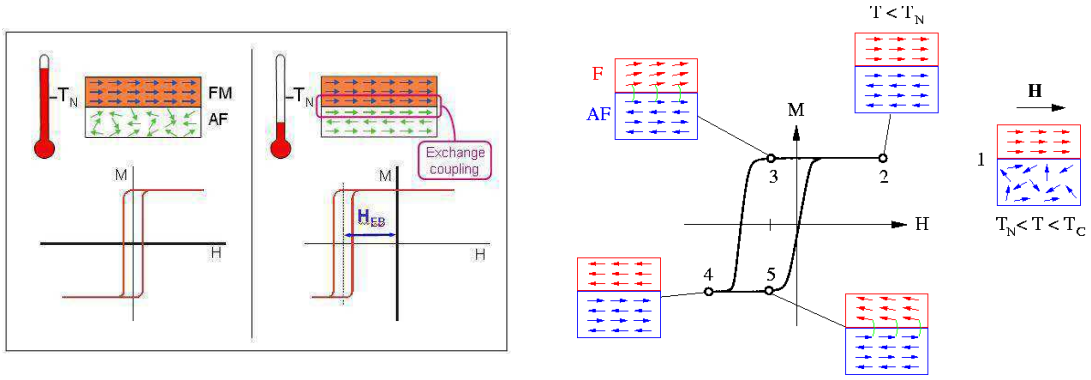

Figure 1.2: Exchange bias causes a shift in the hysteresis loop due to pinning. Taken from Vahid Hemmati, MSc 2011 (Memorial University).

There exists in the literature many models of exchange bias. The first and simple theory explaining EB was given by Meilkejohn and Bean [11], and directly attributed it to exchange interaction across the interface. They utilized a macroscopic phenomenological model with an energy per unit area as [12]

$$E = -HM_F t_F \cos(\theta-\beta)+K_F t_F \sin^2(\beta)+K_{AF} t_A F \sin^2(\alpha)-J_{F/AF}\cos(\beta-\alpha), \quad (1.11)$$

where H is the magnitude of the applied magnetic field, t_F and t_{AF} are the thicknesses of the FM and AF layers respectively, M_F is the magnetization of the FM layer (uniform through the sample), K_F and K_{AF} are bulk anisotropy constants, $J_{F/AF}$ is the exchange coupling constant across the interface, θ is the angle between **H** and

the FM easy axis, and α and β are angles between M_{AF} and M_F and corresponding easy axes. Here the anisotropy axes of the FM and AF are assumed to be parallel. Minimizing the energy and neglecting the FM anisotropy term, which is usually much smaller than the AF anisotropy term, H_{EB} is given by the formula [13]

$$H_{EB} = \frac{J_{F/AF}}{M_F t_F}, \tag{1.12}$$

if the condition

$$K_{AF} t_{AF} \geq J_{F/AF} \tag{1.13}$$

is fullfilled, otherwise $H_{EB} = 0$. However, this simple early model, with reasonable estimates for $J_{F/AF}$ (i.e. comparable to J_F and J_{AF}), gives several orders of magnitude greater values for H_{EB} than is usually observed in experiments. Many other models were developed to overcome this problem, in which attempts to take into account other parameters influencing the Hamiltonian were included. These include the formation of AF and FM domain walls [14], roughness at the interface [15], magnetic field effects on AF spins, etc. All these models are based on some assumptions, especially about interface properties which perhaps poses the biggest difficulties [12], and give good agreement with experiment for some class of systems with suitably adjusted parameter values.

One of the models which significantly influenced further development of theoretical description was proposed by Néel. He considered an uncompensated AF interface layer and assumed ferromagnetic coupling through the interface, uniform magnetization at each layer in AF and FM films, which are allowed to rotate with respect to each other. Then, in order to be in equilibrium the system should satisfy the

equation [12]

$$J_{F/AF}S^2\left(\sin(\frac{\theta_{i+1}-\theta_i}{2})+\sin(\frac{\theta_{i-1}-\theta_i}{2})\right)-2K_{AF}\sin(\theta_i)=0, \tag{1.14}$$

where $\frac{\theta_i}{2}$ is the angle between the magnetization of layer i and the easy axes. In the continuum approximation this equation becomes

$$J_{F/AF}S^2\frac{d^2\theta}{di^2}-4K_{AF}\sin(\theta)=0. \tag{1.15}$$

Under appropriate conditions this equation leads to existence of domain walls both in the AF and FM films, and EB.

In the case of a compensated AF Koon [16] showed that in the magnetic ground state, the FM spins are perpendicular to spins in AF film, though spins in the first AF interfacial layer are slightly canted. As shown by T.C. Schultness and W.H. Butler [17] this by itself does not lead to EB, but to an increase in the coercivity. However, combined with interfacial roughness it does lead to EB with reasonable numbers.

Among other features of EB are:

1. Increasing of coercivity [13].

2. A blocking temperature T_B (which usually is about T_N, but can be considerably lower [13]) below which EB is not observed. It can be attributed to grain size and thickness of the AF film: When the size of the AF is smaller than some critical length, T_N becomes smaller than for bulk systems.

3. While the dependence of H_{EB} on FM film thickness is approximately inversely proportional, $H_{EB}\propto\frac{1}{t_F}$, there is no dependence of H_{EB} on AF film thickness if

the film is sufficiently thick (> 20nm) [13]. As thickness decreases the magnitude of H_{EB} is rapidly decreasing and becomes zero for very thin films. This may be attributed to a violation of the Meiklejohn condition (1.13) $K_{AF}t_{AF} \geq J_{F/AF}$ (both may be due to thickness by itself and changing of magnetocrystalline anisotropy constant with thickness) and decreasing of T_N for thin films.

4. Training effect: H_{EB} decreases with the number of thermal cycles (around T_N) to some constant [13]. This effect occurs mainly in systems with polycrystalline AF films, while it is very small or even absent in systems with single crystal AF.

1.4 Monte Carlo Simulations

Monte Carlo simulations refers to a wide number of algorithms based on repetitive picking of uniformly distributed random numbers. Such algorithms have found a large number of applications in condensed matter, particularly in statistical mechanics because of its inherently probabilistic nature. In statistical mechanics the determination of the statistical sum, or the partition function,

$$Z = \sum_n e^{-\beta E_n}, \tag{1.16}$$

where $\beta = 1/k_B T$ allows one, in principle, to compute any equilibrium property of a macroscopic system. Unfortunately, exact analytical calculations of Z are feasible only for the simplest systems, mainly those without interactions between constituent particles. On the other hand, since statistical mechanics is strictly valid only for infinite systems, direct calculation of the exact partition function by computation is

also impossible.

However, for any thermodynamic system in equilibrium the sum in Eq. (1.16) is dominated by a small range of states, with observable variables that deviate only a small amount from their mean values. Thus there is no need to take into account all possible states, but to focus only on those which have the highest probability.

The basic idea of using MC simulations in statistical physics is as follows: starting with an arbitrary, or some special state, generate a sequence of states which satisfy the Boltzmann distribution, then take averages of interested observables, Q, over this sequence of states

$$Q = \frac{\sum_{i=1}^{N} Q_i}{N}. \tag{1.17}$$

Found in this way these values should give good estimation for the observables found in real experiments. Of course, the size of the systems to be simulated should be taken as large as possible to be considered close to the value in the thermodynamic limit.

Just simply picking states with a Boltzmann probability $e^{-\beta E}/Z$ is not a good choice, since most of states will be rejected. Instead, generating of a sequence of states based on a Markov process, which satisfies two conditions: 1) the transition probability from one state to another state does not depend on time; 2) the transition probability does not depend on previous transitions, i.e. Markov processes are memoryless. The time evolution of the probability $w_i(t)$ of the system at time t to be at state i is governed by the master equation [18]

$$\frac{dw_i}{dt} = \sum_j (w_j(t) R_{j\to i} - w_i(t) R_{i\to j}), \tag{1.18}$$

where $R_{i\to j}$ is a transition rate from state i to j. In the discrete approximation, this

takes the form

$$w_i(t_{n+1}) = \sum_j w_j(t_n) P_{j\to i}, \tag{1.19}$$

where $P_{j\to i}$ is the probability to switch from state j to state i in the time-interval step and satisfies a condition $\sum_i P_{j\to i} = 1$.

The problem of generating new states is essentially in choosing the set of probabilities $P_{j\to i}$. They should be picked in such a way that $w_i(t) \to \frac{e^{-\beta E_i}}{Z}$ as $t \to \infty$, and that something close to this solution is obtained in a reasonable time.

In order to achieve a Boltzmann distribution the process of generating new states must satisfy the requirement of ergodicity, i.e. each state should be possible to be reached through some path starting with any other state. Obviously, if this condition is violated, starting with some state i_0, from which it is impossible to reach state j_f, the solution of master equation at infinite time does not give the Boltzmann distribution, since the probability for the system to get into the state j_f is 0.

As $t \to \infty$ Eq. (1.19) could end up in the situation where the probability distribution $\mathbf{w}$ cycles through a finite number of values

$$\begin{aligned} &\mathbf{w}(t_{N+1}) = P\mathbf{w}(t_N),\ \mathbf{w}(t_{N+2}) = P\mathbf{w}(t_{N+1}),\ \dots,\ \mathbf{w}(t_{N+f}) = P\mathbf{w}(t_{N+f-1})\ , \\ &\mathbf{w}(t_{N+f+1}) = P\mathbf{w}(t_{N+f}) = \mathbf{w}(t_N),\ \dots\ . \end{aligned} \tag{1.20}$$

This is so called dynamical equilibrium. In this case there is no limit of probabilities at infinite time. In order to avoid it, the condition of detailed balance is imposed

$$e^{-\beta E_i} P_{i\to j} = e^{-\beta E_j} P_{j\to i}. \tag{1.21}$$

In other words, the full probability to transit from a state i to j is the same as to transit to state i from state j. Also, in most systems detailed balance is supported

by time-reversal symmetry. In this case, if detailed balance is violated and we reverse the time, in a case of dynamical equilibrium the system still transit from k_i to k_{i+1} state which implies that the system does not go backwards. Given that requirements of ergodicity and detailed balance are fulfilled, it is possible to show that for any selected probabilities $P_{i\to j}$ we have $w_i(t) \to \frac{e^{-\beta E_i}}{Z}$ as $t \to \infty$.

1.4.1 Metropolis Algorithm

One of the standard methods of generating a transition probability $P_{i\to j}$ that satisfies detailed balance which works well for many systems is the Metropolis algorithm. This method was proposed in 1953 by N. Metropolis et al. in [19]. It is convenient to represent transition probabilities as a multiplication of two parts [18]

$$P_{i\to j} = g_{i\to j} A_{i\to j}, \tag{1.22}$$

where $g_{i\to j}$ is called the selection probability and $A_{i\to j}$ is called the acceptance ratio. Their meaning is reflected by their names: first a new state j is generated from state i with probability $g_{i\to j}$ and then this change of state is accepted with probability $A_{i\to j}$. There is a lot of flexibility on how to define these parts. Since the condition of detailed balance always holds for $P_{i\to i}$, the transition probability from i to j, $P_{i\to j}$, can be adjusted by making appropriate changing in $P_{i\to i}$ so, that $\sum_j P_{i\to j} = 1$. Also the condition of detailed balance can be rewritten in the form

$$\frac{P_{i\to j}}{P_{j\to i}} = e^{-\beta(E_j - E_i)} = \frac{g_{i\to j} A_{i\to j}}{g_{j\to i} A_{j\to i}}, \tag{1.23}$$

so changing the ratio $\frac{A_{i\to j}}{A_{j\to i}}$ can be adjusted by making appropriate changes in the ratio $\frac{g_{i\to j}}{g_{j\to i}}$.

For computational efficiency, the bigger the acceptance ratio the better. In the Metropolis algorithm selection probabilities are all equal and the biggest acceptance probability in the ratio (1.23) is taken to be 1, while the other one should be taken to ensure that the ratio

$$\frac{A_{i\to j}}{A_{j\to i}} = e^{-\beta(E_j - E_i)} \tag{1.24}$$

is satisfied. So, if $E_i < E_j$ then $A_{j\to i}$ should be chosen to be 1 and $A_{i\to j} = e^{-\beta(E_j-E_i)}$.

The Metropolis algorithm can be succinctly summarized as:

1. Choose a state i_0 to start with.

2. Generate a new state j given that the selection probability $g_{i\to j}$ is uniform.

3. If $E_j \leq E_i$, change system to state j.

4. If $E_i < E_j$ the state is changed to the state j with probability $e^{-\beta(E_j-E_i)}$ (by comparing with a random number $0 \leq r \leq 1$).

5. Go to item #2 repeatedly to achieve equilibrium.

Using these steps a sequence of states is generated. It is hard to choose an initial state i_0 that is one of the states where the system spends the majority of its time, thus, usually it is necessary to wait some time while the system equilibrates. After equilibration the interesting observables can be calculated at each state and be averaged over.

Since thermodynamical systems spend most of their time in a narrow region of states with close energies, talking about spin systems it is worthwhile to consider transitions between states which differ in the orientation of only one spin. This so

called single-spin-flip dynamics algorithm of choosing a new state obviously possesses the property of ergodicity. We will refer to one sweep of the lattice as a Monte Carlo step (MCS).

1.4.2 Thermodynamic Quantities

In this subsection the question of calculating measurable quantities in MC simulations is considered.

After some large number of MC steps as defined above, the system has reached equilibrium and one can simply calculate the energy, magnetization, etc. by using formula (1.17). Calculation of the specific heat and susceptibility is less straightforward.

As the probability for the system to be in the state with energy E_i is proportional to $e^{-\beta E_i}$ the expectation value of any quantity X is

$$\langle X \rangle = \frac{\sum_i X_i e^{-\beta E_i}}{\sum_i e^{-\beta E_i}}. \tag{1.25}$$

Thus, for the energy and its standard deviation one can derive

$$\langle E \rangle = \frac{\sum_i E_i e^{-\beta E_i}}{\sum_i e^{-\beta E_i}} = -\frac{1}{Z}\frac{\partial Z}{\partial \beta} = -\frac{\partial \log Z}{\partial \beta} \tag{1.26}$$

$$\begin{aligned} \langle E^2 \rangle - \langle E \rangle^2 &= \frac{\sum_i {E_i}^2 e^{-\beta E_i}}{\sum_i e^{-\beta E_i}} - \left(\frac{1}{Z}\frac{\partial Z}{\partial \beta}\right)^2 = \\ &= \frac{1}{Z}\frac{\partial^2 Z}{\partial \beta^2} - \frac{1}{Z^2}\left(\frac{\partial Z}{\partial \beta}\right)^2 = \frac{\partial^2 \log Z}{\partial \beta^2}. \end{aligned} \tag{1.27}$$

The specific heat at constant volume is defined by the formula

$$C_V = \frac{\partial E}{\partial T} = \frac{\partial E}{\partial \beta}\frac{\partial \beta}{\partial T} = -k\beta^2 \frac{\partial E}{\partial \beta} = k\beta^2 \frac{\partial^2 \log Z}{\partial \beta^2}. \tag{1.28}$$

Comparing it with the previous formula gives

$$C_V = k\beta^2 \left(\langle E^2 \rangle - \langle E \rangle^2 \right). \tag{1.29}$$

The susceptibility tensor χ_{mn} $(m, n = x, y, z)$ is defined by the formula

$$\chi_{mn} = \frac{\partial M_m}{\partial H_n}, \tag{1.30}$$

and it is also possible to connect it with the magnetization as follows.

The energy of the system in a magnetic field has the form $E = E_0 - \mathbf{M} \cdot \mathbf{H}$, where E_0 is its energy in the absence of the magnetic field. The expectation value of the m-th component of the magnetization is written as

$$\langle M_m \rangle = \frac{\sum_i M_{im} e^{-\beta E_i}}{\sum_i e^{-\beta E_i}} = \frac{1}{\beta Z} \frac{\partial Z}{\partial H_m} = \frac{1}{\beta} \frac{\partial \log Z}{\partial H_m}. \tag{1.31}$$

Thus

$$\begin{aligned} \langle M_m M_n \rangle - \langle M_m \rangle \langle M_n \rangle &= \frac{\sum_i M_{im} M_{in} e^{-\beta E_i}}{\sum_i e^{-\beta E_i}} - \left(\frac{1}{\beta} \frac{\partial \log Z}{\partial H_m} \right) \left(\frac{1}{\beta} \frac{\partial \log Z}{\partial H_n} \right) = \\ &= \frac{1}{\beta^2 Z} \frac{\partial^2 Z}{\partial H_m \partial H_n} - \frac{1}{\beta^2 Z^2} \frac{\partial Z}{\partial H_m} \frac{\partial Z}{\partial H_n} = \\ &= \frac{1}{\beta^2} \frac{\partial^2 \log Z}{\partial H_m \partial H_n}. \end{aligned} \tag{1.32}$$

On the other hand, the susceptibility can be written as

$$\chi_{mn} = \frac{\partial M_m}{\partial H_n} = \frac{1}{\beta} \frac{\partial^2 \log Z}{\partial H_m \partial H_n}. \tag{1.33}$$

Comparing two last expressions gives

$$\chi_{mn} = \beta \left(\langle M_m M_n \rangle - \langle M_m \rangle \langle M_n \rangle \right). \tag{1.34}$$

In the above expressions, thermodynamic averages are calculated by running the Metropolis MC algorithm over many MC steps, after equilibrium has been achieved.

1.5 Classical Spins on the 2D Kagome Lattice

The 2D kagome lattice is depicted[3] in Fig. 1.3. It is obtained from the triangular lattice by removing 1/4 of its nodes. Obviously, it is not a Bravais lattice, since it is possible to find two types of nodes with different surroundings. Though, it can be described as a triangular Bravais lattice with a three point basis denoted by the numbers $1, 2, 3$ in Fig. 1.3.

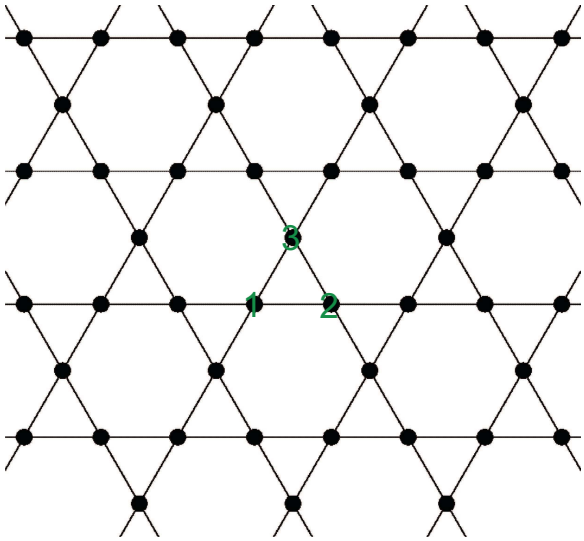

Figure 1.3: 2D kagome lattice.

Let us put classical spins on this lattice and assume that this magnetic system is well described by the Heisenberg hamiltonian with only nearest neighbors interactions with antiferromagnetic coupling. For the ground state ($T = 0$) it is impossible to direct anti-parallel spins on the lattice so that energy of interaction between each

[3]This picture is licensed under the Creative Commons Attribution-Share Alike 2.5 Generic license. Original picture (credit to WilliamSix) is altered.

pair of spins would be minimal (see Fig. 1.4). Such situation is described by the notion of geometrically frustrated antiferromagnetism.

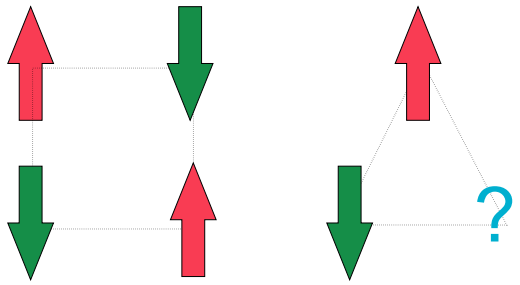

Figure 1.4: Illustration of unfrustrated square and frustrated triangular antiferromagnets.

However, for classical spins it is not hard to find periodic ground states. There are two possible perfectly ordered configurations depicted[4] in Fig. 1.5: $q = 0$ and $\sqrt{3} \times \sqrt{3}$ states [20].

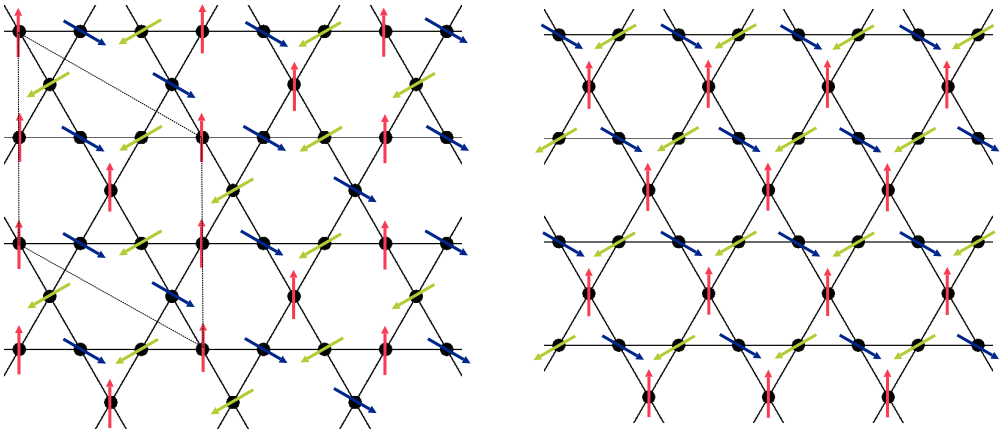

Figure 1.5: $q = 0$ (right) and $\sqrt{3} \times \sqrt{3}$ (left) ground states. The parallelogram is the unit cell.

[4]This picture is licensed under the Creative Commons Attribution-Share Alike 2.5 Generic license. Original picture (credit to WilliamSix) is altered.

In both these states, angles between neighboring spins are 120°, and due to rotational symmetry of the Hamiltonian the spins may lie in any plane. When second and third nearest neighbor interactions are taken into account with J_2 and J_3 exchange constants, the only ground state is $q = 0$ if $J_2 > J_3$ and $\sqrt{3} \times \sqrt{3}$ if $J_2 < J_3$ [20]. With NN interactions only, the configuration $q = 0$ has an opportunity for degeneracy by creating AF domain walls in the system. Indeed, a shift of any line of spins along this line by any of acceptable translation vectors does not change energy of the system, since there are still 120° between nearest spins on each triangle. This is shown[5] in Fig. 1.6. The number of ground-state degrees of freedom of N spins on the kagome lattice is $N/9$ [21], which is an extensive quantity. The consequences of these types of degeneracies on the thermodynamic properties of the 2D kagome lattice has been the subject of many publications for both classical and quantum spins over the past twenty-five years [22, 23, 24, 25].

1.6 $IrMn_3$ structure

Alloys of Ir and Mn are one of the best materials in technology for the AF layer in spin valves as they have good EB properties and a high Néel temperature. Chemically disordered alloys $Ir_xMn_{[1-x]}$ are mainly used for this purpose as the thin film are typically deposited by sputtering. There are two types of $IrMn_3$: chemically disordered γ-$IrMn_3$ where Ir and Mn ions are randomly distributed on fcc lattice sites, and chemically ordered $L1_2-IrMn_3$. Both of these forms have the fcc lattice structure:

[5] This picture is licensed under the Creative Commons Attribution-Share Alike 2.5 Generic license. Original picture (credit to WilliamSix) is altered.

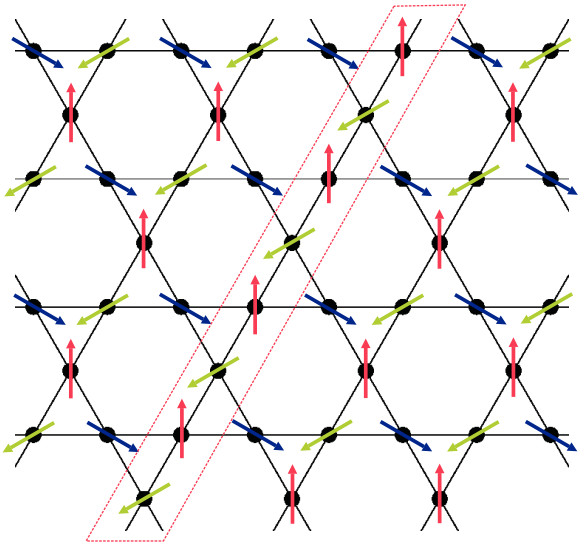

Figure 1.6: Another AF domain (surrounded by the dotted line parallelogram) in $q = 0$ state is formed, costing no energy.

$\gamma-$ phase with lattice spacing $a = 0.378$nm have space group No. 225 and with T_N about 730 K, $L1_2-$ phase with lattice spacing $a = 0.3772$nm and space group No. 221, and T_N about 960 K [26]. The current study is focused on the chemically ordered phase, where Mn ions reside on cube faces and Ir ions at cube corners.

Even though the $L1_2$ phase has cubic symmetry, this is locally broken for each of Mn ions which leads to existence of local easy axes [27]. The magnetic structure of ordered $IrMn_3$ can be also considered as ABC stacked kagome layers along $\langle 111 \rangle$ directions as shown in Fig. 1.7.

Both Mn and Ir are transition metals with the electronic structure of free atoms $[Ar]3d^5 4s^2$ and $[Xe]4f^{14}5d^7 6s^2$, respectively. First principles electronic structure calculations [27] show that the magnetic moment of the Mn ion is $\mu_{\mathrm{Mn}} = 2.66\mu_B$ and has a vanishing value for Ir ions. This value is consistent with orbital quenching if

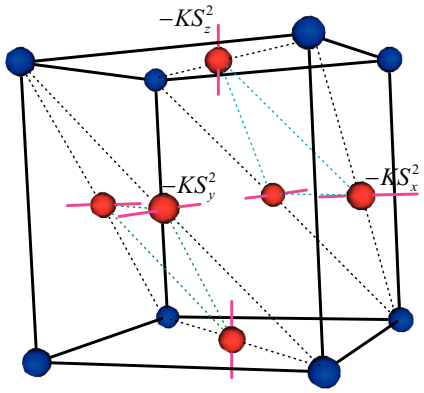

Figure 1.7: Structure of $IrMn_3$. Blue spheres stand for Ir non-magnetic ions, and red spheres stand for magnetic Mn ions. Magnetic anisotropy easy axes are depicted with pink lines.

we assume that Mn ions are left with two electrons in their outer shell: assuming $L = 0$ for Mn gives $\mu_{Mn} = 2\sqrt{S(S+1)} = 2\sqrt{1 \cdot \frac{3}{2}}\mu_B \approx 2.45\mu_B$. Similarly, for Ir ions orbital quenching should imply an entirely empty (or filled) d orbital, however, as Ir has an atomic number in the periodic table of 77 this suggestion may be wrong (Mn's number is 25, thus the spin orbit interaction in Ir ion is about ten times bigger than in Mn). Even though $IrMn_3$ is a system with spin effects which are both localized and itinerant, it can be well approximated with a local atomic spin Hamiltonian according to [27], where the energy spectrum obtained from first principles calculations is mapped onto a local spin Hamiltonian. Based on this work, the spin Hamiltonian for $IrMn_3$ approximately can be taken in the form

$$\mathcal{H} = -\sum_{i \neq j} J_{ij}\mathbf{S}_i \cdot \mathbf{S}_j - K\sum_{\gamma}\sum_{i\epsilon\gamma}(\mathbf{n}_\gamma \cdot \mathbf{S}_i)^2, \tag{1.35}$$

where the first term stands for the isotropic exchange interaction, and the second one stands for the effective MCA; γ denotes the type of an local easy axis (1,2, or 3

directed along $\hat{x}$, $\hat{y}$, or $\hat{z}$, respectively), $\mathbf{n}_\gamma$ are unit vectors along x, y and z axes for $\gamma = 1$, 2 and 3 respectively. More rigorously, the Hamiltonian of the bulk $IrMn_3$ has the form [27]

$$\mathcal{H} = -\sum_{i \neq j} J_{ij} \mathbf{S}_i \cdot \mathbf{S}_j - \sum_{i \neq j} \mathbf{S}_i \mathbf{J}_{ij}^S \mathbf{S}_j - K_0 \sum_\gamma \sum_{i \epsilon \gamma} (\mathbf{n}_\gamma \cdot \mathbf{S}_i)^2, \tag{1.36}$$

where the second term is the two-site anisotropic exchange interaction, and K_0 is an anisotropy constant of local easy axes mentioned above. The effective MCA term in Eq. (1.35) accounts effects of both two-site and on-site anisotropies.

In the same article [27], the exchange constants J_{ij} and anisotropy constant K are calculated. The results state that J_{ij} almost vanishes beyond fourth nearest neighbors, for first NN $J_{ij} \approx -20$meV, for second NN $J_{ij} \approx 5$meV, for third NN $J_{ij} \approx -5$meV, for fourth NN $J_{ij} \approx 4$meV (for second and fourth NN interaction there are ions with different environments, so the maximum values are listed). Considering only magnetic Mn ions, each of them has 8 first NNs, 6 second NNs and 16 third NNs. Thus, the ratio of energy interaction with NN beyond first (and not including fourth NN) to the energy interaction with first NNs is about $22/32 = 0.6875$. This number is not small, however, it is reasonable to suggest that including only first NN interactions in the Hamiltonian (1.35) will not change results qualitatively. In fact, it can be shown that the $q = 0$ spin structure survives in this 3D fcc kagome lattice [2] and that it is consistent with the type (AF or F) of longer-range exchange interactions found by the electronic structure interactions. In support of this analysis is experimental data [28] showing that the ground state of $L1_2$−$IrMn_3$ is that so called $T1$ state, where spins lie within one of (111) planes along $\langle 112 \rangle$ directions and form the $q = 0$ state, as in corresponding 2D kagome lattices (though MCA slightly deforms the $T1$

state [3]). In the case of NN interactions it is easy to show that configuration with $\sqrt{3}\times\sqrt{3}$ state in each $\langle 111\rangle$ plane does not form a ground state. However, taking into consideration only first NN, one should not expect good quantitative results using the value of J for first NN interaction indicated above. In reduced units, the exchange constant J is taken to be -1, and the Boltzmann constant $k_B = 1$. Then, according to the electronic structure calculations in [27] K may be evaluated as about 0.1. Temperature in Kelvins may be recalculated from the reduced temperature by the formula $\tilde{T} = \frac{\tilde{J}}{k_B}T$, where quantities with a tilde are taken in non reduced units.

MC simulations on the 3D fcc kagome lattice without anisotropy [2] and with anisotropy [3] serve as a starting point for the present work. The focus here will be thin film (multilayer) systems. Since the free surface layers do not have cubic symmetry, we introduce uni-axial easy axes (perpendicular to the film in the $\langle 111\rangle$ direction) on the surface layers, while maintaining cubic anisotropy in middle layers. Phase transitions and spin order are examined. A goal of this work is that it serves as a prelude to the study of exchange bias in the case where a ferromagnet film is added. The impact of introducing non-magnetic vacancies on the surface, as a means to mimic non-ideal sputtered films, is also briefly studied.

Preliminary to reviewing these new results, the next chapter demonstrates that the MC code used in this work can reproduce the key features found in the previous MC studies of the 3D systems [2], [3]. In Ch. 3 the spin structure of the ground state is discussed. In Ch. 4 MC simulation results for thin films of ordered phase of $IrMn_3$ are presented. In Ch. 5 preliminary MC results for thin films with vacancies on the one of the surfaces are shown. Ch. 6 summarizes the obtained results and contains conclusions as well as prospective future work.

Chapter 2

Bulk $IrMn_3$ Simulations

As a precursor to MC simulations on thin films we first ensure that our MC code can reproduce results obtained previously on bulk $L1_2-IrMn_3$ with cubic anisotropy [3]. In this chapter we present the results of a series of MC calculations based on the Hamiltonian given by Eq. (1.35) and compare the results with those obtained in [3].

In the Hamiltonian (1.35) only nearest neighbors interactions are taken into account, $J = -1$ (reduced units, Boltzmann constant $k_B = 1$), and the effective constant of cubic anisotropy K is varied (according to [27] for chemically ordered $IrMn_3$ K is about 10% of J). So, the Hamiltonian has the form

$$\mathcal{H} = -J \sum_{NN} \mathbf{S}_i \cdot \mathbf{S}_j - K \sum_{\gamma} \sum_{i\epsilon\gamma} (\mathbf{n}_\gamma \cdot \mathbf{S}_i)^2 \tag{2.1}$$

Simulations have been carried out for the system of size $18 \times 18 \times 18$ with periodic boundary conditions to better simulate a bulk system. Number of MC steps is 10^6 with 10% of these discarded for equilibration. Two order parameters can be defined

in this system

$$M_t = \frac{1}{N} \left\langle \sum_{\gamma} \left| \sum_{i \epsilon \gamma} \mathbf{S}_i \right| \right\rangle \tag{2.2}$$

and

$$M_f = \frac{1}{N} \left| \left\langle \sum_{i} \mathbf{S}_i \right\rangle \right| \tag{2.3}$$

Angle brackets here stand for statistical averaging through states obtained during simulations, N is the number of spins in the system. M_t defines degree of collinearity of spins in the ferromagnetic sublattices, while M_f is a modulus of the total system magnetization per spin.

Results for the specific heat and the order parameter susceptibility

$$\chi = \beta \left(\langle M_t^2 \rangle - \langle M_t \rangle^2 \right) \tag{2.4}$$

are presented in Figs. 2.1 and 2.2. From the MC data we see that the specific heat and the susceptibility give approximately the same transition temperatures T_N. Fig. 2.3 shows the transition temperature T_N obtained from the peaks in C *vs* T as a function of K.

These results are in good agreement with those of [3]. From Fig. 2.3 it is seen that at first increasing K causes the value of T_N to grow up to around $K = 5$, where it peaks, after which T_N decreases with increasing K. As established in [3], the transition is continuous for finite anisotropy, unlike the case without anisotropy which shows a discontinuous transition [2]. A possible qualitative explanation of this may be as follows. The transition temperature is associated with long range order, and in the Hamiltonian (1.35) the exchange interaction term is responsible for this order. When $K = 0$, due to rotational symmetry of the Hamiltonian any plane may be a plane where spins lie. Thus, spins at different part of the system may begin establish

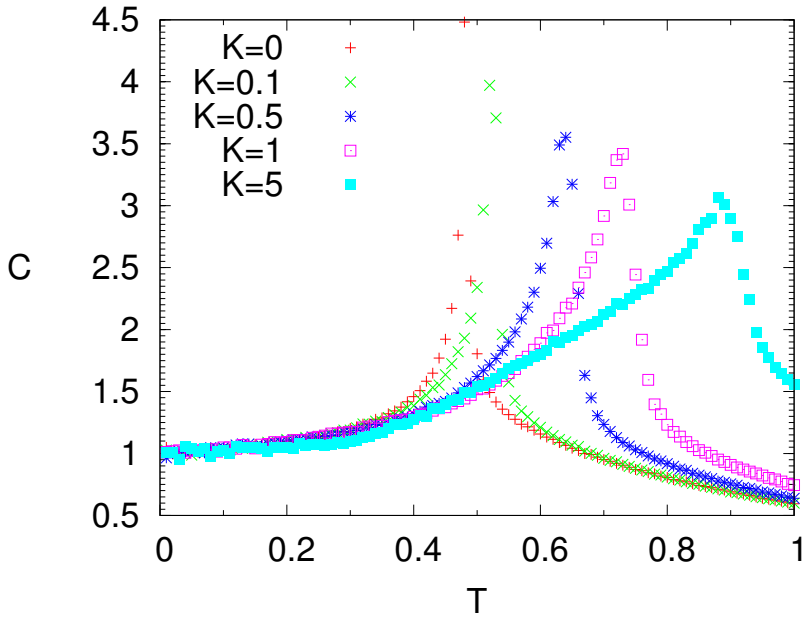

Figure 2.1: Specific heat per spin vs temperature for a range of anisotropy values.

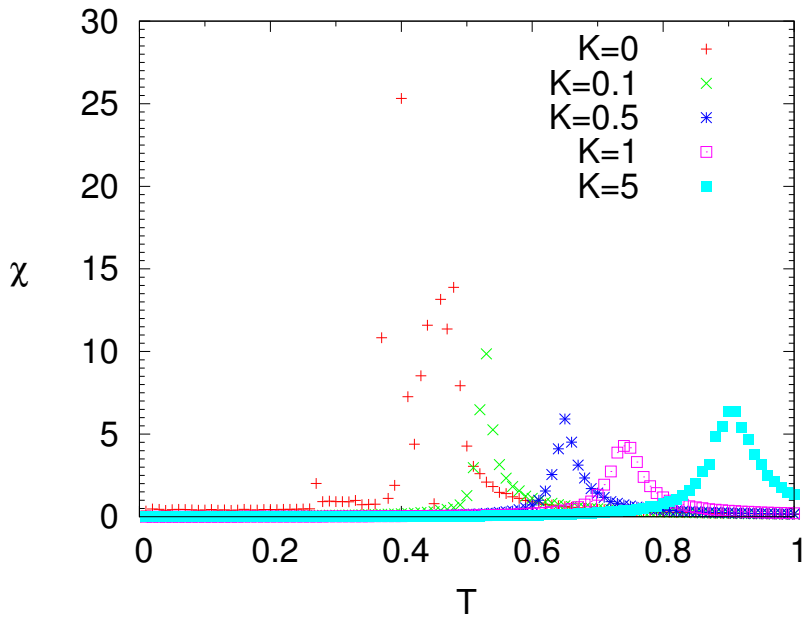

Figure 2.2: Susceptibility per spin vs temperature for a range of anisotropy values.

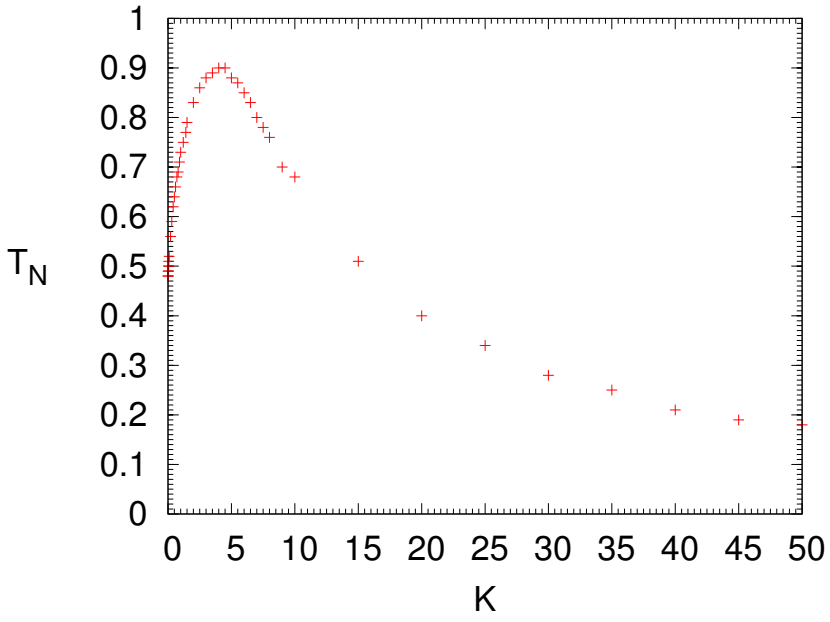

Figure 2.3: Transition temperature as a function of anisotropy.

long range order in different directions, which leads to the coexistence of ordered and disordered phases. While $K \neq 0$ the system acquires preferred directions: $\hat{x}$, $\hat{y}$ and $\hat{z}$ for spins in different sublattices. When K is not big, it is easier for the system to establish long range order as spins which are far from each other have larger chances to start order coherently in one direction favoring only one phase, characteristic of a continuous phase transition. If K is too big compared to the exchange term, the relative significance of exchange interaction is reduced, and in the limit $K/J \to \infty$, one expects no long range order.

Figure 2.4 shows the order parameter M_t as a function of T. In the completely ordered ground state, i.e. where all three sublattices are pure, $M_t = 1$. The fact that for small K we see that M_t does not achieve saturation may be attributed to low energy metastable states in which the spins from different sublattices interchange their

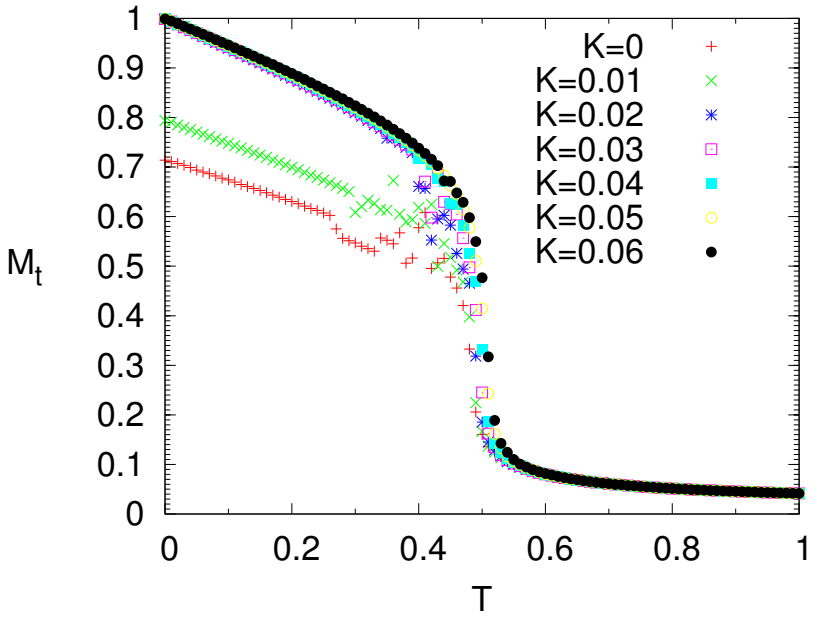

Figure 2.4: Order parameter M_t vs temperature over a range of anisotropy values.

orientation with each other. Such metastable states can persist to low temperatures and lock in at $T = 0$ preventing full saturation of the order parameter M_t. As reported in [3] when $K \geq 0.06$, M_t always tends to unity as $T \to 0$. On the order parameter susceptibility graph in Fig. 2.2 the scattering of points for $K = 0$ is due to switching between different ground states.

The total magnetization per spin is plotted in the Fig. 2.5 as a function of temperature. As expected, it is zero for $K = 0$, corresponding to the $T1$ state. For the estimated value of K for $IrMn_3$, which is about 0.1, the magnetization is still very small. This non-zero magnetization comes from z-components (the z-axis is directed normal to one of $\langle 111 \rangle$ planes, in which the spins almost lie) of spins.

All graphs are in good agreement with those presented in [3].

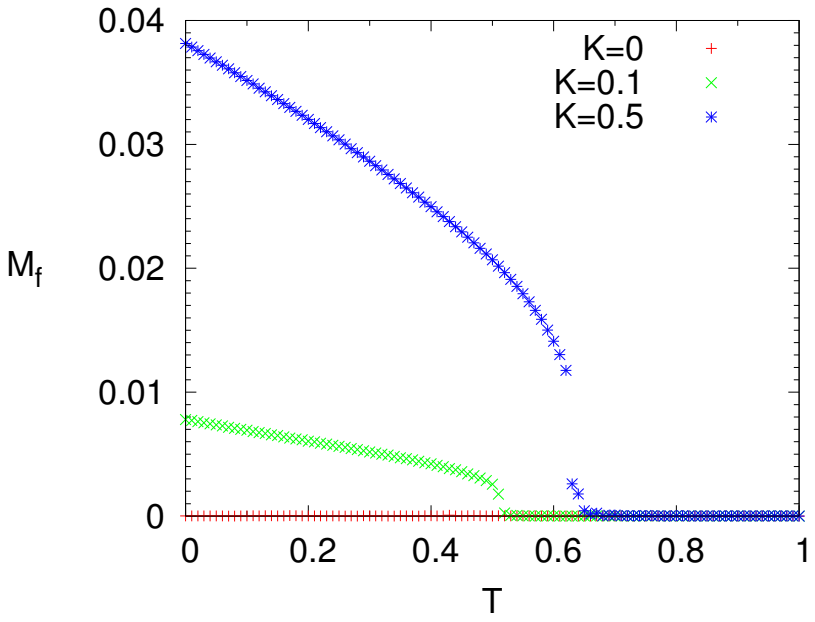

Figure 2.5: Modulus of the total magnetization per spin vs temperature.

Chapter 3

Thin Films: Zero and Low-T Spin Configurations

In this chapter the ground states for thin films of $L1_2-IrMn_3$ alloy are discussed. The thin films consist of ABC stacked kagome layers, in which the layers of the films coincide with the (111) plane of bulk $L1_2-IrMn_3$ (see Fig. 3.1).

It is assumed that the bulk atomic structure is preserved at the surfaces. The effect of surfaces is to change the coordination number of the surface spins (where there are 6 nearest neighbors: 4 in plane and 2 in the layer above or below), and to break the cubic symmetry of the infinite (bulk) lattice. This leads to an easy axis anisotropy perpendicular to the surfaces as the symmetry is now that of the kagome plane. Thus, it is necessary to distinguish surface and middle (interior) layer spins. The effective Hamiltonian may be written in the form

$$\mathcal{H} = -J \sum_{<n.n>} \mathbf{S}_i \cdot \mathbf{S}_j - K \sum_{\gamma \,\epsilon \text{ interior}} \sum_{i \,\epsilon\, \gamma} (\mathbf{n}_\gamma \cdot \mathbf{S}_i)^2 - D \sum_{i \,\epsilon \text{ surface}} (\mathbf{n} \cdot \mathbf{S}_i)^2. \qquad (3.1)$$

In this expression all previously defined symbols keep their meaning, and D is the

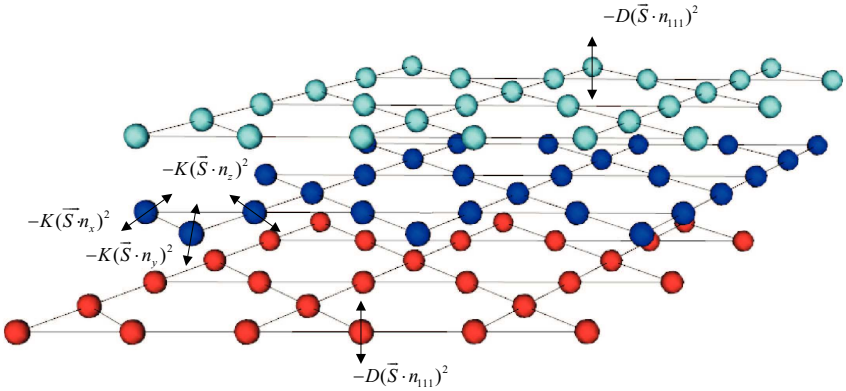

Figure 3.1: Schematic picture of the thin film. Only magnetic Mn ions are depicted. Easy axes for cubic (K) and axial surface (D) symmetries are shown as two-sided arrows.

uniaxial anisotropy constant at the surface. In the following simulations we chose $J = -1$ and, based on Ref. [27] $K = 0.1$. There is no estimate for D, but following general considerations, the lower the symmetry the greater the constant of anisotropy, it may be quite significant. Consequently, we therefore consider a wide range of values of D.

It is noteworthy that for a thin film with $D = 0$ and $K = 0$ the reduced number of nearest neighbors at the surfaces does not lead to a different ground spin configurations. They are still the same as for the infinite lattice (bulk) case. Since 120^o angles between neighboring spins minimize the local energy of interaction in each triangle of nearest neighbors it is still the $q = 0$ state in each layer. The proof of this may be stated as follows.

Let us consider a film consisting of only two layers coinciding with a (111) *plane of the infinite crystal. Its energy may be written as a sum of three terms:* $E =$

$E_1 + E_2 + E_{12}$, where E_i is the energy of interaction between spins within the i^{th} layer only and E_{12} is the energy of interaction between layers 1 and 2. The energies E_1 and E_2 are minimized with the $q = 0$ state. The system also can be considered as stacked parts of kagome layers along $[11\bar{1}]$ direction, and then E_{12} is minimized also with the $q = 0$ state. Since it is possible to set up the $q = 0$ state in each of the four $\{111\}$ planes in the case of the bulk $IrMn_3$, it is also possible in the case of the two layer system. Thus the energy of the system E is minimized as all terms in the sum are minimized. Extension to bigger number of layers does not change this scenario.

Unless indicated otherwise, the simulations presented in this chapter have been carried out for systems consisting of three or six layers of size 18×18. Periodic boundary conditions were used at lateral sides of the system and free boundary conditions were applied at the surfaces. The number of MC steps is 10^6 with 10% of these discarded for equilibration.

3.1 Near Ground State from MC Simulations

Similar to the infinite lattice (bulk), for the case of thin films, governed by the Hamiltonian (3.1), there are only three types of spin directions in each layer in the ground state. Also, for $K = 0$ and $D \neq 0$ the degeneracy arising from the formation of AF walls is still observed. However, unlike the bulk case, where switching at low temperature between ground states is unlikely for $K = 0.1$, for the thin films this switch is observed even for $K = 0.1$. This happens due to the fact that the K term is not present at the surfaces. The perfectly ordered ground state (i.e. in which all ferromagnetic sublattices are fully saturated) is most convenient for analyzing angles

between spins, so in order to construct a state close to it, first simulations with $K = 1$ in a cooling cycle (ended at $T = 0.01$) were performed to create the perfectly ordered state, then K was slowly changed from 1 to 0.1 at $T = 10^{-6}$ with MCS=10^6. $T = 10^{-6}$ is a very low temperature for MC simulations for calculating thermodynamic quantities, since the acceptance rate for new configurations with higher energy than at the previous configuration is very low. Meanwhile, every new spin configuration with lower energy than previous configuration is always accepted. The purpose is to obtain the ground state but not to calculate thermodynamic quantities, so rejecting configurations with higher energies is desirable.

For further reference, let us call at each layer those spins, which have the smallest angle with the normal to the surface, spins of type 3. Then other two types of spin directions are called of type 1 and 2. Angles between different types of spins as a function of D are shown in Fig. 3.3–3.8 for three- and six- layer thin films, where symbols S_{ij} denote a spin of type j in the i^{th} layer (see Fig. 3.2), and $\widehat{S_{ij}S_{kl}}$ stands for an angle between spins S_{ij} and S_{kl}. For making these graphs the approximate ground state spin configurations, obtained as described in the previous paragraph, were used. At first the angles were calculated for each pair of adjacent spins and then averaged over the lattice.

According to the graphs, for small D the angles between spins are almost 120°, as expected. For the surface layers, as D increases, spins of type 3 tend to point along the normal to the surface (up or down) and the other two types tend to point in the opposite direction. For the interior layers this is not the case. Spins of type 3 at these layers tend to point in the same direction as the surface spins of type 3, however, the angles between spins in these layers are almost 120° for any D and tend to the value

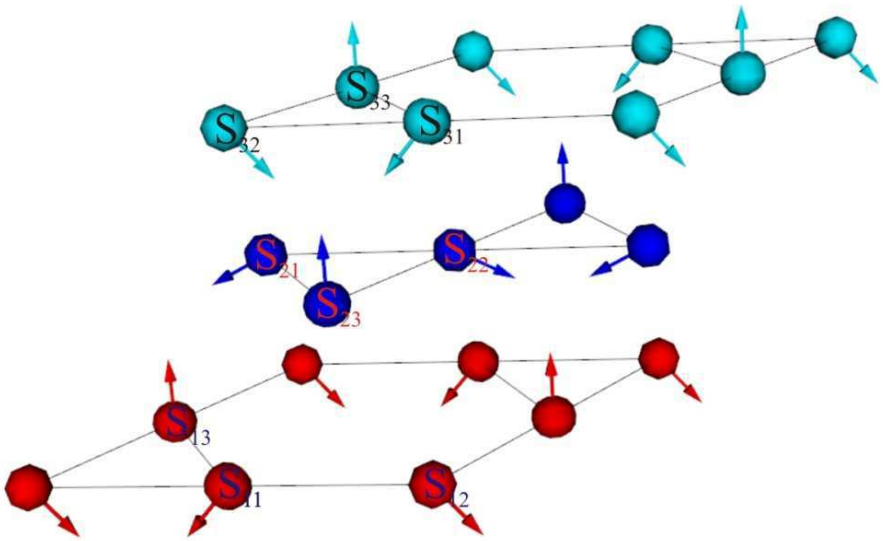

Figure 3.2: Ground state of the 3-layer system with $D = 1$ and $K = 0.1$.

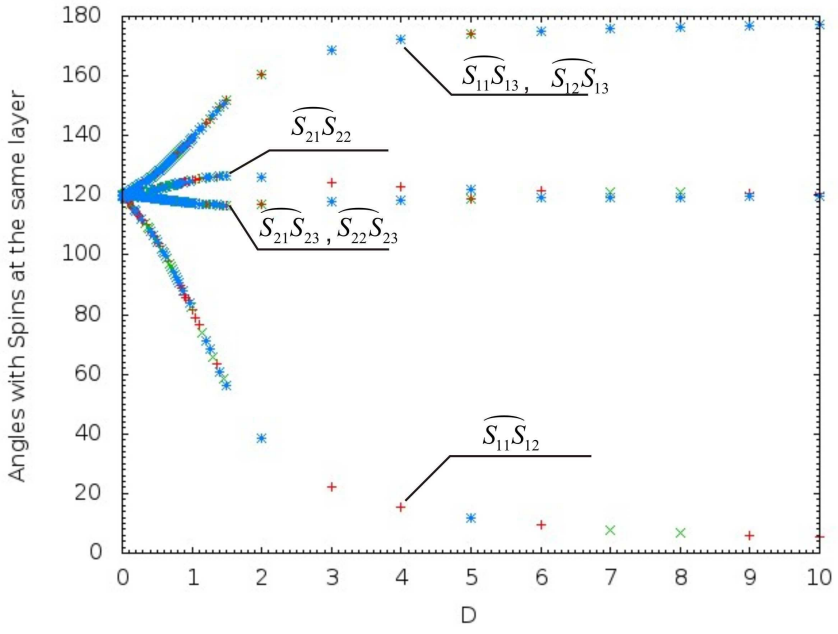

Figure 3.3: Ground state angles for the the 3-layer system between spins in the same layer (layer 1 and layer 2) as a function of surface anisotropy.

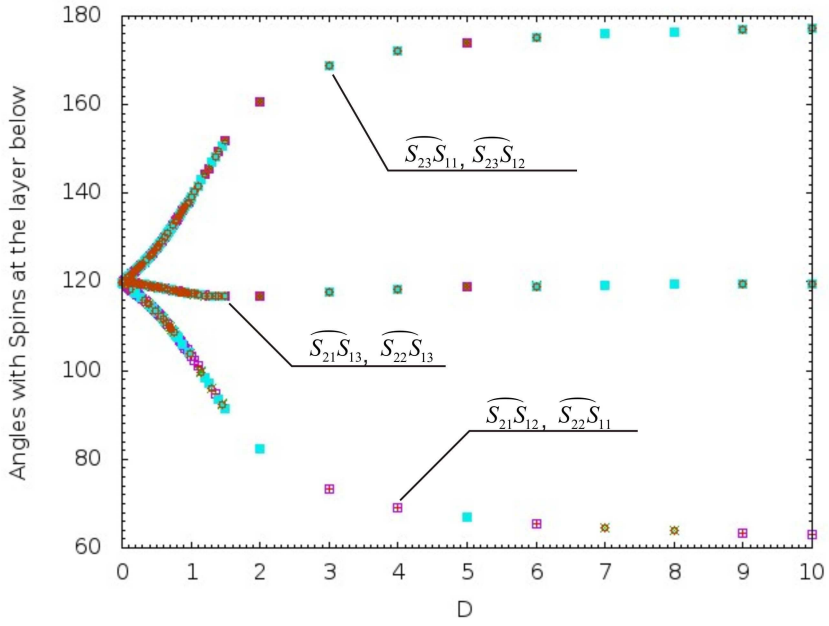

Figure 3.4: Ground state angles for the 3-layer system between spins in adjacent layers as a function of surface anisotropy.

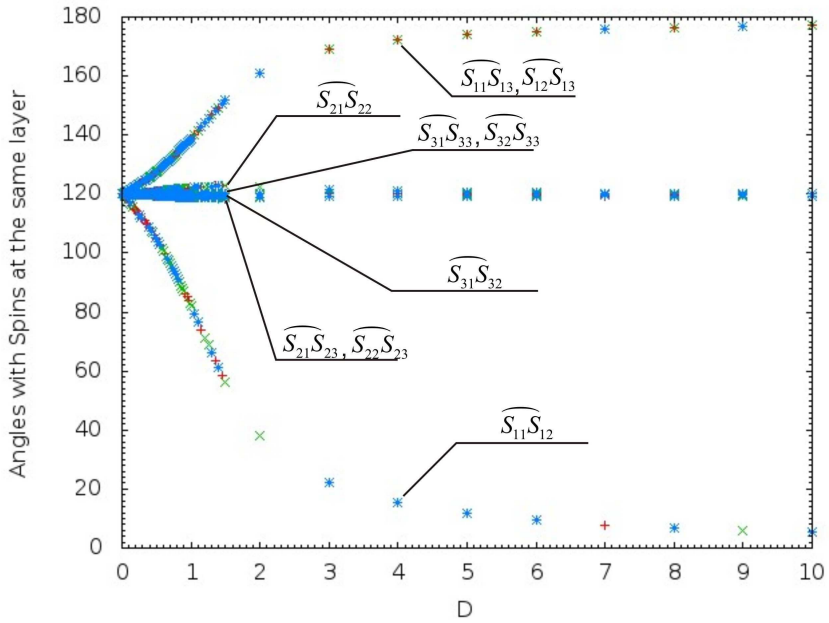

Figure 3.5: Ground state angles for the 6-layer system between spins in the same layer (layers 1, 2, and 3) as a function of surface anisotropy.

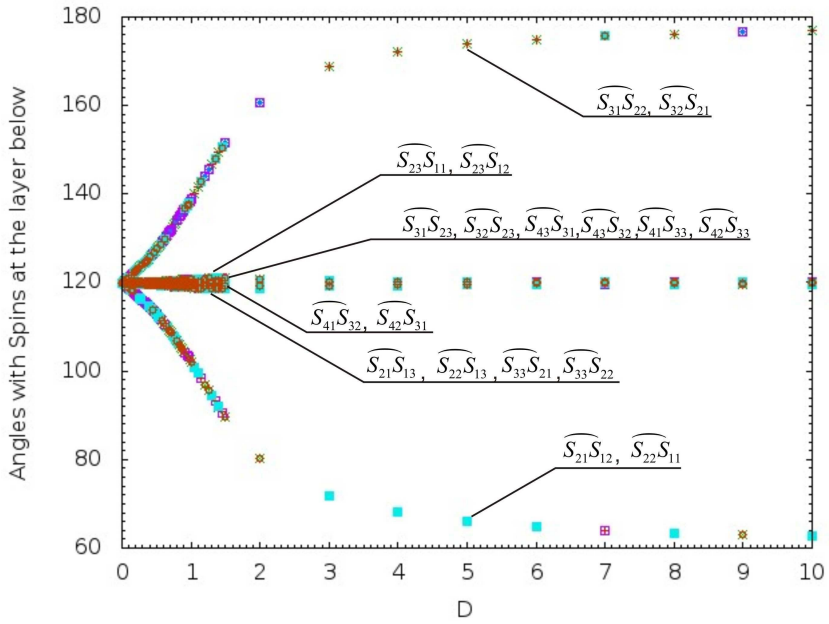

Figure 3.6: Ground state angles for the 6-layer system between spins in adjacent layers as a function of surface anisotropy.

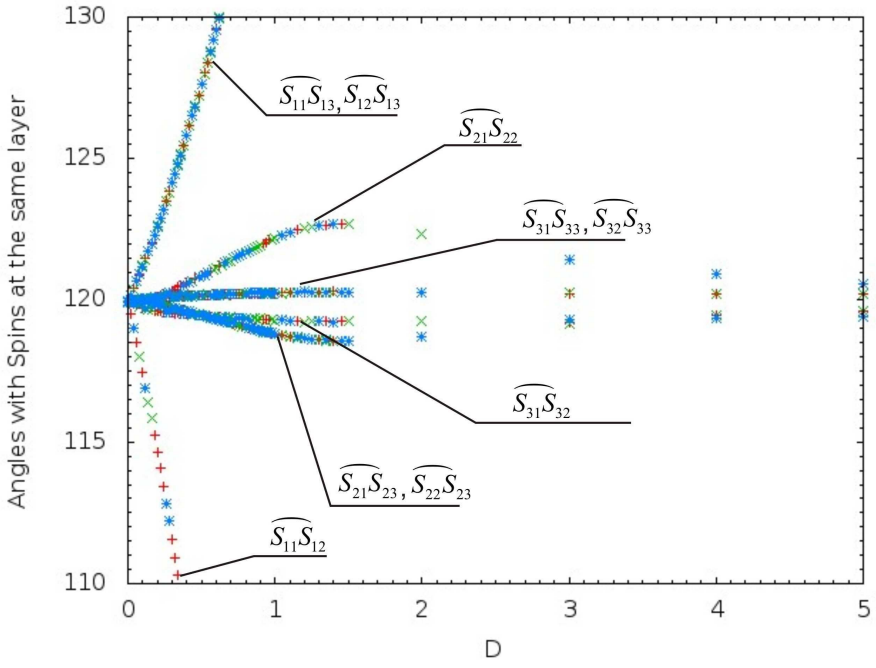

Figure 3.7: Zoomed part from the graph in Fig. 3.5.

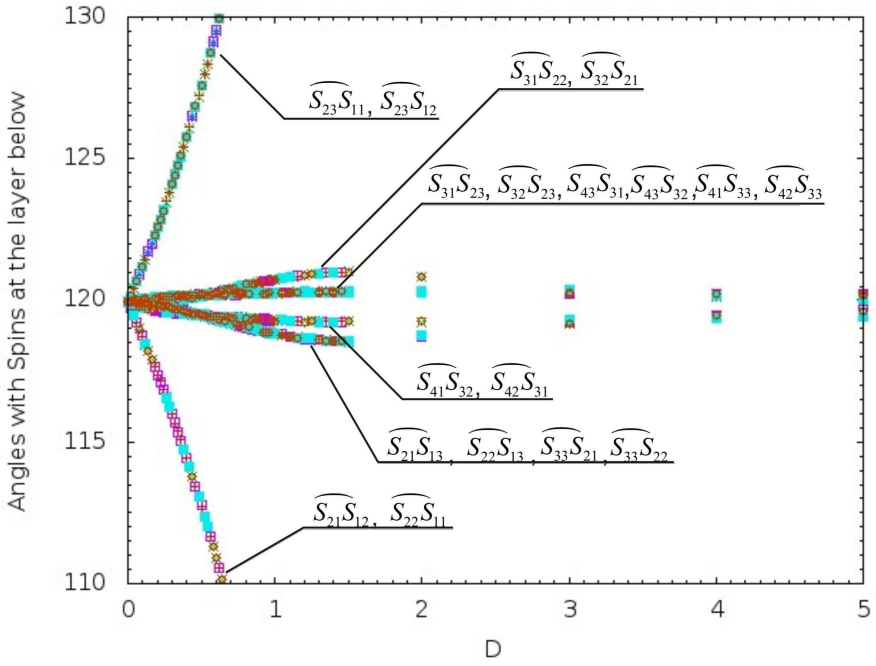

Figure 3.8: Zoomed part from the graph in Fig. 3.6.

close to 120° for large D.

When $D = 0$ and $K \neq 0$ there are 8 possible domains, which we can classify by the possible four $\{111\}$ planes [3], in which the spins tend to lie when K tends to 0, and two directions: Spins point either out of a triangle or towards the center. When D is slightly increased from zero, one of the $\{111\}$ planes, namely the one which coincides with the surface plane, is not suitable for characterization of the ground state. This is because an angle between spins lying in this plane and the D easy axis is much larger than for the other planes. So, we are left with only three planes. Any one of spins in a triangle can become the spin of type 3, which may be attributed to the C_3 rotational symmetry of the kagome lattice. Also, the spin of third type can point either up or down, thus, excluding the rotational symmetry factor, there are 6 possible domains.

3.2 Analytic calculations for the ground state

The following consideration is carried out for three-layer films in the Cartesian system using the conventional unit cell of the corresponding infinite (bulk) fcc crystal (i.e. thin films constitute a part of the infinite fcc crystal).

The energy per spin can be obtained by counting number of bonds per spin. Let us denote surface spins as $\mathbf{S_1}, \mathbf{S_2}, \mathbf{S_3}$, and spins in the middle as $\mathbf{M_1}, \mathbf{M_2}, \mathbf{M_3}$ so, that spins with the index 1 border only with spins which have indices 2 and 3, spins with the index 2 border with spins with indices 1 and 3, etc.. The local cubic anisotropy axis for spins M_1, M_2, and M_3 are $\hat{x}$, $\hat{y}$, and $\hat{z}$ respectively. In the surface layers there are $S_1 - S_2, S_1 - S_3$, and $S_2 - S_3$ types of bonds, in the middle layer $M_1 - M_2, M_1 - M_3$, and $M_2 - M_3$ types of bonds. Between layers there are $M_1 - S_2$, $M_1 - S_3$, $M_2 - S_3$, $M_2 - S_1$, $M_2 - S_3$, $M_3 - S_1$, and $M_3 - S_2$ bonds. On average a spin in the surface and a spin in the middle have exchange energies

$$E_{\text{in}}{}^{(\text{s})} = -J\frac{2\mathbf{S_1}\cdot\mathbf{S_2} + 2\mathbf{S_1}\cdot\mathbf{S_3} + 2\mathbf{S_2}\cdot\mathbf{S_3}}{3}, \tag{3.2}$$

$$E_{\text{in}}{}^{(\text{m})} = -J\frac{2\mathbf{M_1}\cdot\mathbf{M_2} + 2\mathbf{M_1}\cdot\mathbf{M_3} + 2\mathbf{M_2}\cdot\mathbf{M_3}}{3} \tag{3.3}$$

for spins in the same layer respectively. The average energy of interactions with spins between different layers is

$$E_{\text{between}} = -\frac{4}{3}J\frac{\mathbf{M_1}\cdot\mathbf{S_2} + \mathbf{M_1}\cdot\mathbf{S_3} + \mathbf{M_2}\cdot\mathbf{S_1} + \mathbf{M_2}\cdot\mathbf{S_3} + \mathbf{M_3}\cdot\mathbf{S_1} + \mathbf{M_3}\cdot\mathbf{S_2}}{6}, \tag{3.4}$$

where the ratio involving spin bonds is the average energy per bond, and the coefficient $\frac{4}{3}$ is due to the fact that per a line of three spins (each in the different layer) there are four bonds. Finally, introducing anisotropy terms, the total energy per spin

is given by

$$
\begin{aligned}
E = \frac{1}{3}\left(-2J\frac{2\mathbf{S_1}\cdot\mathbf{S_2}+2\mathbf{S_1}\cdot\mathbf{S_3}+2\mathbf{S_2}\cdot\mathbf{S_3}}{3} - J\frac{2\mathbf{M_1}\cdot\mathbf{M_2}+2\mathbf{M_1}\cdot\mathbf{M_3}+2\mathbf{M_2}\cdot\mathbf{M_3}}{3}\right) \\
- \frac{4}{3}J\frac{\mathbf{M_1}\cdot\mathbf{S_2}+\mathbf{M_1}\cdot\mathbf{S_3}+\mathbf{M_2}\cdot\mathbf{S_1}+\mathbf{M_2}\cdot\mathbf{S_3}+\mathbf{M_3}\cdot\mathbf{S_1}+\mathbf{M_3}\cdot\mathbf{S_2}}{6} \\
- \frac{2}{3}\cdot\frac{1}{3}\left(\frac{D}{3}[S_{1x}+S_{1y}+S_{1z}]^2+[S_{2x}+S_{2y}+S_{2z}]^2+[S_{3x}+S_{3y}+S_{3z}]^2\right) \\
- \frac{1}{3}\cdot\frac{1}{3}\left(K{M_{1x}}^2+K{M_{2y}}^2+K{M_{3z}}^2\right). \qquad (3.5)
\end{aligned}
$$

The location of the axes of the anisotropy with respect to the chosen coordinate system and the results of the previous section suggest that $S_{1x} = S_{2y}$, $S_{1y} = S_{2x}$, $S_{1z} = S_{2z}$, $S_{3x} = S_{3y}$, and similarly for the middle spins. Although this reduces the number of independent variables, an analytic solution for the minimization of this energy expression remains elusive. However, given that $K = 0.1$ is small compared to J it is possible to use perturbation methods in the case where D is also small.

A case of $D \to \infty$ is also feasible. It is known that in this case spins at the surface in the ground state point normal to the (111) surface, so they may be chosen as $S_{3x} = S_{3y} = S_{3z} = \frac{1}{\sqrt{3}}$ and $S_{1x} = S_{1y} = S_{1z} = -\frac{1}{\sqrt{3}} = S_{2x} = S_{2y} = S_{2z}$. Expression (3.5) thus becomes

$$
\begin{aligned}
E &= \frac{1}{3}\left(\frac{4J}{3} - 2J\frac{\mathbf{M_1}\cdot\mathbf{M_2}+\mathbf{M_1}\cdot\mathbf{M_3}+\mathbf{M_2}\cdot\mathbf{M_3}}{3}\right) \\
&\quad - \frac{4}{3}J\frac{\mathbf{M_3}\cdot\mathbf{S_1}+\mathbf{M_3}\cdot\mathbf{S_2}}{6} - \frac{2}{3}D - \frac{K}{9}\left({M_{1x}}^2+{M_{2y}}^2+{M_{3z}}^2\right) \\
&= -2J\frac{\mathbf{M_1}\cdot\mathbf{M_2}+\mathbf{M_1}\cdot\mathbf{M_3}+\mathbf{M_2}\cdot\mathbf{M_3}}{9} - \frac{K}{9}\left({M_{1x}}^2+{M_{2y}}^2+{M_{3z}}^2\right) \\
&\quad - \frac{2}{3}D + \frac{4J}{9} + \frac{4}{\sqrt{3}}J\frac{M_{3x}+M_{3y}+M_{3z}}{9}. \qquad (3.6)
\end{aligned}
$$

From here it immediately follows that for $K = 0$ the solution for the middle layer spins is the 120° structure with $\mathbf{M_3}$ pointing in the [111] direction. This is so because

the first term is minimized with the 120° structure and is isotropic, and the last term depends on only coordinates of $\mathbf{M_3}$ which determines its direction. This explains the behavior of Figs. 3.3–3.8 at large D.

For $0 < D << |J|$, $0 < K << |J|$. In this case it is possible to use perturbation theory to obtain the solution which minimizes the energy. For a zeroth order approximation let us choose the solution for the case with $D = 0,\ K = 0$ when spins lie in the $(11\bar{1})$ plane. It is known [3] that in this case spins are

$$\mathbf{S}_1 = (-\sqrt{\frac{2}{3}}, \frac{1}{\sqrt{6}}, -\frac{1}{\sqrt{6}}), \mathbf{S}_2 = (\frac{1}{\sqrt{6}}, -\sqrt{\frac{2}{3}}, -\frac{1}{\sqrt{6}}), \mathbf{S}_3 = (\frac{1}{\sqrt{6}}, \frac{1}{\sqrt{6}}, \sqrt{\frac{2}{3}}). \qquad (3.7)$$

It is convenient to work in a polar coordinate system, since while minimizing, the condition ${S_{ix}}^2 + {S_{iy}}^2 + {S_{iz}}^2 = 1$ is fulfilled automatically. Then, spins $\mathbf{S}_1$, $\mathbf{S}_2$, $\mathbf{M}_1$, and $\mathbf{M}_2$ are described with a polar and an azimuthal angles (θ_1, ϕ_1), $(\theta_1, \frac{\pi}{2} - \phi_1)$, (α_1, β_1) and $(\alpha_1, \frac{\pi}{2} - \beta_1)$ respectively, and spins $\mathbf{S}_3$ and $\mathbf{M}_3$ are described by angles $(\theta_3, \frac{\pi}{4})$ and $(\alpha_3, \frac{\pi}{4})$. The energy in the polar coordinates, after some simplification, may be rewritten as

$$\begin{aligned}
E = &-\frac{4}{9}J\left[\sin^2\theta_1 \sin 2\phi_1 + \cos^2\theta_1 + 2\sin\theta_1 \sin\theta_3 \cos(\phi_1 - \frac{\pi}{4}) + 2\cos\theta_1 \cos\theta_3\right] \\
&-\frac{4}{9}J\left[\sin^2\alpha_1 \sin 2\beta_1 + \cos^2\alpha_1 + 2\sin\alpha_1 \sin\alpha_3 \cos(\beta_1 - \frac{\pi}{4}) + 2\cos\alpha_1 \cos\alpha_3\right] \\
&-\frac{4}{9}J[\sin\alpha_1 \sin\theta_1 \sin(\phi_1 + \beta_1) + \cos\alpha_1 \cos\theta_1 + \sin\alpha_1 \sin\theta_3 \cos(\beta_1 - \frac{\pi}{4}) + \\
&+\cos\alpha_1 \cos\theta_3 + \sin\alpha_3 \sin\theta_1 \cos(\phi_1 - \frac{\pi}{4}) + \cos\alpha_3 \cos\theta_1] \\
&-\frac{2}{27}D\left[2(1 + \sin^2\theta_1 \sin 2\phi_1 + \sin 2\theta_1(\cos\phi_1 + \sin\phi_1)) + 1 + \sin^2\theta_3 + \sqrt{2}\sin 2\theta_3\right] \\
&-\frac{K}{9}\left[2\sin^2\alpha_1 \cos^2\beta_1 + \cos^2\alpha_3\right]. \qquad (3.8)
\end{aligned}$$

One may express the angles which minimizes the energy in the form

$$\begin{aligned} \theta_1 &= \theta_1^{(0)} + \theta_1^{(1)} \qquad \phi_1 = \phi_1^{(0)} + \phi_1^{(1)} \qquad \theta_3 = \theta_3^{(0)} + \theta_3^{(1)} \\ \alpha_1 &= \alpha_1^{(0)} + \alpha_1^{(1)} \qquad \beta_1 = \beta_1^{(0)} + \beta_1^{(1)} \qquad \alpha_3 = \alpha_3^{(0)} + \alpha_3^{(1)}. \end{aligned} \tag{3.9}$$

where $\theta_1^{(1)}, \phi_1^{(1)}, \theta_3^{(1)}, \alpha_1^{(1)}, \beta_1^{(1)}, \alpha_3^{(1)}$ are small angles, and

$$\begin{aligned} \theta_1^{(0)} &= \arccos\frac{1}{\sqrt{6}} \qquad \phi_1^{(0)} = -\arctan\frac{1}{2} \qquad \theta_3^{(0)} = \arccos\sqrt{\frac{2}{3}} \\ \alpha_1^{(0)} &= \arccos\frac{1}{\sqrt{6}} \qquad \beta_1^{(0)} = -\arctan\frac{1}{2} \qquad \alpha_3^{(0)} = \arccos\sqrt{\frac{2}{3}}. \end{aligned} \tag{3.10}$$

After the expansion up to second order the energy reduces to

$$\begin{aligned} E = &-\frac{4}{9}J\left[-\frac{3}{2} + \frac{17}{10}\theta_1^{(1)2} - \frac{1}{\sqrt{5}}\theta_1^{(1)}\phi_1^{(1)} + \frac{3}{2}\phi_1^{(1)2} + \frac{1}{2}\theta_2^{(1)2} + \frac{2\sqrt{2}}{\sqrt{5}}\theta_1^{(1)}\theta_3^{(1)} - \sqrt{2}\theta_3^{(1)}\phi_1^{(1)}\right] \\ &-\frac{2}{9}J\left[-\frac{3}{2} + \frac{17}{10}\alpha_1^{(1)2} - \frac{1}{\sqrt{5}}\alpha_1^{(1)}\beta_1^{(1)} + \frac{3}{2}\beta_1^{(1)2} + \frac{1}{2}\alpha_2^{(1)2} + \frac{2\sqrt{2}}{\sqrt{5}}\alpha_1^{(1)}\alpha_3^{(1)} - \sqrt{2}\alpha_3^{(1)}\beta_1^{(1)}\right] \\ &-\frac{4}{9}J[-\frac{3}{2} + \frac{1}{2}\theta_1^{(1)2} + \frac{5}{12}\phi_1^{(1)2} + \frac{1}{4}\theta_3^{(1)2} + \frac{1}{2}\alpha_1^{(1)2} + \frac{5}{12}\beta_1^{(1)2} + \frac{1}{4}\alpha_3^{(1)2} - \frac{7}{10}\theta_1^{(1)}\alpha_1^{(1)} \\ &-\frac{1}{2\sqrt{5}}\theta_1^{(1)}\beta_1^{(1)} + \frac{2}{\sqrt{10}}\theta_1^{(1)}\alpha_3^{(1)} - \frac{1}{2\sqrt{5}}\phi_1^{(1)}\alpha_1^{(1)} - \frac{1}{\sqrt{2}}\phi_1^{(1)}\alpha_3^{(1)} + \frac{2}{3}\phi_1^{(1)}\beta_1^{(1)} + \frac{2}{\sqrt{10}}\theta_3^{(1)}\alpha_1^{(1)} \\ &-\frac{1}{\sqrt{2}}\theta_3^{(1)}\beta_1^{(1)}] \\ &-\frac{2}{27}D\left[4 + \frac{16}{3\sqrt{5}}\theta_1^{(1)} + 4\phi_1^{(1)} + \frac{4\sqrt{2}}{3}\theta_3^{(1)} - \frac{4}{15}\theta_1^{(1)2} + \frac{7}{3}\phi_1^{(1)2} - \frac{7}{3}\theta_3^{(1)2} + \frac{4}{\sqrt{5}}\theta_1^{(1)}\phi_1^{(1)}\right] \\ &-\frac{K}{9}\left[2 - \frac{8}{3\sqrt{5}}\alpha_1^{(1)} + \frac{4}{3}\beta_1^{(1)} + \frac{2\sqrt{2}}{3}\alpha_3^{(1)} - \frac{16}{15}\alpha_1^{(1)2} - \beta_1^{(1)2} - \frac{1}{3}\alpha_3^{(1)2} - \frac{8}{3\sqrt{5}}\alpha_1^{(1)}\beta_1^{(1)}\right]. \end{aligned} \tag{3.11}$$

After taking derivatives we find the following matrix equation is obtained

$$\begin{pmatrix} \frac{16D}{405} - \frac{88J}{45} & -\frac{8D}{27\sqrt{5}} + \frac{4J}{9\sqrt{5}} & -\frac{8\sqrt{2}J}{9\sqrt{5}} & -\frac{14J}{45} & \frac{2J}{9\sqrt{5}} & -\frac{4}{9}\sqrt{\frac{2}{5}}J \\ -\frac{8D}{27\sqrt{5}} + \frac{4J}{9\sqrt{5}} & -\frac{28D}{81} - \frac{46J}{27} & \frac{4\sqrt{2}J}{9} & \frac{2J}{9\sqrt{5}} & -\frac{8J}{27} & \frac{2\sqrt{2}J}{9} \\ -\frac{8\sqrt{2}J}{9\sqrt{5}} & \frac{4\sqrt{2}J}{9} & \frac{28D}{81} - \frac{2J}{3} & -\frac{4}{9}\sqrt{\frac{2}{5}}J & \frac{2\sqrt{2}J}{9} & 0 \\ -\frac{14J}{45} & \frac{2J}{9\sqrt{5}} & -\frac{4}{9}\sqrt{\frac{2}{5}}J & -\frac{6J}{5} + \frac{32K}{135} & \frac{2J}{9\sqrt{5}} + \frac{8K1}{27\sqrt{5}} & -\frac{4\sqrt{2}J}{9\sqrt{5}} \\ \frac{2J}{9\sqrt{5}} & -\frac{8J}{27} & \frac{2\sqrt{2}J}{9} & \frac{2J}{9\sqrt{5}} + \frac{8K}{27\sqrt{5}} & -\frac{28J}{27} + \frac{2K}{9} & \frac{2\sqrt{2}J}{9} \\ -\frac{4}{9}\sqrt{\frac{2}{5}}J & \frac{2\sqrt{2}J}{9} & 0 & -\frac{4\sqrt{2}J}{9\sqrt{5}} & \frac{2\sqrt{2}J}{9} & -\frac{4J}{9} + \frac{2K}{27} \end{pmatrix} \begin{pmatrix} \theta_1^{(1)} \\ \phi_1^{(1)} \\ \theta_3^{(1)} \\ \alpha_1^{(1)} \\ \beta_1^{(1)} \\ \alpha_3^{(1)} \end{pmatrix} = \begin{pmatrix} \frac{32D}{81\sqrt{5}} \\ \frac{8D}{27} \\ \frac{8\sqrt{2}D}{81} \\ -\frac{8K}{27\sqrt{5}} \\ \frac{4K}{27} \\ -\frac{2\sqrt{2}K}{27} \end{pmatrix}. \tag{3.12}$$

The general solution of this system is quite formidable, and that is why it is not shown here. It may be found with the Gaussian elimination method, and here it was implemented by using the function Rowreduce in Wolfram Mathematica software. The energy and normal to the film spin components obtained with this solution are shown in Tables 3.1 and 3.2, respectively.

The energy obtained is in good agreement with the exact energy (obtained with Wolfram Mathematica by direct numerical minimization of the energy Eq. (3.5) and the effective field method (see below)) for small values of D. Futher increasing the accuracy for small D is possible by extending the expansion to include higher order terms and using the method of successive approximations, in which variables are expressed in the form $x = x^{(0)} + x^{(1)} + x^{(2)} + ...$.

3.3 Effective Field Method

The effective field method [29] is an algorithm to find the $T = 0$ ground state numerically. The basic idea of this method is to minimize the energy locally by changing

direction of one (or several) spin(s) at a time. Starting with a random spin configuration, the minimization of a local energy is carried out for every spin in one sweep, after which another sweep is carried out. This procedure is repeated iteratively until a local minimum of the energy of the system is achieved or some criteria is fulfilled, for example, until after 10^5 sweeps a relative changing in energy is less than 10^{-10}. If there is no proof that the obtained state is the global minimum of the system's energy, this procedure should be done for a large number of initial random configurations in order to feel safe that the obtained minimum is global, or at least close to it. The name of this method came from the fact that in a case of a Hamiltonian, without single-site anisotropy terms, the local minimization is achieved by directing a spin antiparallel to the effective field created by its neighbors, $\mathbf{H}_i^{eff}$. However, in presence of local anisotropy (e.g. along the z-axis) local minimization is not achieved by directing spins antiparallel to an effective field. In this case, the necessary condition of minimum for the i^{th} spin is

$$\sum_j J_{ij} S_{j\alpha} - 2K\delta_{\alpha z} S_{iz} = \lambda S_{i\alpha}, \tag{3.13}$$

where λ is a Lagrange multiplier for the constraint $S_{ix}^2 + S_{iy}^2 + S_{iz}^2 = 1$, $\alpha = x, y, z$, $\delta_{\alpha z}$ is Kronecker delta function, and i, j are the magnetic ion sites. It is possible to rewrite the last formula in the form $\mathbf{H}_i^{eff} = \lambda \mathbf{S_i}$, where $\mathbf{H}_i^{eff}$ would be dependent of the i^{th} spin's coordinates. Thus, directing the spin antiparrallel to the $\mathbf{H}_i^{eff}$, in general, changes the direction and magnitude of the $\mathbf{H}_i^{eff}$, which, in general, even does not guarantee decreasing in energy. Instead, the solution of Eqs. (3.13) or numerical minimization of a local energy is needed.

Using the Cartesian coordinate system as defined in the previous section, for local

minimization of a spin in the middle layers with the easy axis along the $\hat{x}$ direction one may find stationary points of the function

$$F = -J_x S_x - J_y S_y - J_z S_z - K {S_x}^2 - \lambda({S_x}^2 + {S_y}^2 + {S_z}^2), \tag{3.14}$$

where λ is a Lagrange multiplier, $J_\alpha = \sum_{NN} S_{j\alpha}$ and $\alpha = x, y, z$. This leads to a set of equations

$$-J_x - 2KS_x - 2\lambda S_x = 0 \tag{3.15}$$

$$-J_y - 2\lambda S_y = 0 \tag{3.16}$$

$$-J_z - 2\lambda S_z = 0. \tag{3.17}$$

Together with the constraint ${S_x}^2 + {S_y}^2 + {S_z}^2 = 1$, these equations may be reduced to

$$4\lambda^4 + 8K\lambda^3 + [4K^2 - ({J_x}^2 + {J_y}^2 + {J_z}^2)]\lambda^2 - 2K({J_y}^2 + {J_z}^2)\lambda - K^2({J_y}^2 + {J_z}^2) = 0. \tag{3.18}$$

This equation can be solved analytically. For the other spins with the easy axes along $\hat{y}$ and $\hat{z}$ directions, the equation for minimization is easily obtained from Eq. (3.18) by cyclic permutation of indices x, y, and z. Out of four possible solutions of Eq. (3.18) we choose one which produces real values of S_x, S_y, S_z and minimizes the local energy.

For surface spins, instead of minimization in the current coordinate system, it is convenient to switch to a coordinate system with $\hat{z}$ normal to the surface. This coordinate system is obtained from old one by rotation by an angle $\theta = \arccos\frac{1}{\sqrt{3}}$ about the $[1\bar{1}0]$ axis with the transformation matrix

$$A = \begin{pmatrix} \frac{1}{2} + \frac{1}{\sqrt{12}} & -\frac{1}{2} + \frac{1}{\sqrt{12}} & -\frac{1}{\sqrt{3}} \\ -\frac{1}{2} + \frac{1}{\sqrt{12}} & \frac{1}{2} + \frac{1}{\sqrt{12}} & -\frac{1}{\sqrt{3}} \\ \frac{1}{\sqrt{3}} & \frac{1}{\sqrt{3}} & \frac{1}{\sqrt{3}} \end{pmatrix}. \tag{3.19}$$

Returning to the old system, of course, is made with the inverse matrix.

There are only three types of spin directions in each layer in the ground state, and periodic boundary conditions ensure that any spin in a ground state on a lattice with integer number of unit cells has the same neighbors as in the case of an infinite system. This implies that the ground energy per spin does not depend on the lattice lateral size, and for this reason computations were done on the small $6 \times 6 \times 3$ film. Results from these computations, MC simulations, analytical calculations by expansion the energy up to second order, and numerical minimization of the formula (3.5) by means of Wolfram Mathematica software (with the function "Minimize") are displayed in the Table 3.1. Results in Figs. 3.3–3.8 are confirmed by the effective field method as well. For example, for $D = 1$ the result obtained from the effective field method gives $\widehat{S_1S_3}$= 139.145, $\overset{frown}{S_1S_2} = 81.7066$, from MC simulations these angles are: $\widehat{S_1S_3}$= 139.08, $\widehat{S_1S_2}$= 81.68.

From this table a very good agreement between the Mathematica numerical minimization and the effective field computations can be seen. Though, for $D = 3, 5, 10$ the energy in the effective field column is $\approx 10^{-14}$ less than in the Mathematica column. This may be attributed to the fact that in the effective field method, the C++ code uses double precision. The energy per spin of the prepared near-ground state in the MC simulations with the precision at least to 10^{-4} coincides with the effective method field results, which shows it may be considered as a good approximation.

Table 3.1: Comparison of the ground state energy per spin of the 6x6x3 system obtained by different methods.

D	Mathematica	2^{nd} order	MC simulations	Effective field
0	-1.6891028159428623	-1.68910278	x	-1.689102815942711
0.01	-1.6922055300448742	-1.69213	x	-1.692205530044869
0.02	-1.695453665463186	-1.69494	-1.69532	-1.695453665463181
0.1	-1.722387722628923	-1.71393	-1.72232	-1.722387722628919
0.5	-1.867922139962391	-1.82554	-1.86791	-1.86792213996239
1	-2.083071483463267	-1.96848	-2.08307	-2.08307148362216
3	-3.281524672022323	-0.43010	-3.28152	-3.281524672022326
5	-4.597199860922256	x	-4.59719	-4.597199860922261
10	-7.91981272045046	x	-7.9198	-7.919812720450472

Table 3.2: Comparison of the normal components of S_3 and M_3 in the 6×6×3 system obtained by numerical minimization in Mathematica and second order expansion. The precision of numbers is 5×10^{-7}.

D	$S_{3\perp}$, Mathematica	$M_{3\perp}$, Mathematica	$S_{3\perp}$, 2^{nd} order	$M_{3\perp}$, 2^{nd} order
0	0.944098	0.938184	0.944884	0.938998
0.01	0.979547	0.975092	0.984602	0.980489
0.02	0.990731	0.987499	0.99681	0.994548
0.1	0.999471	0.998512	0.986538	0.990369
0.5	0.999992	0.999728	0.947025	0.941393
1	1	0.999869	0.908886	0.860604
3	0.999998	0.999968	-0.886559	0.738214

Chapter 4

Finite Temperature MC Simulations

4.1 Energy and Specific Heat

Unless indicated otherwise, the MC simulations presented in this chapter have been carried out for systems consisting of L layers of size 18×18 with increasing temperature (heating), starting from a near-ground state obtained as described in section 3.1.

Figures 4.1 and 4.2 show the energy of the system per spin, and Figs. 4.3 and 4.4 show the specific heat per spin. Simulation results over a larger range of temperature (Figs. 4.5 and 4.6) show that in the case of the system with 3 layers, in addition to the sharp peak at the transition temperature, there is another broad shoulder at a higher temperature for higher values of D.

Since the high T shoulder is observed only for 3-layer film it appears to be a

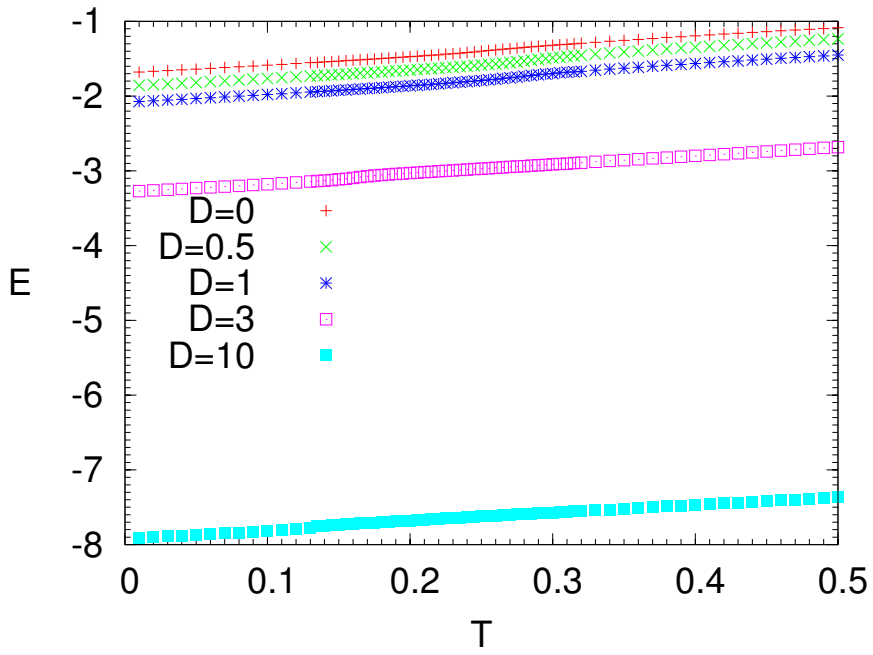

Figure 4.1: Energy per spin of the thin film with 3 layers vs temperature, with varying axial anisotropy values.

surface effect, and this is clearly shown on Figs. 4.7- 4.10 where values C_{surf} and C_{int} are depicted. Here, C_{surf} accounts only for the energy fluctuations of the surface spins and C_{int} accounts only for the energy fluctuations of the interior, using the formulas

$$C_{\text{surf}} = k\beta^2 \left(\langle E_{\text{surf}}^2 \rangle - \langle E_{\text{surf}} \rangle^2 \right) \tag{4.1}$$

$$C_{\text{int}} = k\beta^2 \left(\langle E_{\text{int}}^2 \rangle - \langle E_{\text{int}} \rangle^2 \right). \tag{4.2}$$

While calculating E_{surf} and E_{int}, bonds between surface spins and spins from adjacent layers are still accounted for.

The high T shoulder is a Schottky anomaly [4] due to the D term in the Hamiltonian. A similar effect was found at large K in $IrMn_3$ [3].

At low temperature C_{surf} and C_{int} for large values of D are considerably greater than one. This may be associated with the fact that they are proportional to math-

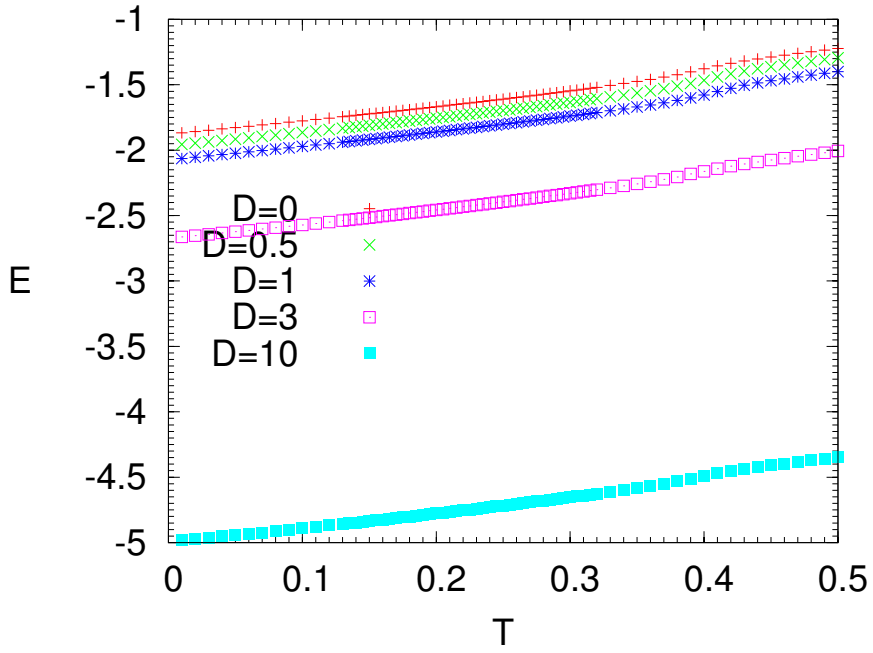

Figure 4.2: Energy per spin of the thin film with 6 layers vs temperature, with varying axial anisotropy values.

ematical expectations of $(E_{\text{surf}} - \bar{E}_{\text{surf}})^2$ and $(E_{\text{int}} - \bar{E}_{\text{int}})^2$, where the bar means an expected value of the quantities. While at low T the system spends most its time at the lowest energy levels, the modulus of the deviations of E_{surf} and E_{int} may be larger than the modulus of the corresponding deviation of the total energy E, where deviations of E_{surf} to one side from zero may be compensated by deviations of the energy interaction between the middle layer spins to another side, which, at the same time, may be considered as deviations of E_{int} in one side are compensated by deviations of the energy interaction between the surface layer spins.

Figure 4.11 shows the transition temperature for both $L = 3$ and $L = 6$ as a function of D estimated from the peaks in the specific heat. For $L = 3$, there is well formed maximum near $D = 0.85$. A similar peak is observed for $L = 6$, but it is

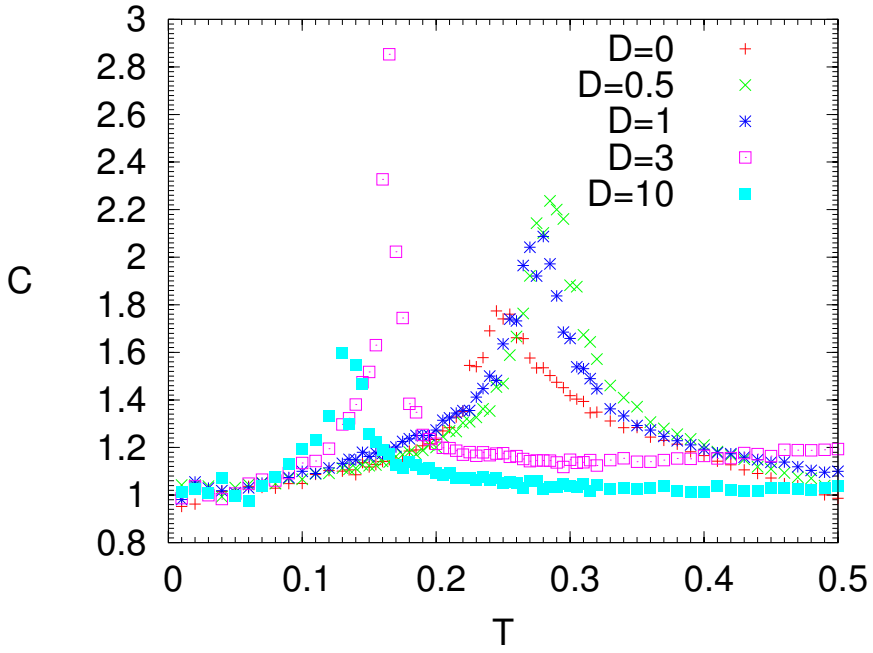

Figure 4.3: Specific heat per spin of the thin film with 3 layers vs temperature, with varying axial anisotropy values.

less pronounced. These maxima have basically the same qualitative explanation as peaks in the T_N *vs* K plot in Chapter 2. The difference here is that as $D \to \infty$ T_N does not tend to 0, but to some constant value (about 0.13 and 0.4 for $L = 3$ and $L = 6$, respectively). This is because the D term acts only on the surface spins and the system can still establish long range order through coupling to the middle layers. For the 3D case at $K = 0.1$, the transition temperature is about 0.52. For $D = 0$ in thin films with $L = 6$, it is about 0.41, and for $L = 3$, it is about 0.25. This is consistent with the tendency of surface effects to diminish with increasing number of layers [30].

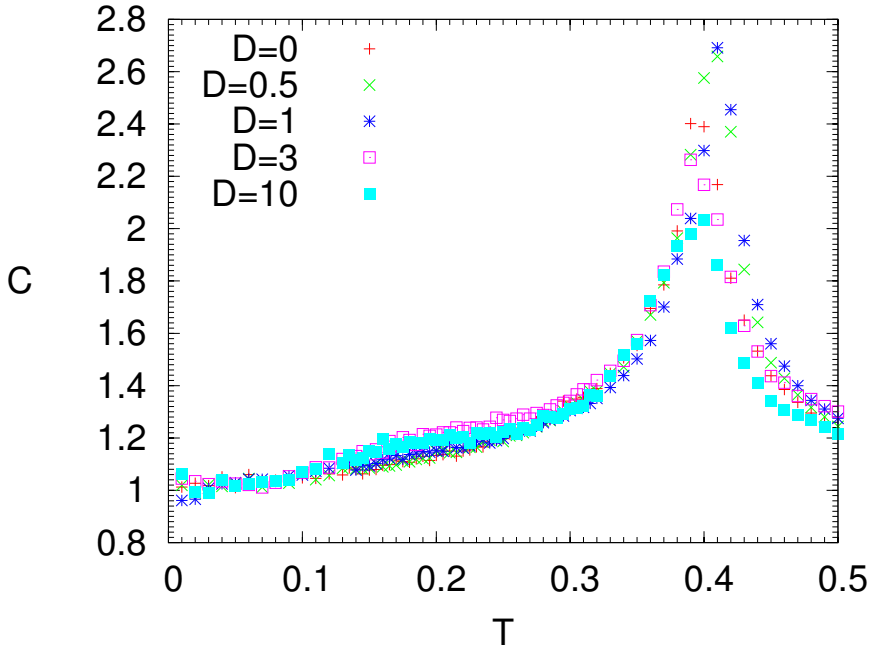

Figure 4.4: Specific heat per spin of the thin film with 6 layers vs temperature, with varying axial anisotropy values.

4.2 Order Parameter

The order parameter M_t calculated for both heating and cooling cycles (for 18x18 size in plane) is shown in Figs. 4.12, 4.13 and Figs. 4.14, 4.15, respectively. However, the order parameters in cooling and heating runs were calculated in a little bit different ways. They both also differ from the order parameter for the bulk system determined by Eq. (2.2), because it is good to account for the fact that each layer has their own three ferromagnetic sublattices. In heating runs the order parameter was calculated as

$$M_t = \frac{1}{N} \left\langle \sum_{layers} \sum_{\gamma} \left| \sum_{i \epsilon \gamma} \mathbf{S}_i \right| \right\rangle , \tag{4.3}$$

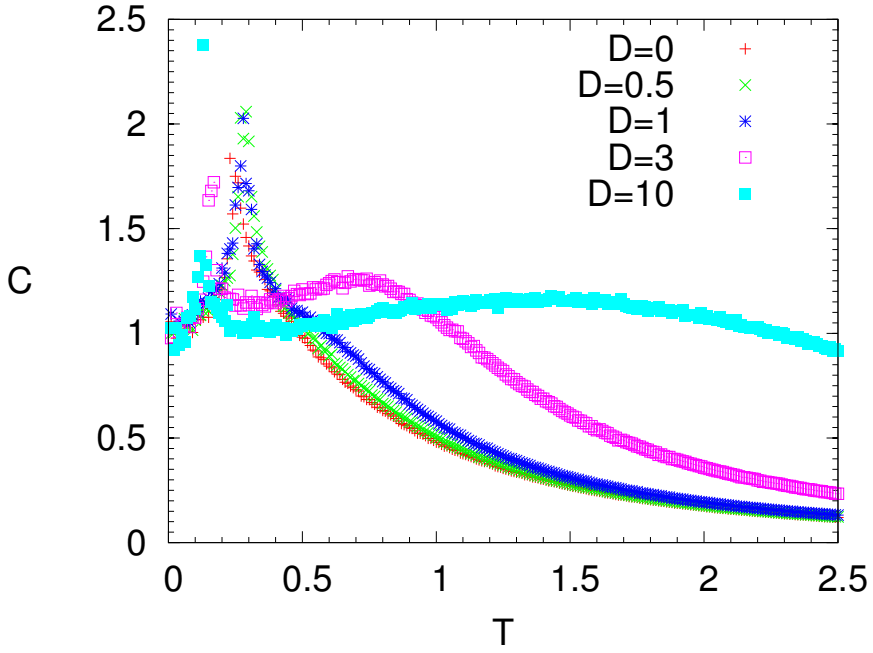

Figure 4.5: Specific heat per spin vs temperature in a wide range of $T = (0; 2.5]$ for 3-layer films, with varying axial anisotropy values. From cooling run with MCS=250000.

while in cooling runs the formula

$$M_t = \frac{1}{N} \sum_{layers} \sum_{\gamma} \left| \left\langle \sum_{i \epsilon \gamma} \mathbf{S}_i \right\rangle \right| \tag{4.4}$$

was used. The difference is in the order of the modulus and averaging operations. Because in the formula (4.3) the modulus operation is performed after the summation of the spin vectors over a small size lattice, this leads to non-zero values for the order parameter at high temperature in heating cycle graphs on Figs. 4.12 and 4.13. Although averaging before the modulus operation is more correct, the formula (4.3) is needed for calculating the order parameter susceptibility, since one needs to calculate the mean square root deviations.

From Figs. 4.12 and 4.13 we see that for heating cycle M_t is always saturated at low temperature (since the initial spin configuration is fully ordered), while for

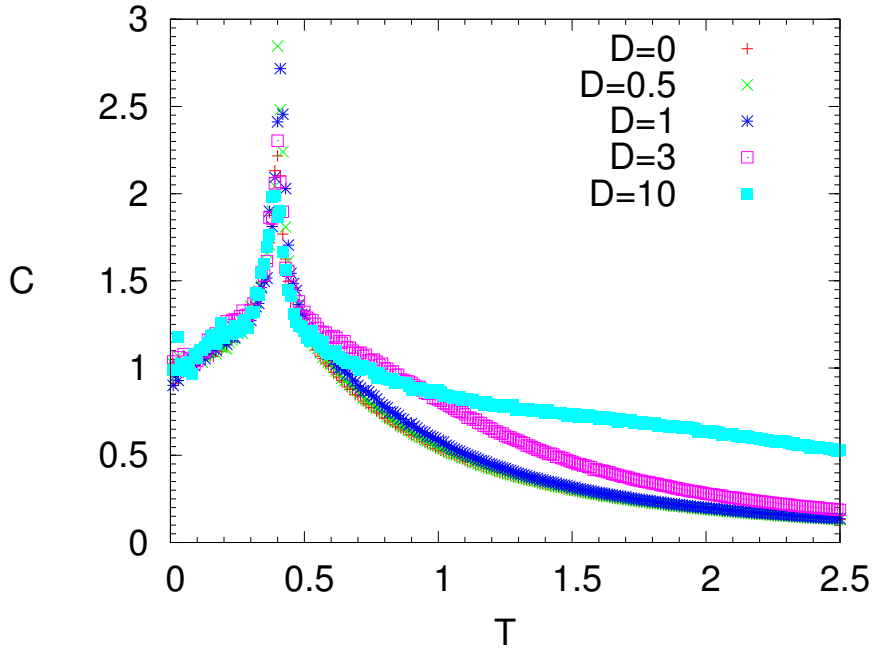

Figure 4.6: Specific heat per spin vs temperature in a wide range of $T = (0; 2.5]$ for 6-layer films, with varying axial anisotropy values. From cooling run with MCS=200000.

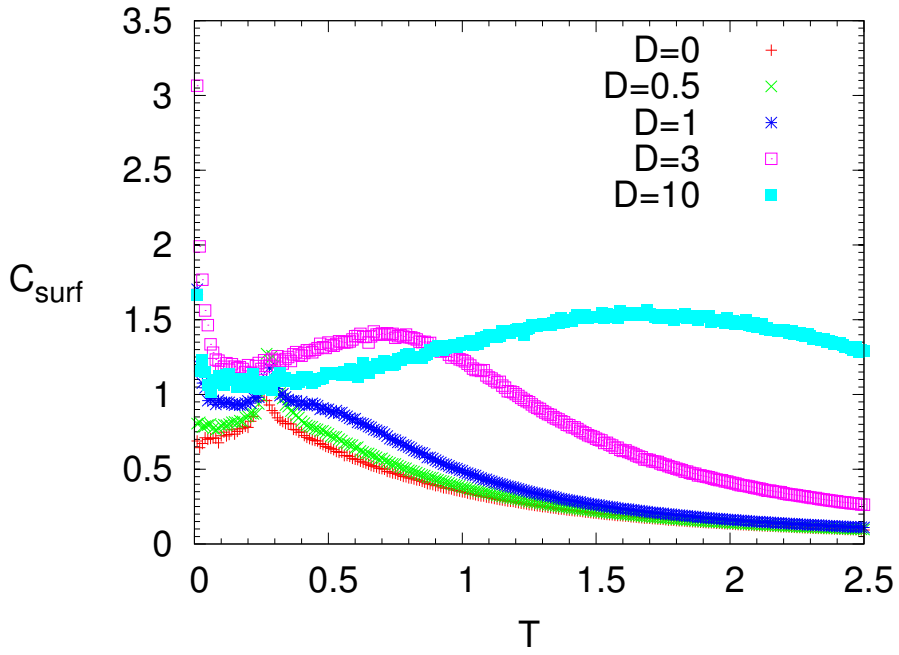

Figure 4.7: C_{surf} vs T, 3-layer thin films. From cooling run with MCS=250000.

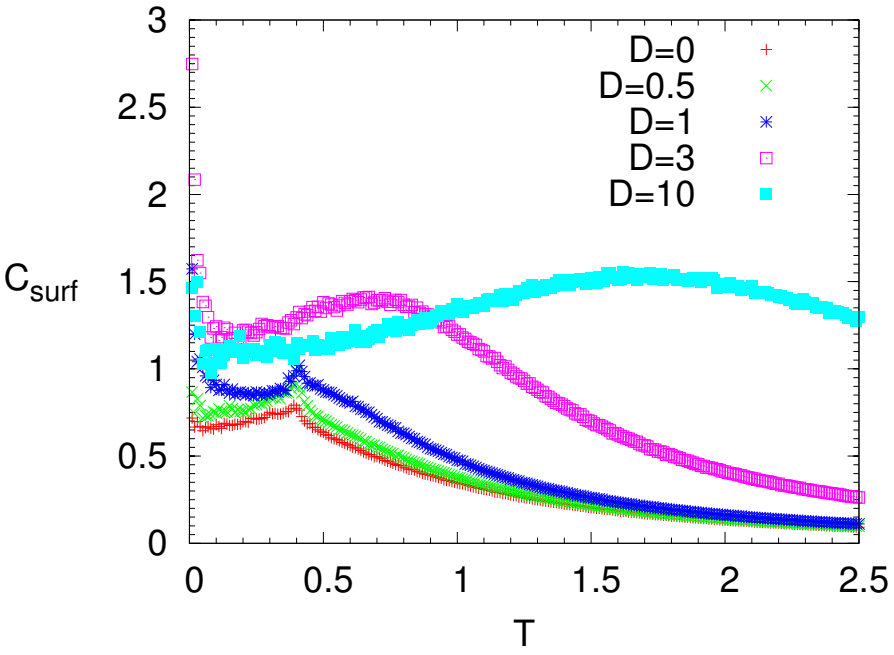

Figure 4.8: C_{surf} vs T, 6-layer thin films. From cooling run with MCS=200000.

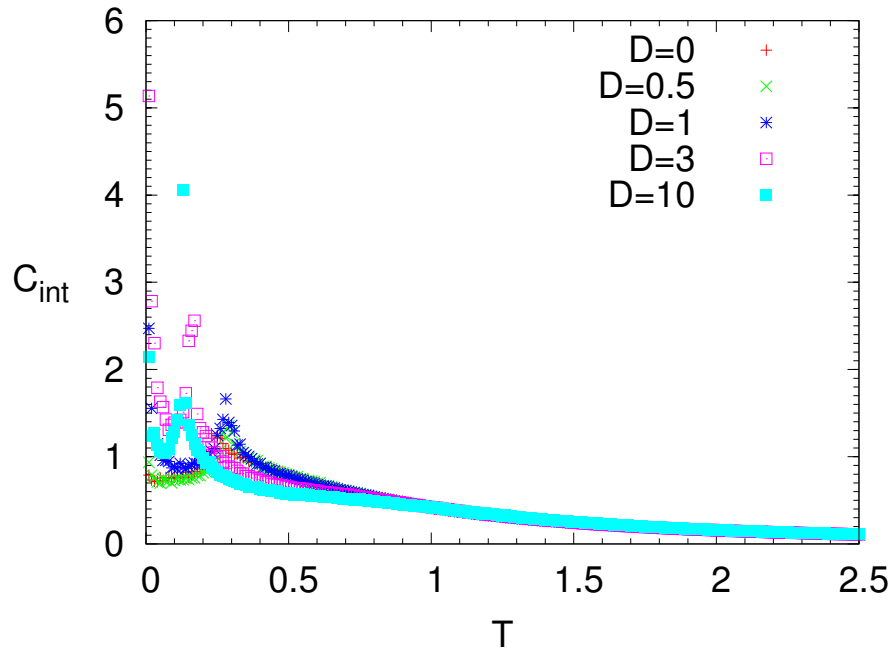

Figure 4.9: C_{int} vs T, 3-layer thin films.

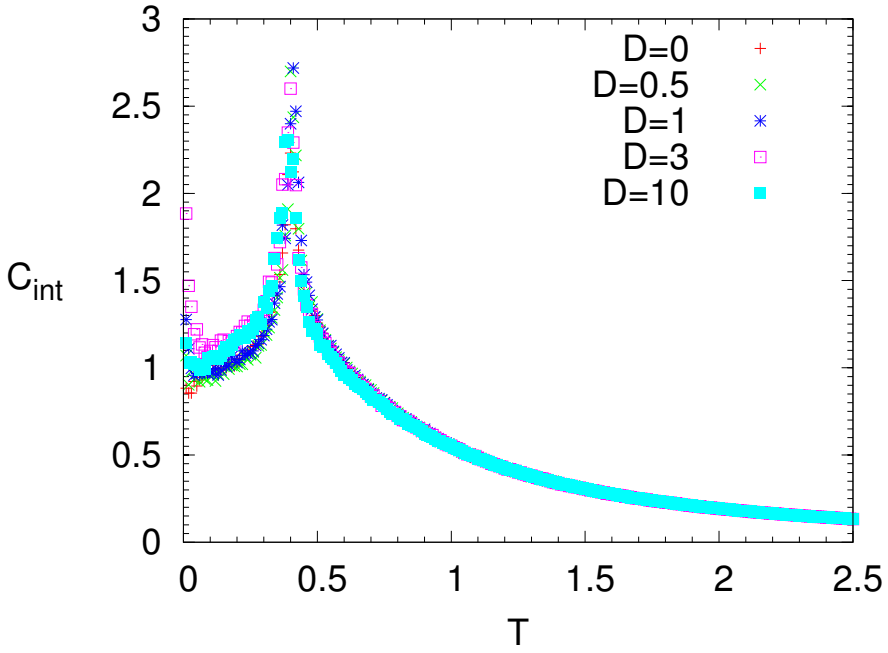

Figure 4.10: C_{int} vs T, 6-layer thin films.

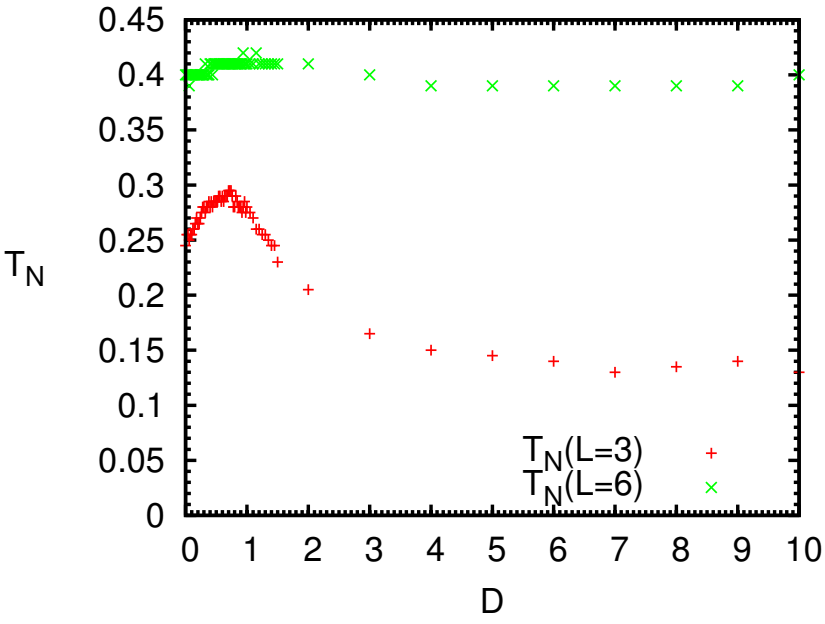

Figure 4.11: Transition temperature from specific heat plots vs surface anisotropy values.

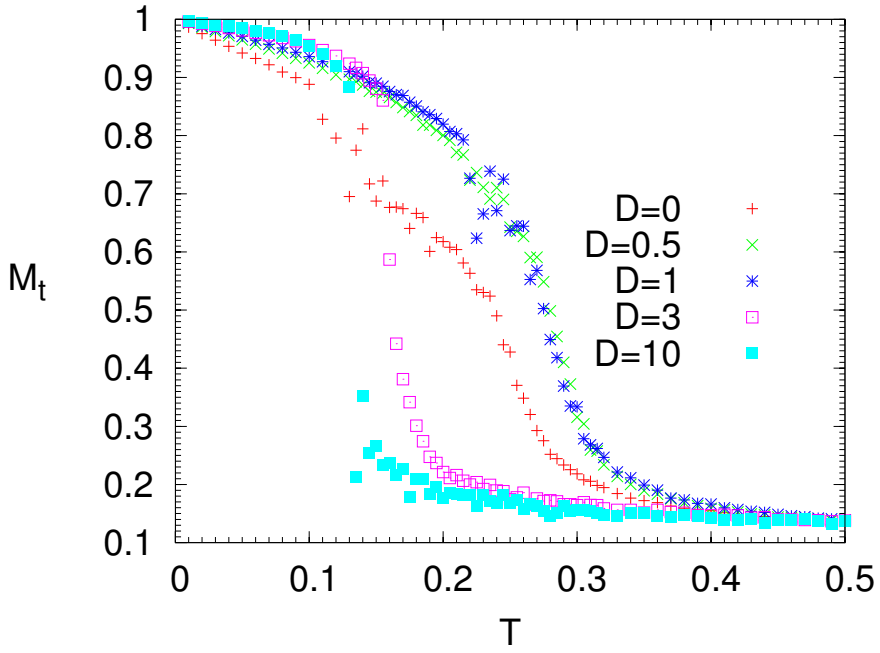

Figure 4.12: M_t of the thin films with 3 layers vs temperature, obtained from the heating cycle.

cooling cycle for the 3-layer film case (Fig. 4.14) this is not always achieved. There are also a well formed discontinuity for some lines of points. This may be attributed to the switching between low-energy states as was described in the Ch. 2 (as in the 3D case for small K). Even though for a cooling cycle for the 6-layer films (Fig. 4.15) M_t achieves unity for every values of D presented, it is also possible that M_t does not tend to unity at low temperature, though the probability for this is lower than in the case of the 3-layer film. This is naturally associated with the thickness of the film. The term responsible for hindering switching between metastable low-energy states is the K-term (since it depends on the site position in the lattice; the D-term has no influence on switching, since it is the same for any site on the surface) which is present in the middle layers. In the 3D case a value of $K = 0.1$ is sufficient to

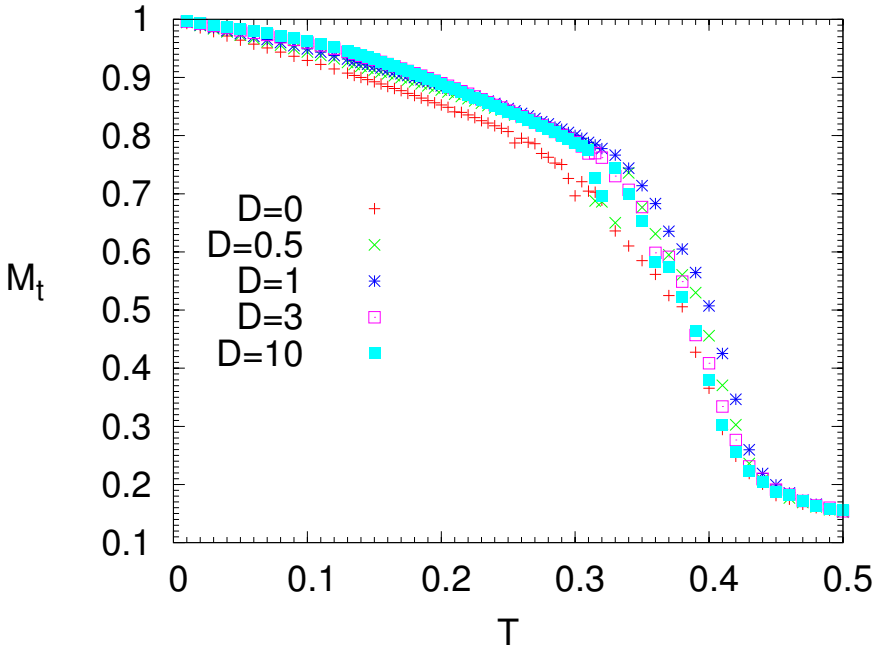

Figure 4.13: M_t of the thin films with 6 layers vs temperature, obtained from the heating cycle.

completely prevent the switching between different spin states, thus increasing the number of middle layers increases the contribution of the K-term, and thus leads to less probability of the switching.

4.3 Magnetization

The total magnetization per spin M_f, magnetization per spin of the interior only (M_{int}) and surface only (M_{surf}) are displayed in Figs. 4.16, 4.17, and 4.18, 4.19, and 4.20, 4.21, respectively. Projections of the magnetizations of the first; second, and third layers onto the normal to the film (z-axis) are shown on Figs. 4.22, 4.23; 4.24, 4.25, and 4.26, 4.27, respectively. Due to the symmetry, magnetizations of the

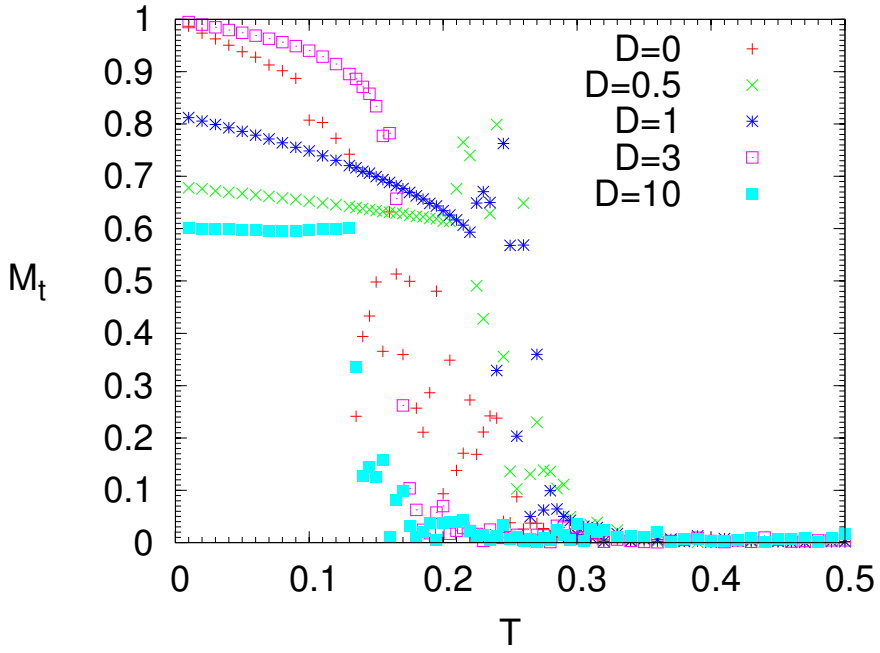

Figure 4.14: M_t of the thin films with 3 layers vs temperature, obtained from the cooling cycle.

other three planes in the case of the film with 6 layers are the same and therefore are not shown. There is no particular direction (up or down) along the z axis, and this implies that the projections may be positive or negative with equal probability.

The magnetization in the interior is very small for all values of D. For the 3-layer film from Fig. 4.18 we see that its magnitude at zero temperature first increases as D increases from 0, and then decreases. This is consistent with the angle graphs provided in Ch. 3, where the small deviations from the $q = 0$ state is most significant in the range of D from ≈ 0 to about 5. The graphs for surface magnetization presented in Figs. 4.20 and 4.21 and their z components in Figs. 4.22 and 4.23 clearly show $M_{\text{surf}} \to 1/3$ as D increases. This corresponds to a surface structure in the limit $D \to \infty$, in which one of spins in a triangle points up (down) and other two respectively down

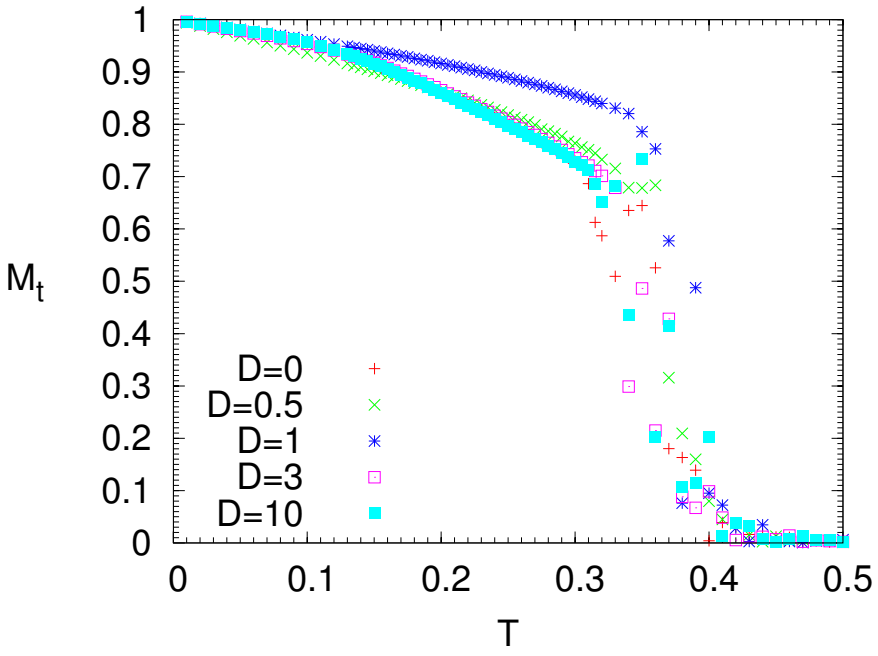

Figure 4.15: M_t of the thin films with 6 layers vs temperature, obtained from the cooling cycle.

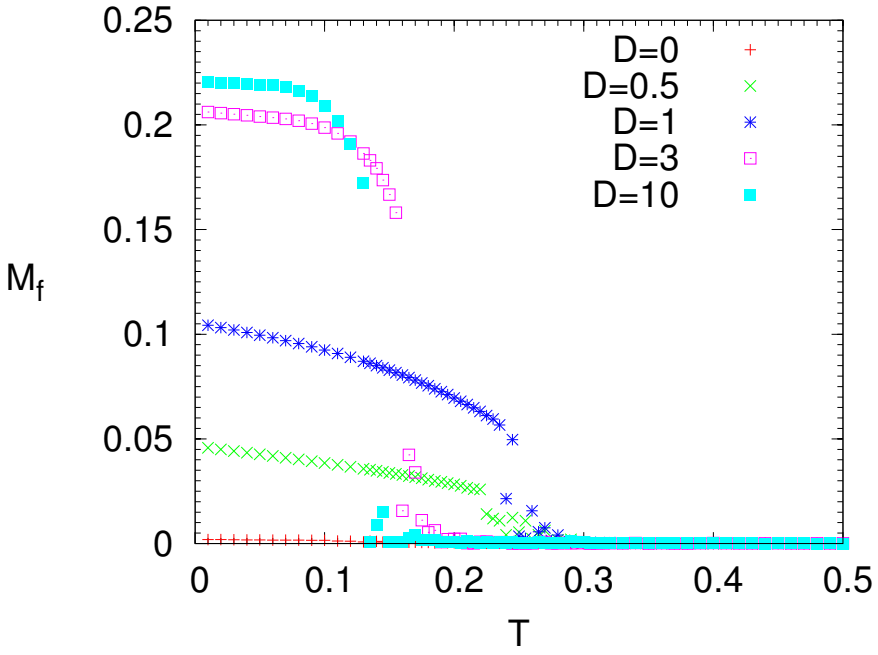

Figure 4.16: Total magnetization M_f of the thin films with 3 layers vs temperature.

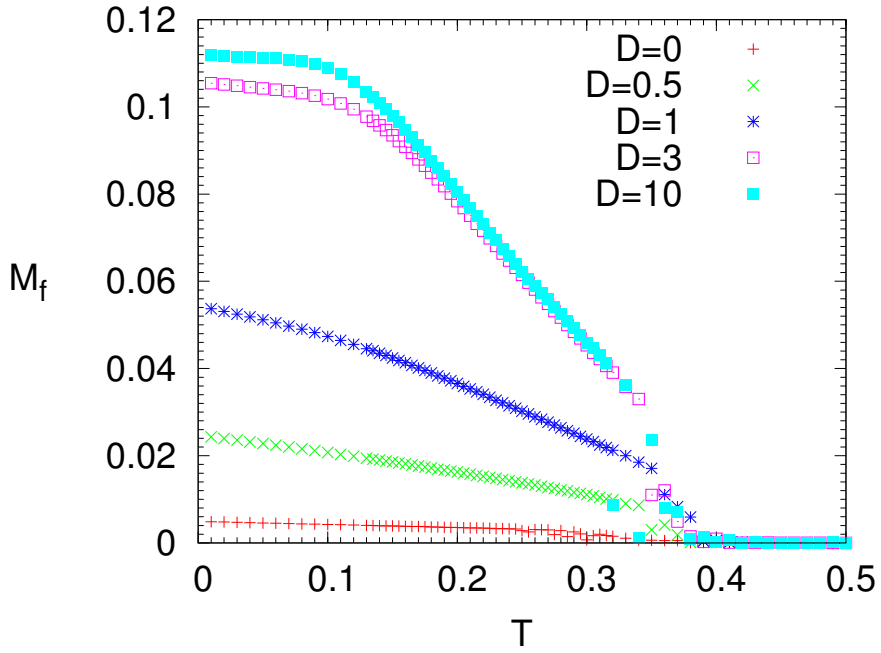

Figure 4.17: Total magnetization M_f of the thin films with 6 layers vs temperature.

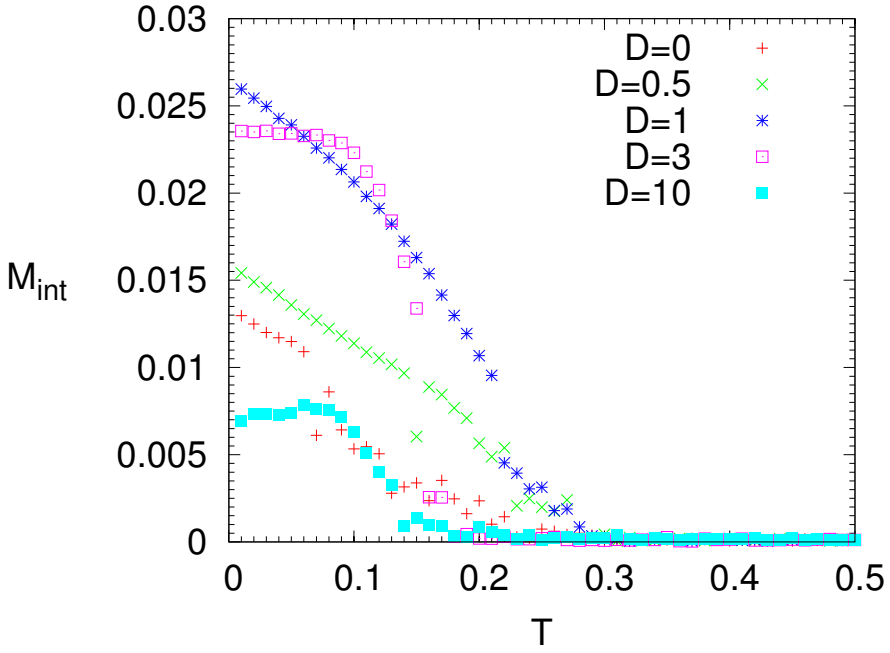

Figure 4.18: Magnetization in the middle M_{int} of the thin films with 3 layers vs temperature. Lateral size is 12x12.

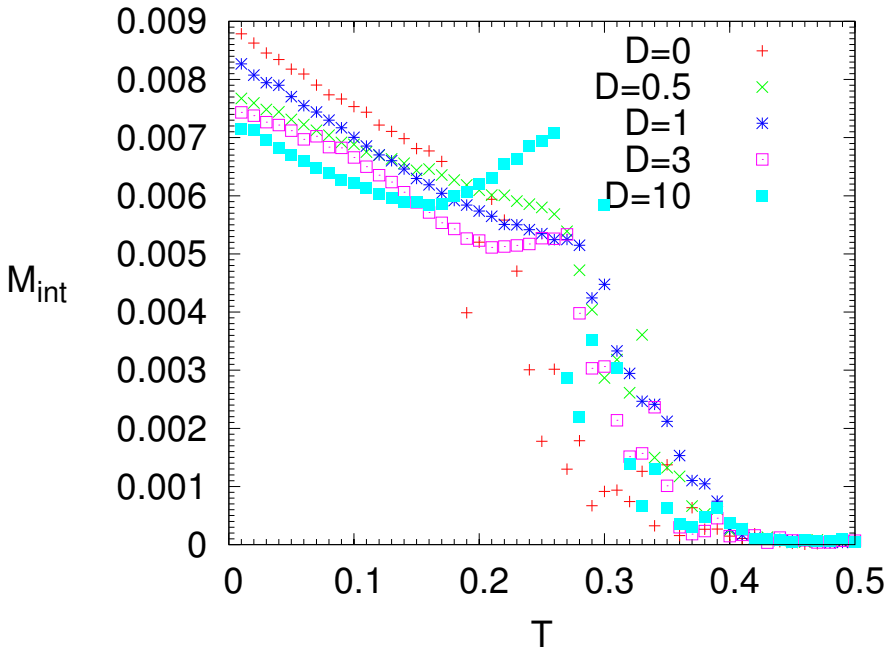

Figure 4.19: Magnetization in the middle M_{int} of the thin films with 6 layers vs temperature. Lateral size is 12x12.

(up). The comparison of results for z components with those for interior and surface magnetizations shows the existence of a tiny inplane component of the magnetization. This is expected since in the case of very small D, when spins almost lie in the $(11\bar{1})$ plane (or in the two other equivalent, but not in the (111) plane), according to the 3D simulations the total magnetization should point almost perpendicular to the plane of spins. It is interesting that in the case of three layers, z components of the surface and middle are opposite in signs. A possible explanation of this result is that an effective coupling between layers is antiferromagnetic, which implies that layer's magnetizations would rather create an obtuse angle between them. In the case of six layers, z component of the second layer magnetization changes its sign as T decreases from high and has maximum and minimum at non-zero temperature. It

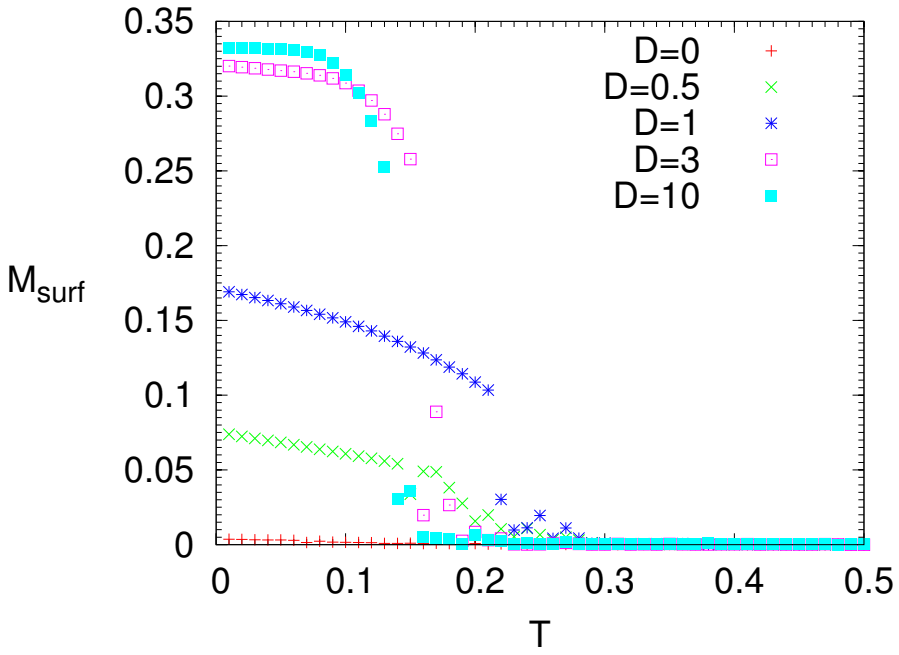

Figure 4.20: Magnetization of the surface M_{surf} of the thin films with 3 layers vs temperature. Lateral size is 12x12.

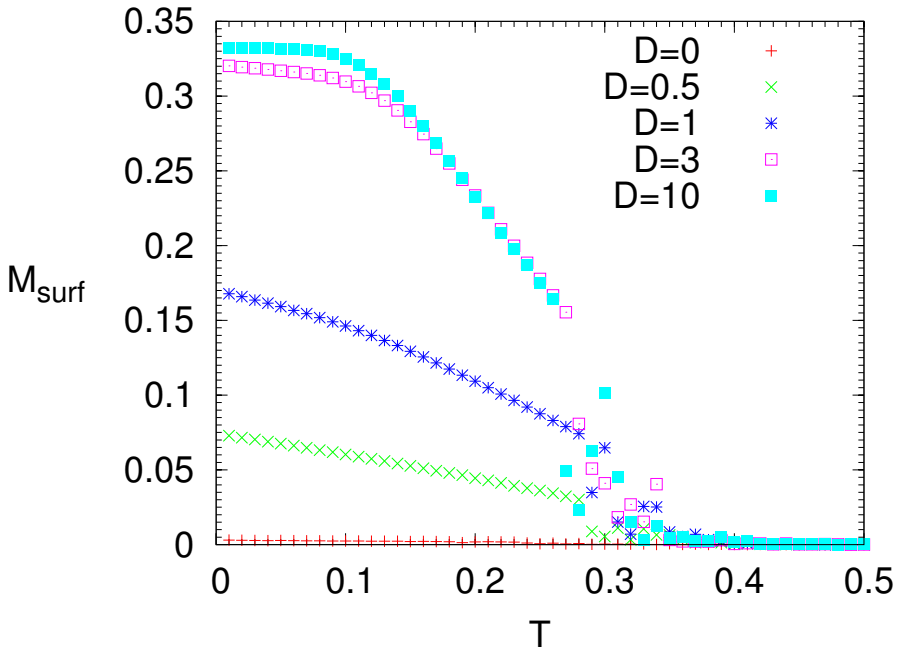

Figure 4.21: Magnetization of the surface M_{surf} of the thin films with 6 layers vs temperature. Lateral size is 12x12.

is worth noting that the peak in M_{int} appears to be connnected to this maximum in the z component of the second layer. each other except for different transition temperatures. This is because the structures in the bulk in both of these cases are almost identical.

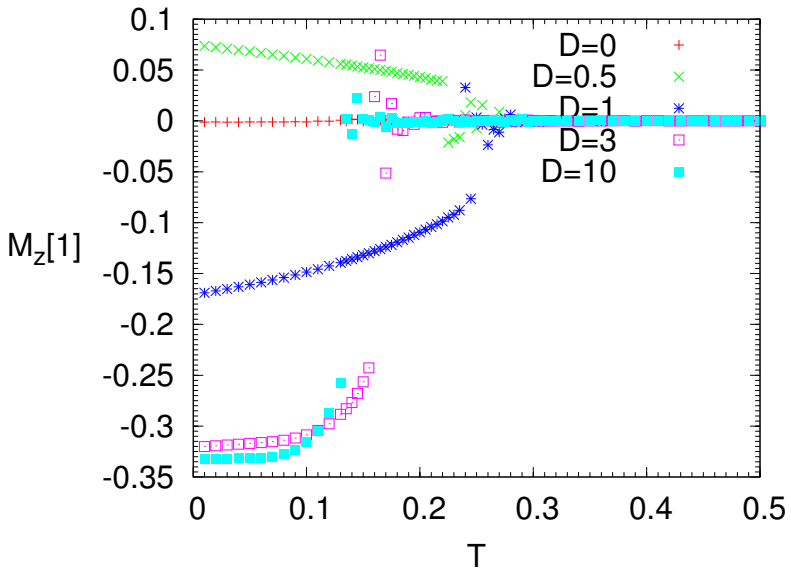

Figure 4.22: z component of the magnetization of the first layer (surface) of the thin films with 3 layers vs temperature.

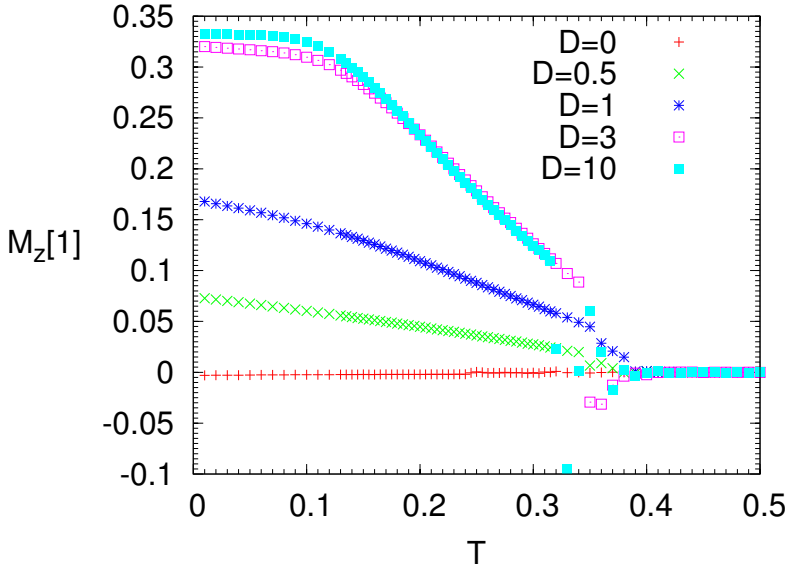

Figure 4.23: z component of the magnetization of the first layer (surface) of the thin films with 6 layers vs temperature.

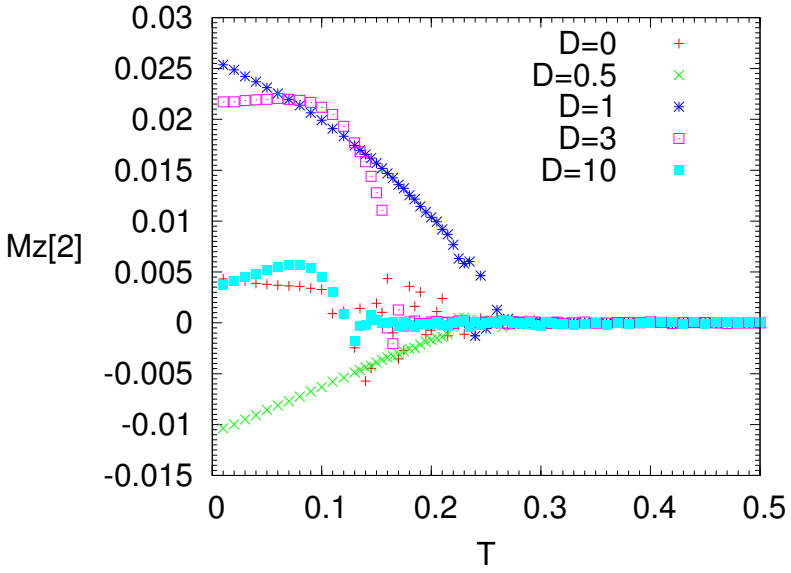

Figure 4.24: z component of the magnetization of the second layer (middle) of the thin films with 3 layers vs temperature.

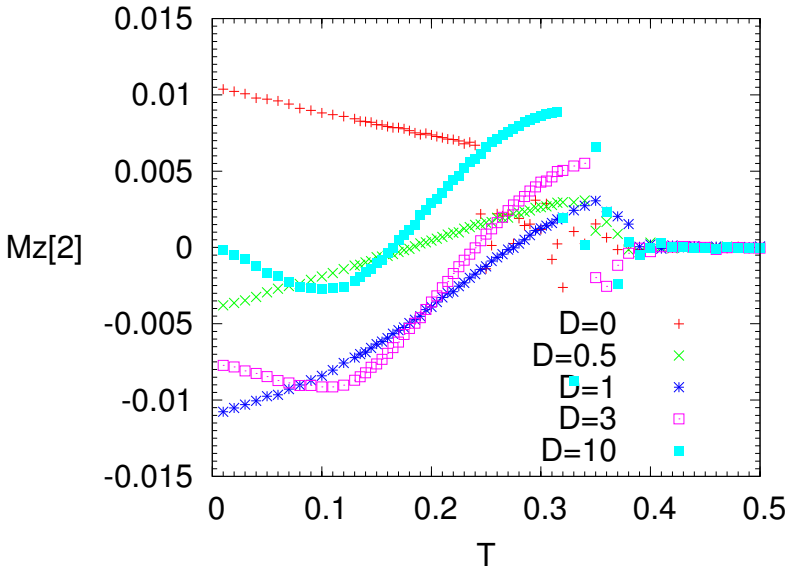

Figure 4.25: z component of the magnetization of the second layer (middle) of the thin films with 6 layers vs temperature.

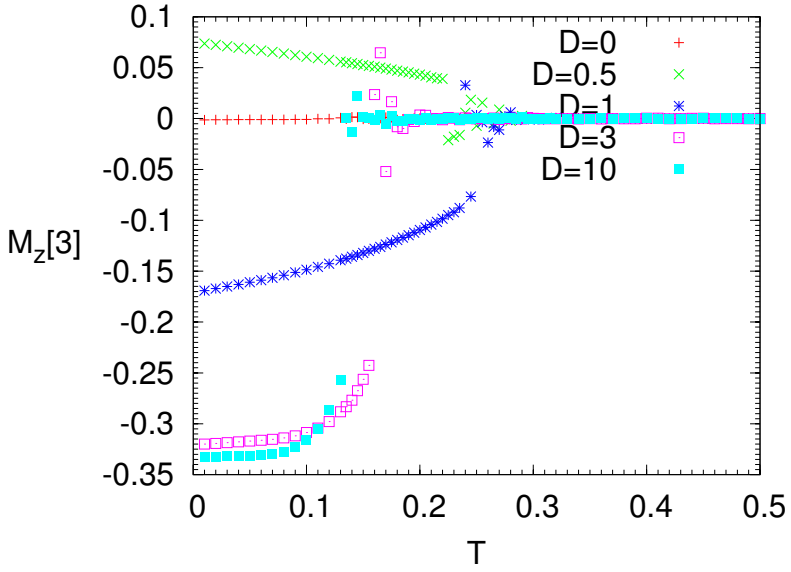

Figure 4.26: z component of the magnetization of the third layer (surface) of the thin films with 3 layers vs temperature.

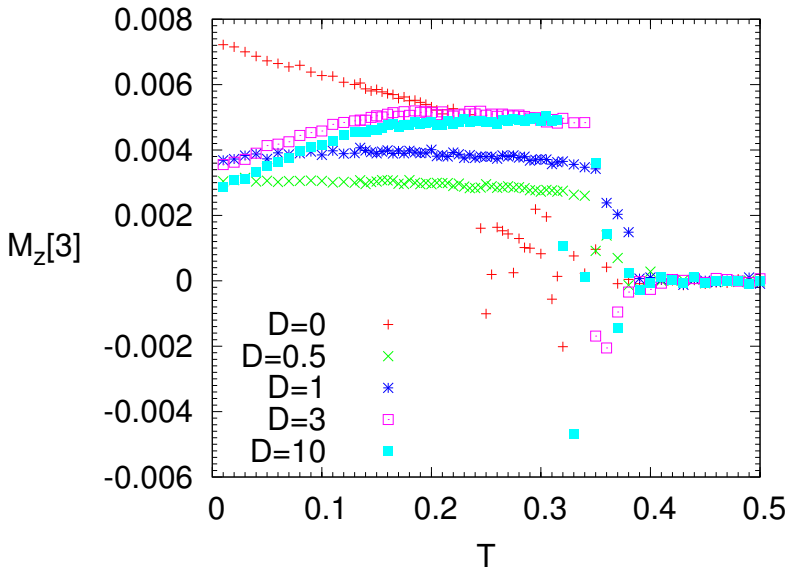

Figure 4.27: z component of the magnetization of the third layer (middle) of the thin films with 6 layers vs temperature.

4.4 Effect of lateral size

Figs. 4.28-4.31 shows the specific heat calculated in simulations for thin films with three and six layers and different lattice size in plane, and with MCS=10^6.

As can be seen the transition temperature is almost unchanged with varying lattice size for $L' > 12$. As expected, the height of curves rises as the size increases, since in the case of an infinite size system $C \to \infty$. Thus, using 18x18 for most of the results shown in this thesis should be reliable.

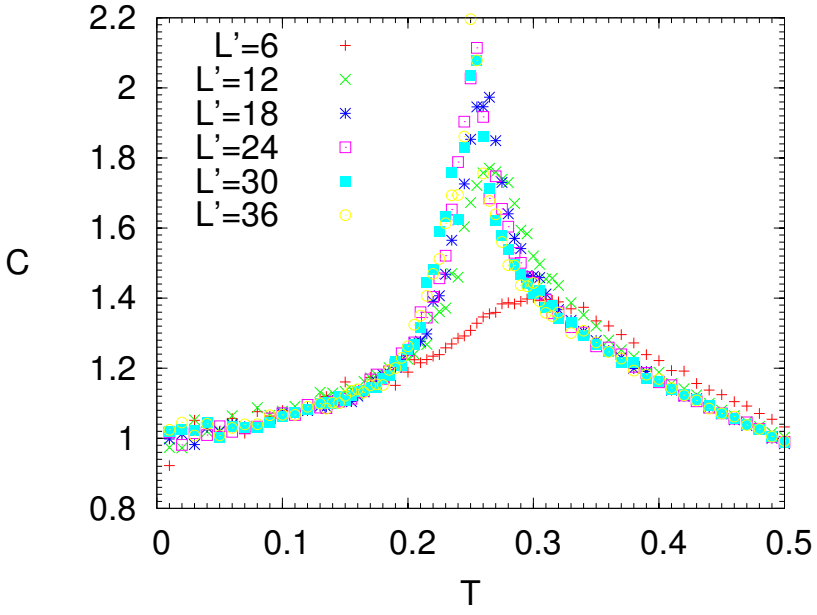

Figure 4.28: Specific heat for three-layer films vs temperature, with different in plane lattice sizes at $D = 0.1$.

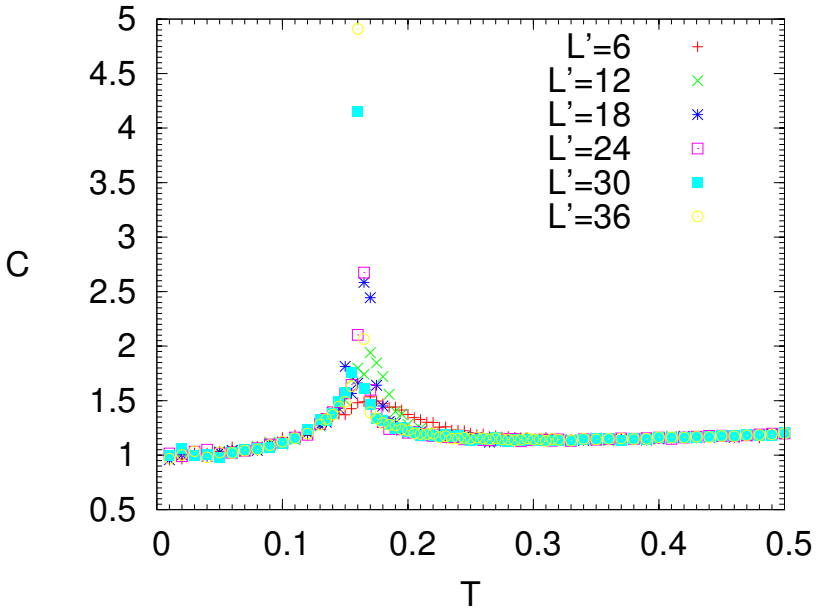

Figure 4.29: Specific heat for three-layer films vs temperature, with different in plane lattice sizes at $D = 3$.

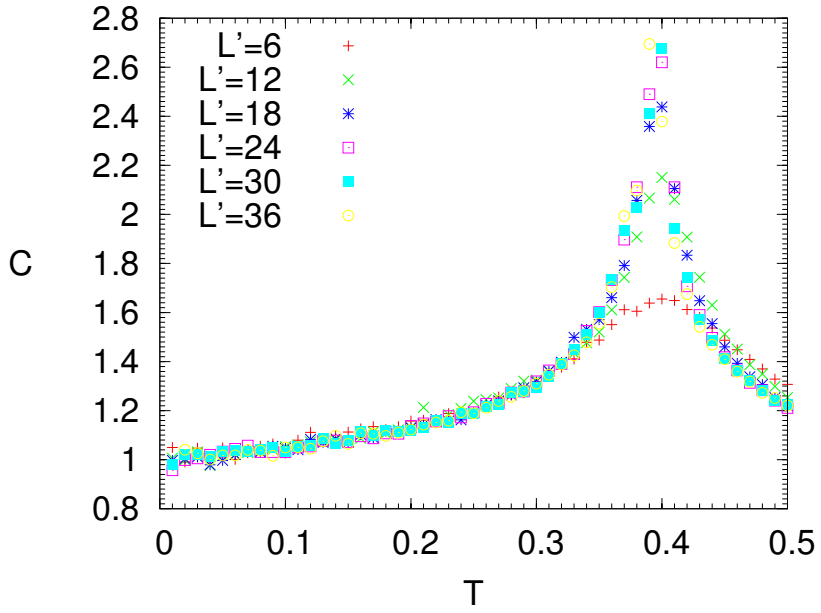

Figure 4.30: Specific heat for six-layer films vs temperature, with different in plane lattice sizes at $D = 0.1$.

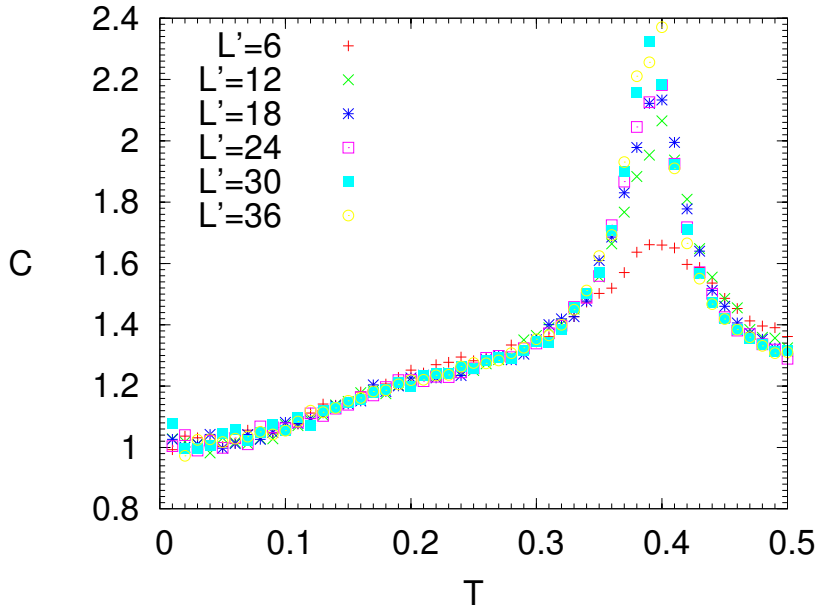

Figure 4.31: Specific heat for six-layer films vs temperature, with different in plane lattice sizes at $D = 3$.

Chapter 5

Simulations with Vacancies

In this chapter the effects of non-magnetic impurities randomly located on one of the surfaces of the thin films are investigated. This study is motivated by the fact that most magnetic thin films are fabricated with imperfections that mostly occur on the surface. It is not clear how to model the system Hamiltonian with these magnetic vacancies as they lead to broken plane symmetry at the surface. The first reason for this is that the lattice will be deformed, and not only on the surface. As well, even with the assumption of a perfect lattice structure, vacancy sites will differ from magnetic ones, which leads to a variation of local symmetry: magnetic ions can have a number of different neighbouring vacancies, and thus different magnetic symmetries. Thus, in general, an MCA term at sites with broken symmetry has the form

$$H_{MCA} = -D_1 S_x^2 - D_2 S_y^2 - D_3 S_z^2 - D_{12} S_x S_y - D_{13} S_x S_z - D_{23} S_y S_z + \\ + \textit{higher order terms}. \qquad (5.1)$$

However, for simplicity we assume here that the lattice structure is not deformed, and symmetry is the same for all the magnetic ions. The surface term $-DS_z^2$ is thus

used here, as before.

Results of MC simulations presented here were performed with cooling cycles for thin films with three and six layers with MCS=10^6 for different values of D, and for different fractions of non-magnetic ions on the surface, p, and do not include averaging over disorder. The size of the films in a plane is 18x18.

5.1 Three Layers

The specific heat per lattice site for the 3-layer films for three different fractions of vacancies $p = 0.01, 0.1$, and 0.2 is shown in Figs. 5.1– 5.3. With increasing p peaks becomes lower and broader, and sometimes it is hard to claim that there is a peak at all. The transition temperature estimated from the specific heat peaks as a function of vacancies fraction p is depicted on Fig. 5.4. A general trend of reducing the transition temperature is clearly seen, though deviations from the average are also substantial. The transition temperatures estimated in the same way from repeated MC runs (see Fig. 5.5) differ somewhat from Fig. 5.4. These results and those in Fig. 5.6, which show that values of the transition temperature are significantly scattered within small range of D for $p = 0.1, 0.2$, suggest that these deviations are due to different random arrangements of the vacancies. The decreasing of the transition temperature may be understood since magnetic bonds between lattice sites are reduced thus reducing the effective exchange interaction. Fig. 5.5 shows that T_N for some values of p at $D = 0.5$ and $D = 1$ are slightly larger (no more than 0.01) than those for $p = 0$ for the same D. This may be attributed to errors in estimating the transition temperature due to the finite size of the lattice (which can be expected to have a bigger impact

when vacancies are present). Also, the temperature step in the vicinity of the T_N for simulations, used for building these graphs, was taken 0.005, thus, the minimal error is about 0.003.

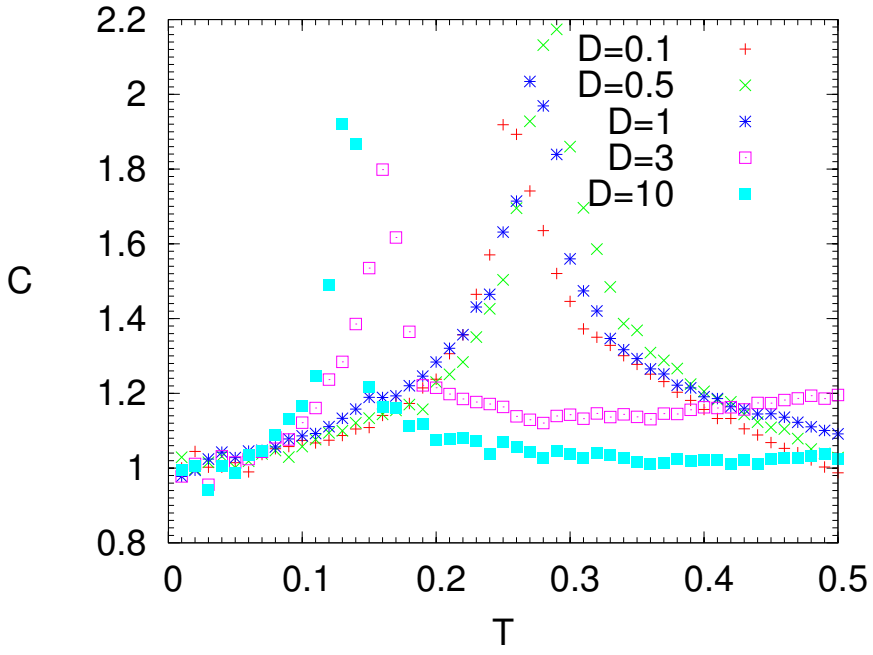

Figure 5.1: Specific heat vs temperature of the 3-layer films for $p = 0.01$.

The temperature dependence of the total magnetization per lattice node for different number of vacancies is depicted in Figs. 5.7– 5.9, and the total magnetization per lattice site at $T = 0.01$ as a function of p is depicted in Fig. 5.10.

Again, there is a general trend for decreasing the total magnetization as p increases with some substantial variations, which are likely due to different random arrangements of vacancies. The matter of interest is the projection of the magnetization onto the plane of a film, as increasing $M_{inplane}$ may facilitate EB in a magnetic field parallel to the plane of the film. Here, only graphs for this projection of the

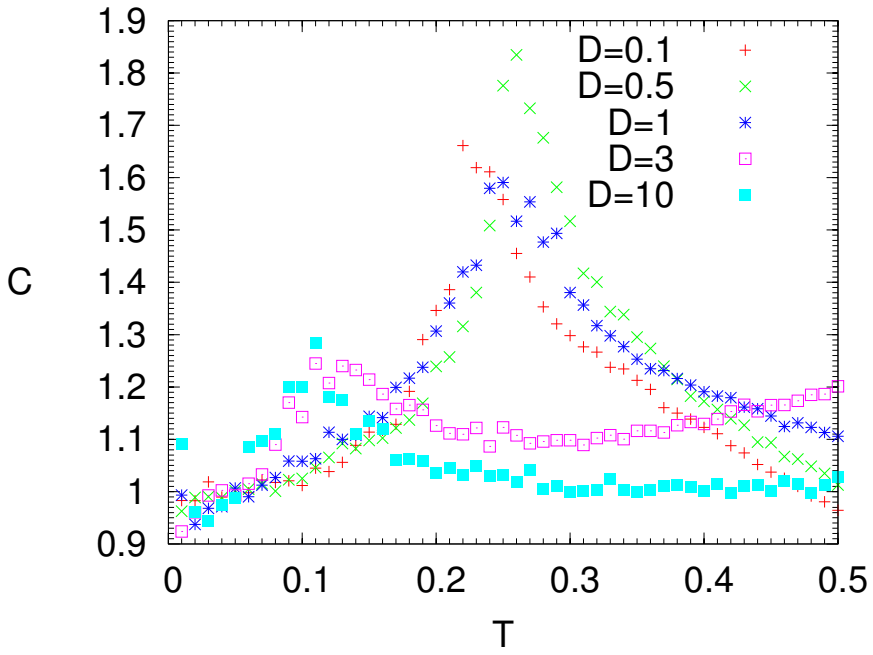

Figure 5.2: Specific heat vs temperature of the 3-layer films for $p = 0.1$.

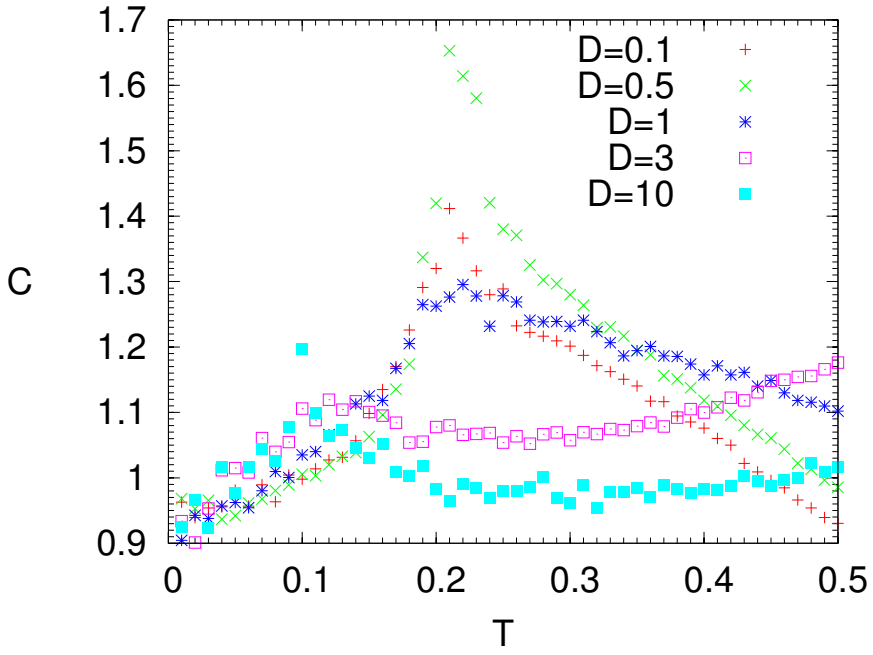

Figure 5.3: Specific heat vs temperature of the 3-layer films for $p = 0.2$.

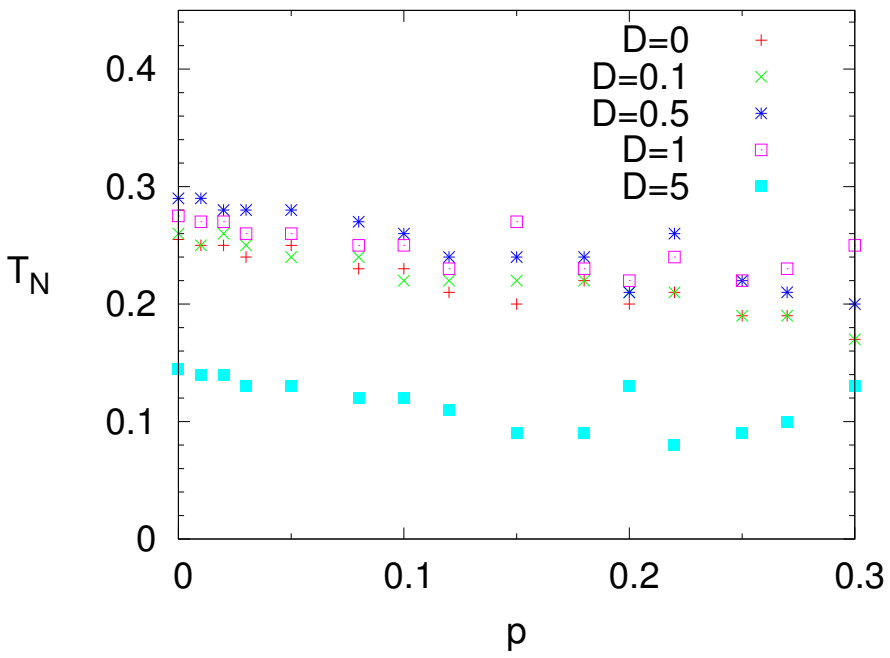

Figure 5.4: Transition temperature as a function of surface vacancy fraction p in the 3-layer films.

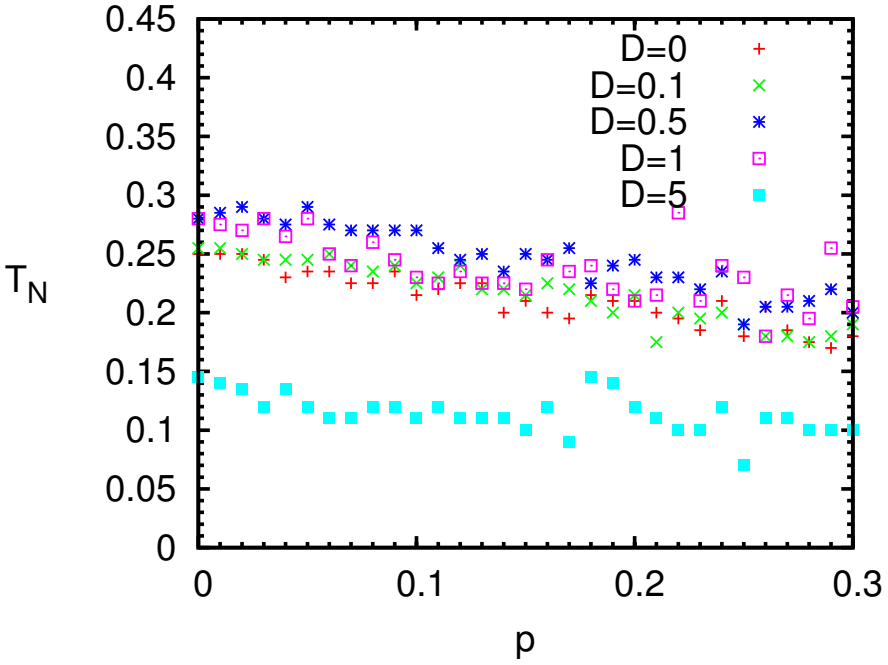

Figure 5.5: Transition temperature as a function of surface vacancy fraction p in the 3-layer films for a repeated set of simulations, as in Fig. 5.4.

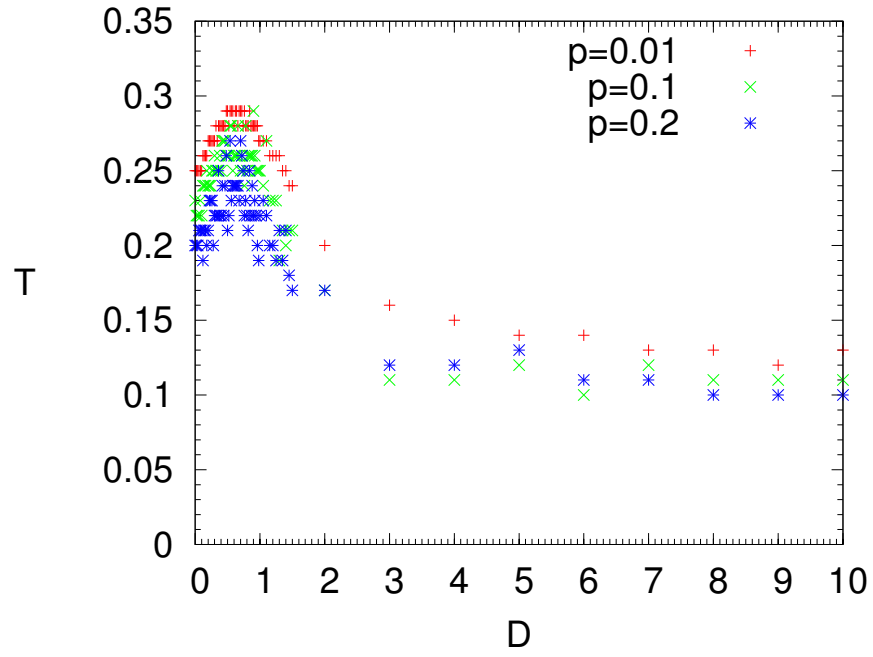

Figure 5.6: Transition temperature vs D of the 3-layer film for $p = 0.01, 0.1, 0.2$.

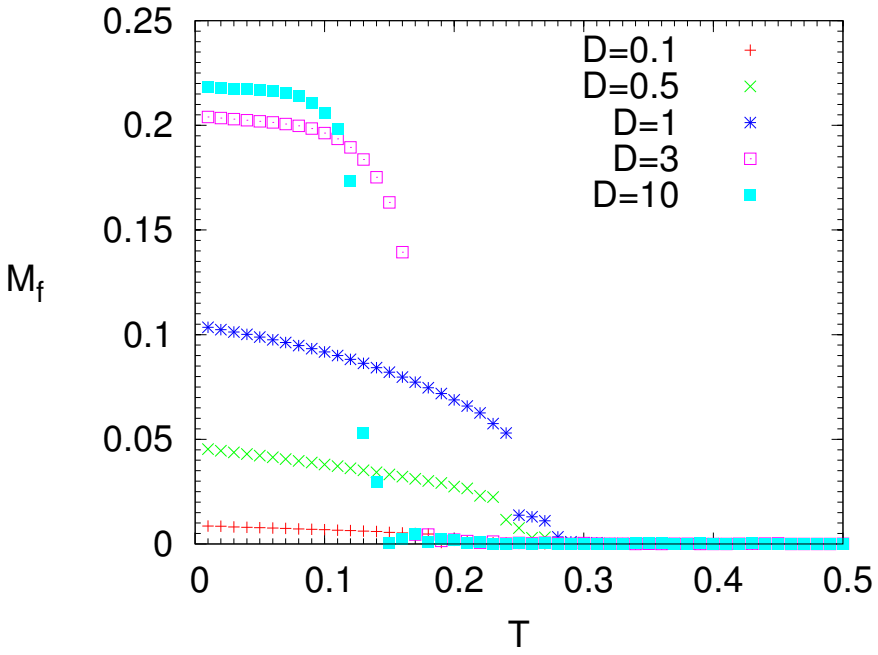

Figure 5.7: Total magnetization vs temperature of the 3-layer films for $p = 0.01$.

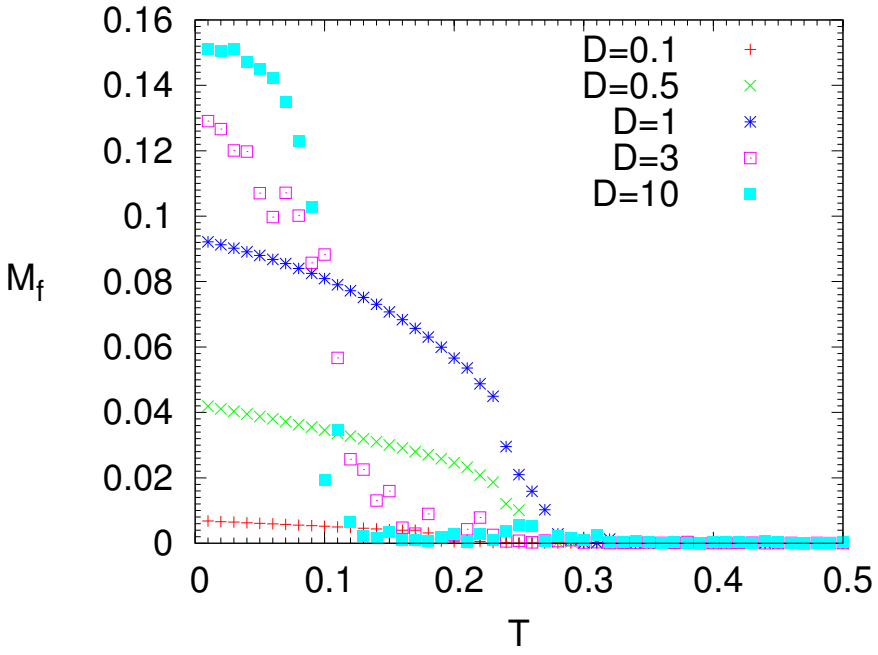

Figure 5.8: Total magnetization vs temperature of the 3-layer films for $p = 0.1$.

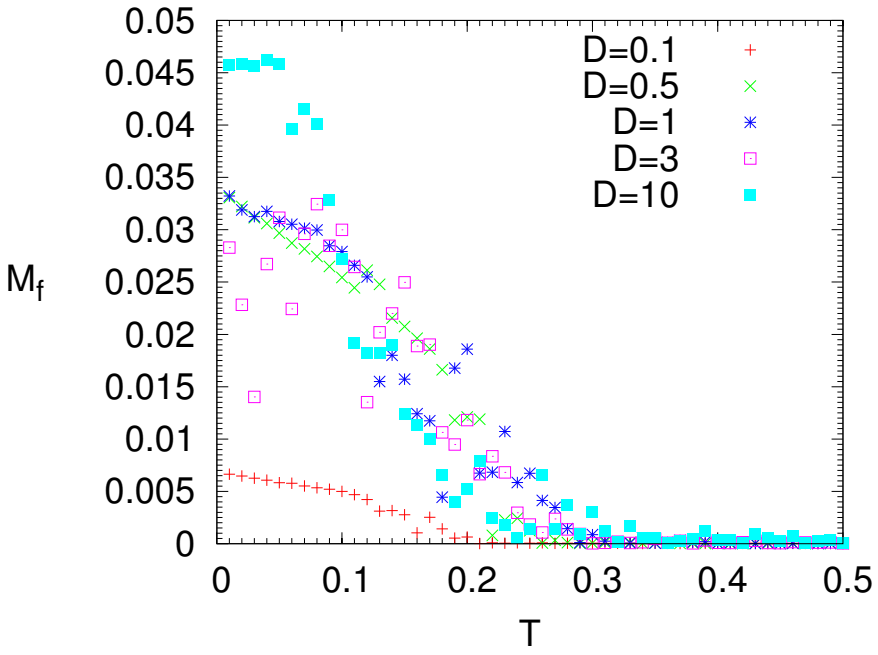

Figure 5.9: Total magnetization vs temperature of the 3-layer films for $p = 0.2$.

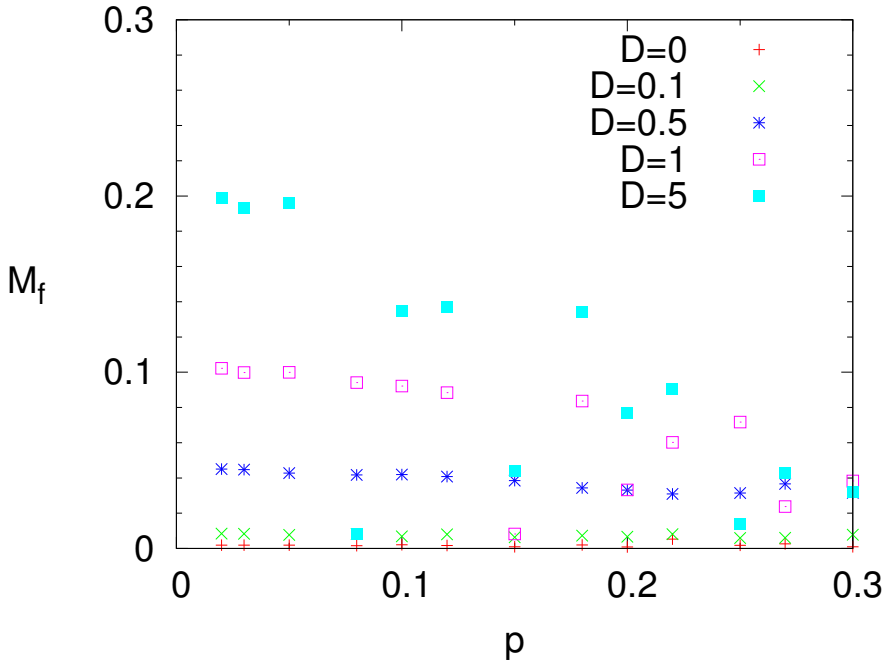

Figure 5.10: Total magnetization at $T = 0.01$ of the 3-layer films as a function of vacancy fraction.

magnetization of the surface layer with vacancies is shown (Figs. 5.11–5.14) as it is assumed that this layer will be in direct contact with a FM film.

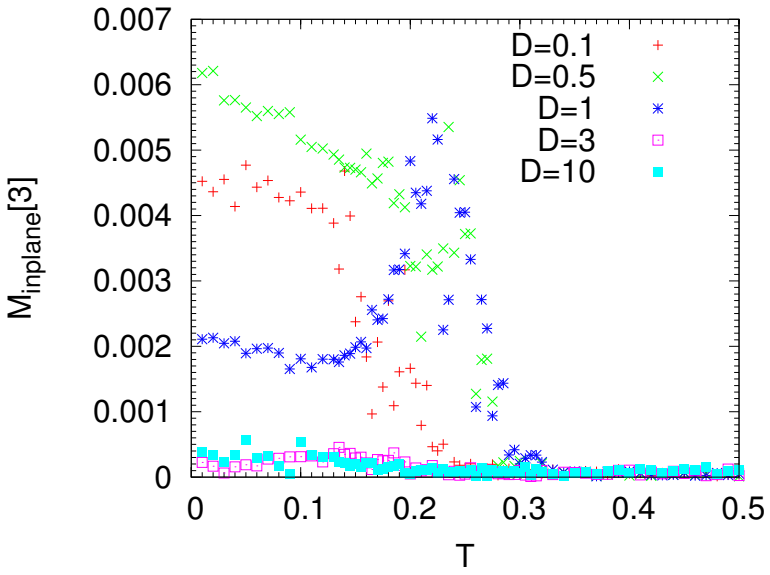

Figure 5.11: In-plane component of the magnetization of the third layer (with vacancies) vs temperature of the 3-layer films for $p = 0.1$.

It is seen from Fig. 5.14 that it is quite possible to get a larger in-plane component of the magnetization with a nonzero fraction of vacancies for any value of D than in the case of no vacancies, sometimes by a factor of three. Along with it, the supposed dependence on vacancies arrangement is again seen, and decreasing of the in-plane component is also possible. Values of $M_{inplane}$ are typically smaller for larger values of D, since in the case of large D spins tend to lie almost in a plane normal to the film.

Figure 5.15 shows the order parameter calculated by Eq. (4.4), and Fig. 5.16 shows the corresponding susceptibility, for $p = 0.15$. The transition temperatures estimated

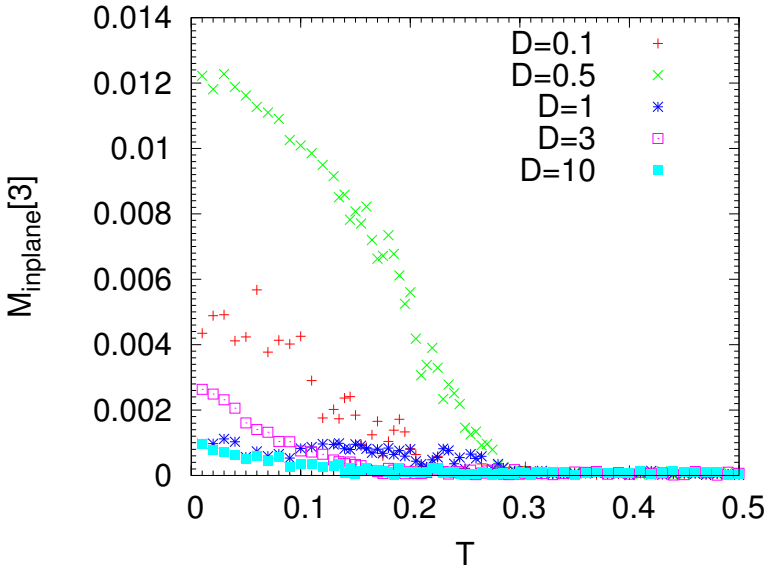

Figure 5.12: In-plane component of the magnetization of the third layer (with vacancies) vs temperature of the 3-layer films for $p = 0.2$.

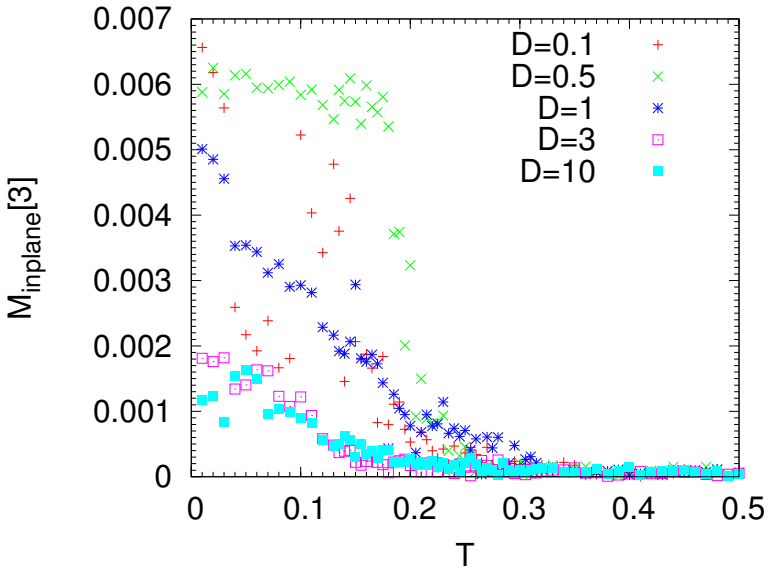

Figure 5.13: In-plane component of the magnetization of the third layer (with vacancies) vs temperature of the 3-layer films for $p = 0.3$.

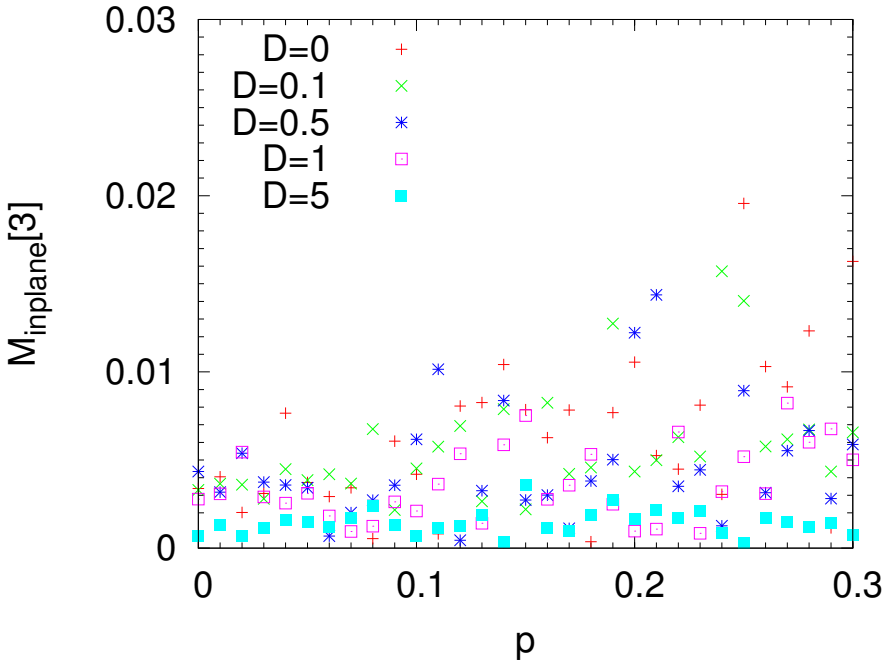

Figure 5.14: In-plane component of the magnetization of the third layer (with vacancies) at $T = 0.01$ of the 3-layer films as a function of p.

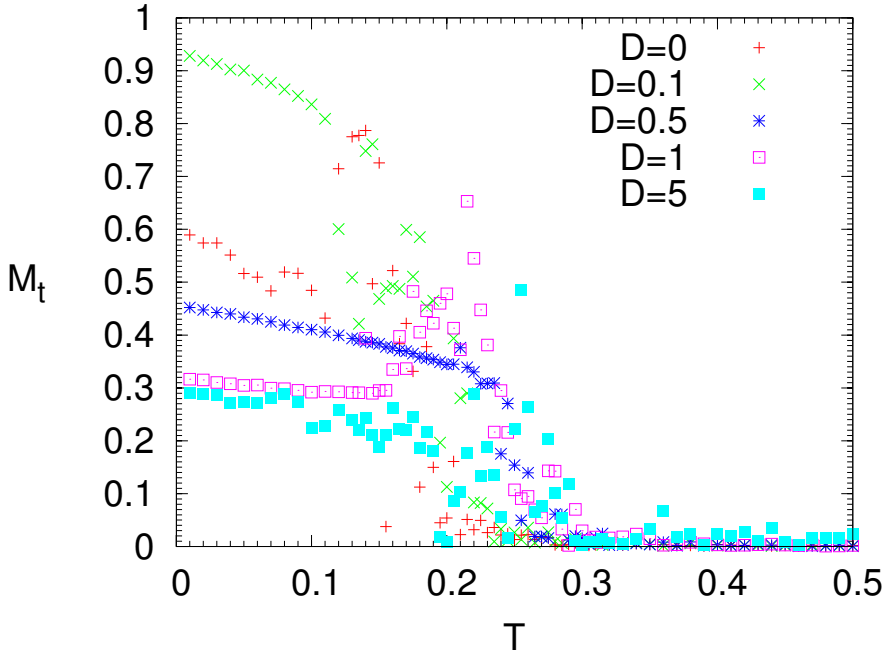

Figure 5.15: M_t vs temperature of the 3-layer films for $p = 0.15$.

from these results give values close to those obtained from the specific heat graphs, except for $D = 5$. For this value it is hardly possible to say that this is a good order parameter due to large scatter at high temperature.

To finish this section, an example spin structure at $T = 0.01$ and $D = 3$ for $p = 0.2$ is depicted in Fig. 5.17. This shows a significant influence of surface vacancies on the middle and the bottom layers. For example, the structure 'one spin up, two spins down' is broken at the bottom surface, spins pointed up may have neighbors which also point up, and in the middle layer spins point in more than these three directions.

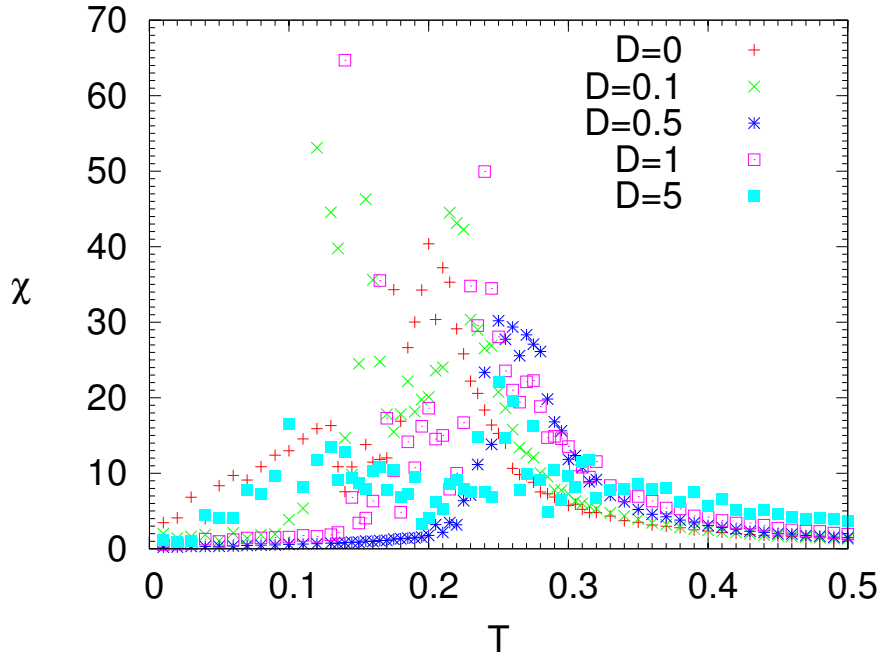

Figure 5.16: Susceptibility of M_t vs temperature of the 3-layer films for $p = 0.15$.

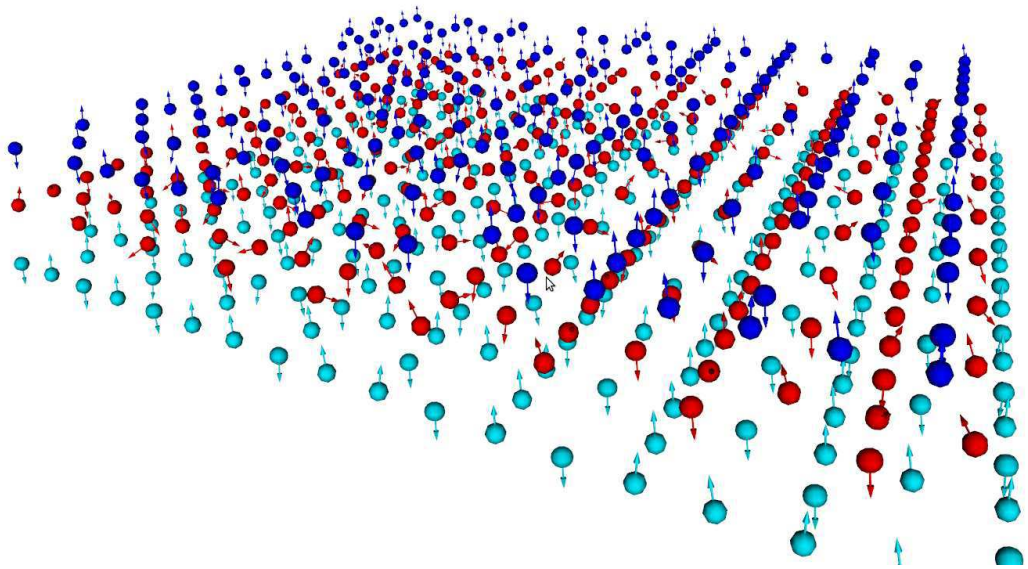

Figure 5.17: Spin structure at $T = 0.01$ of the 3-layer film with $p = 0.2$ at $D = 3$ and $T = 0.01$.

5.2 Six Layers

The specific heat per lattice site for the 6-layer films for different fractions of vacancies p is shown in Figs. 5.18–5.20. The transition temperature estimated from the specific heat peaks as a function of p is depicted in Fig. 5.21. In contrast with the case of three layers, the peaks in the specific heat graphs are always well formed. It also may be concluded that on average the transition temperature is reduced as p increases. However, this happens much slower, and is again accompanied by scattering of its values around the average. This is expected as at the same p, the overall fraction of vacancies in the case of 6 layers is smaller than in the 3-layer film. In Fig. 5.21 the line of points corresponding to $D = 5$ is interesting: For small fractions of vacancies there are values of T_N larger than in the case of no vacancies. In these simulations, the temperature step was 0.01, so the minimal error is about 0.005. However, the maximum difference in the T_N values is 0.02. This could be again attributed to finite size effects, however, this may also have another explanation. As previously mentioned, the large values of D hinder establishing long range order. While vacancies in general also hinder it, the presence of vacancies may reduce the significance of the D term in the Hamiltonian. This suggests that the vacancy effect of reducing the impact of anisotropy may be larger than the effect of hindering long range order.

The temperature dependence of the total magnetization per lattice node for different p is depicted in Figs. 5.22–5.24, and the total magnetization per lattice site is shown in Fig. 5.25. Again, in general, the total magnetization decreases as p increases, but slower than in the case of 3 layers. And the variations from average are much smaller than in the case of 3 layers.

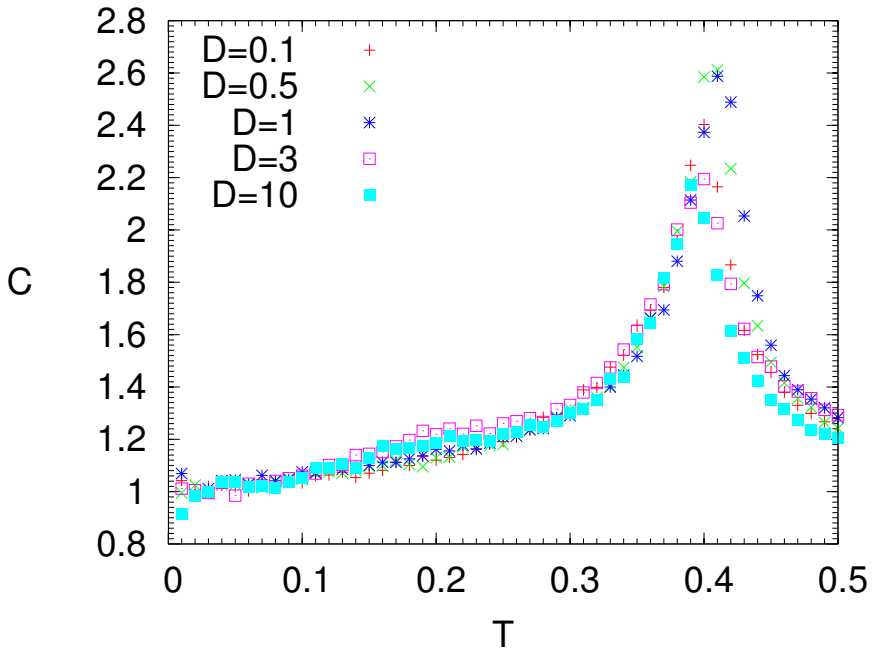

Figure 5.18: Specific heat per spin of the 6-layer films vs temperature for $p = 0.01$.

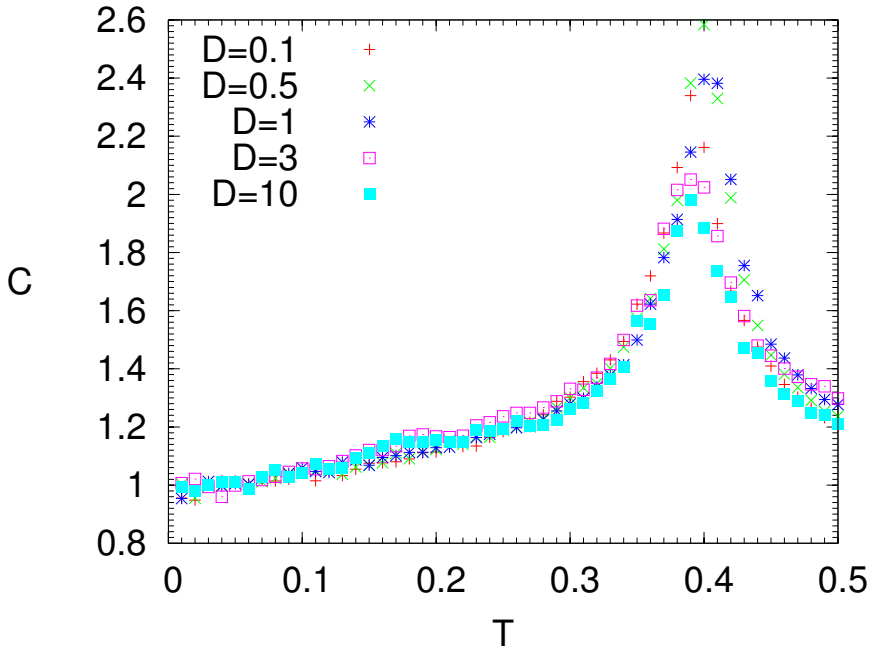

Figure 5.19: Specific heat per spin of the 6-layer films vs temperature for $p = 0.1$.

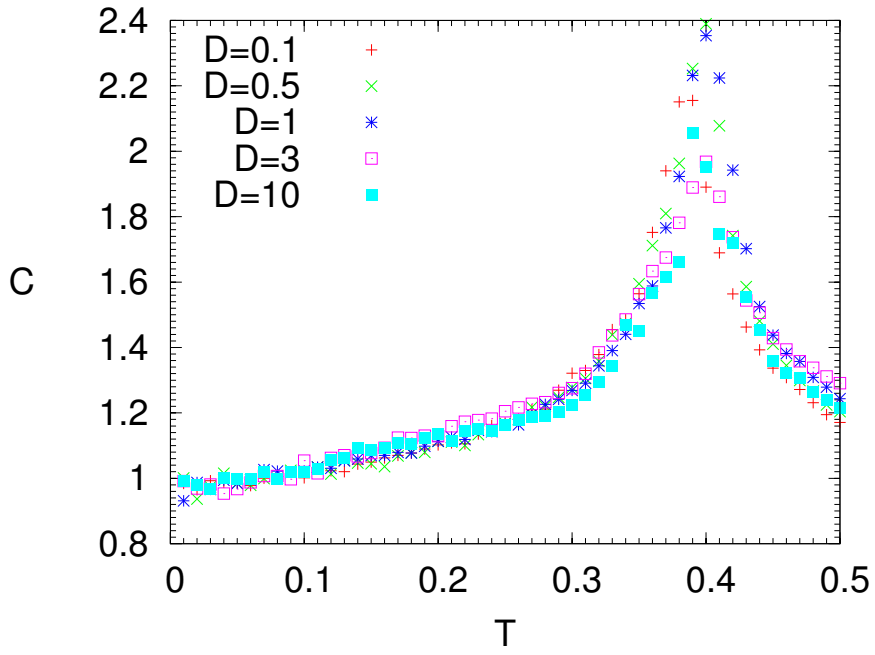

Figure 5.20: Specific heat per spin of the 6-layer films vs temperature for $p = 0.2$.

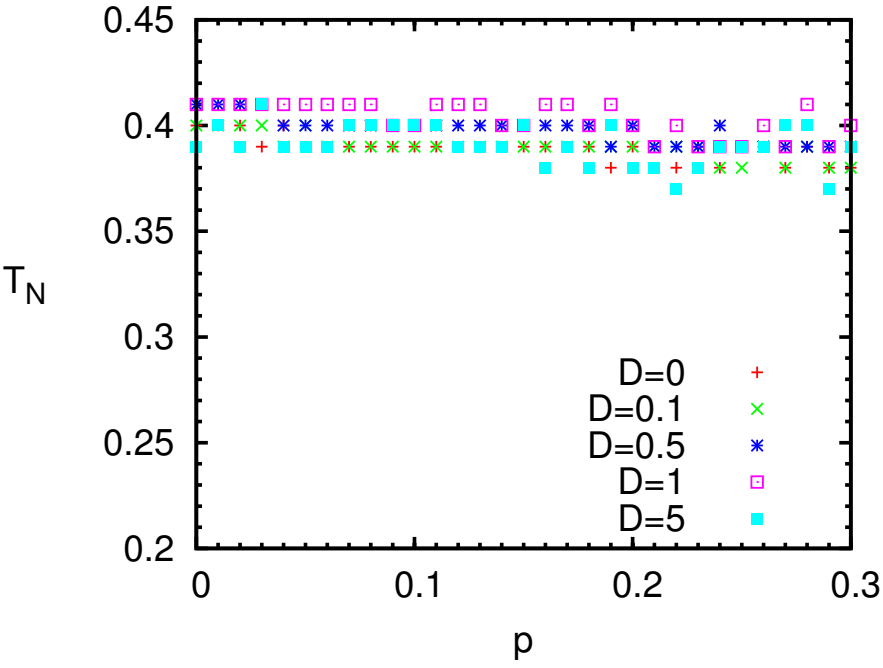

Figure 5.21: Transition temperature as a function of surface vacancy fraction p in the 6-layer films.

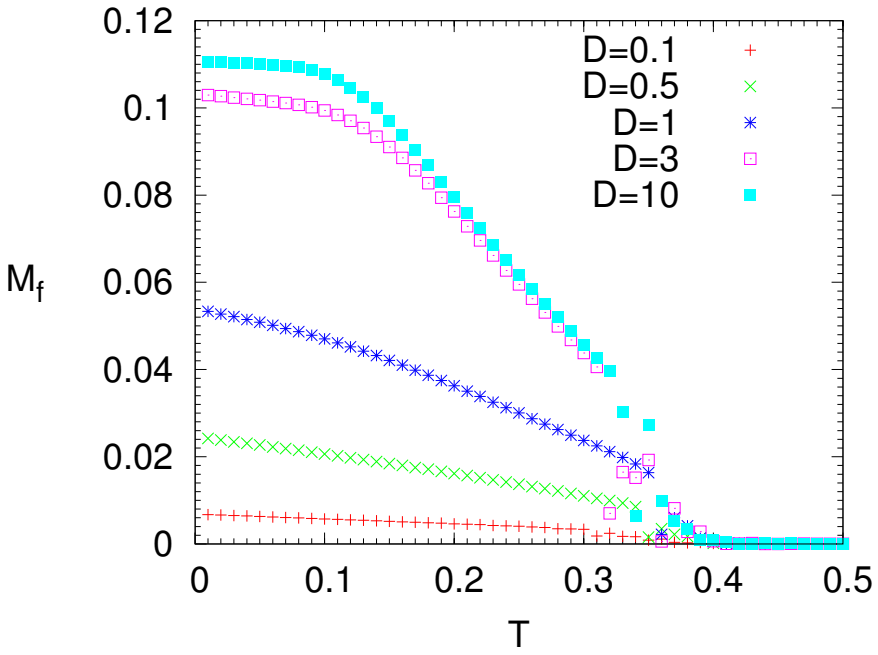

Figure 5.22: Total magnetization of the 6-layer films vs temperature for $p = 0.01$.

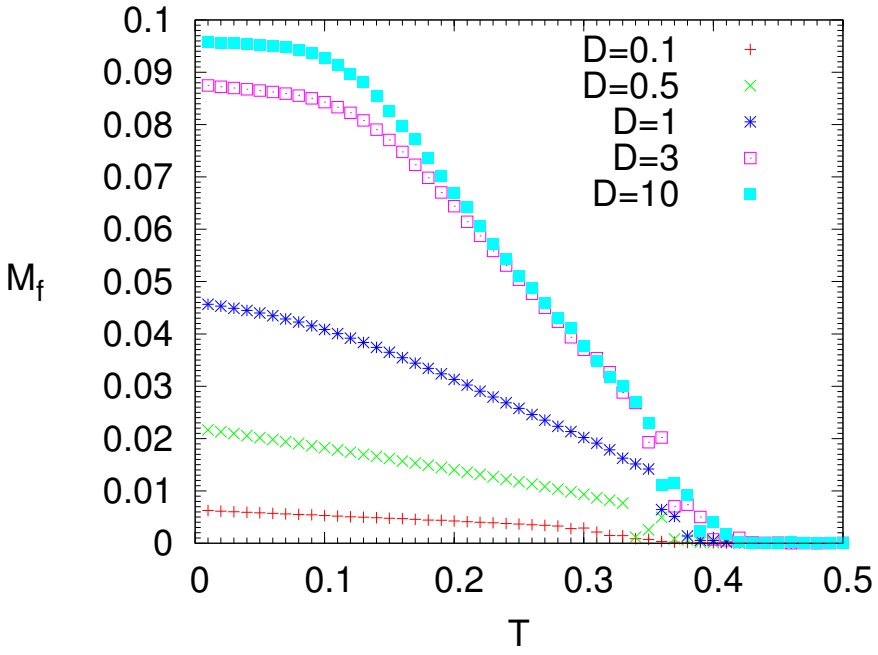

Figure 5.23: Total magnetization of the 6-layer films vs temperature for $p = 0.1$.

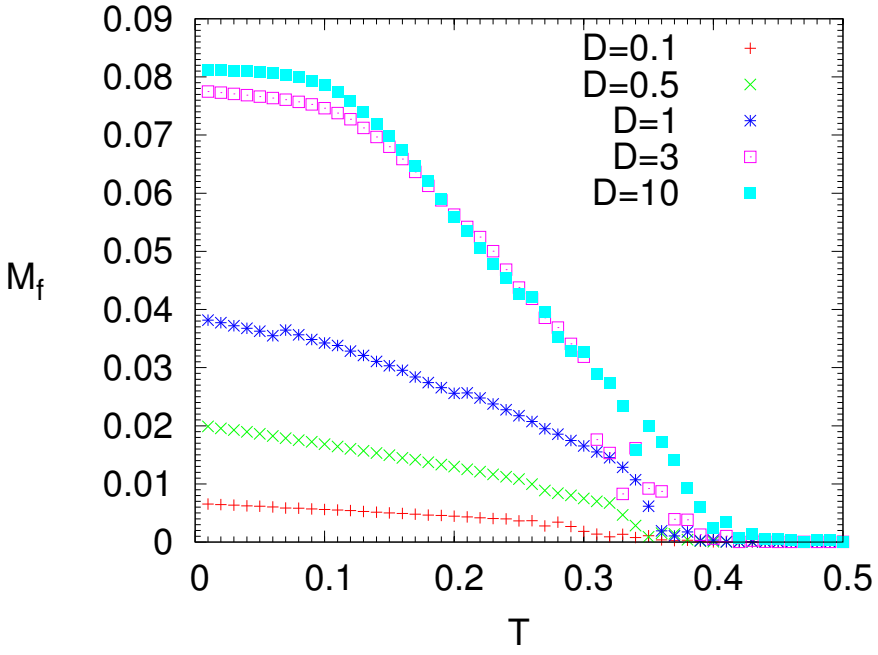

Figure 5.24: Total magnetization of the 6-layer films vs temperature for $p = 0.2$.

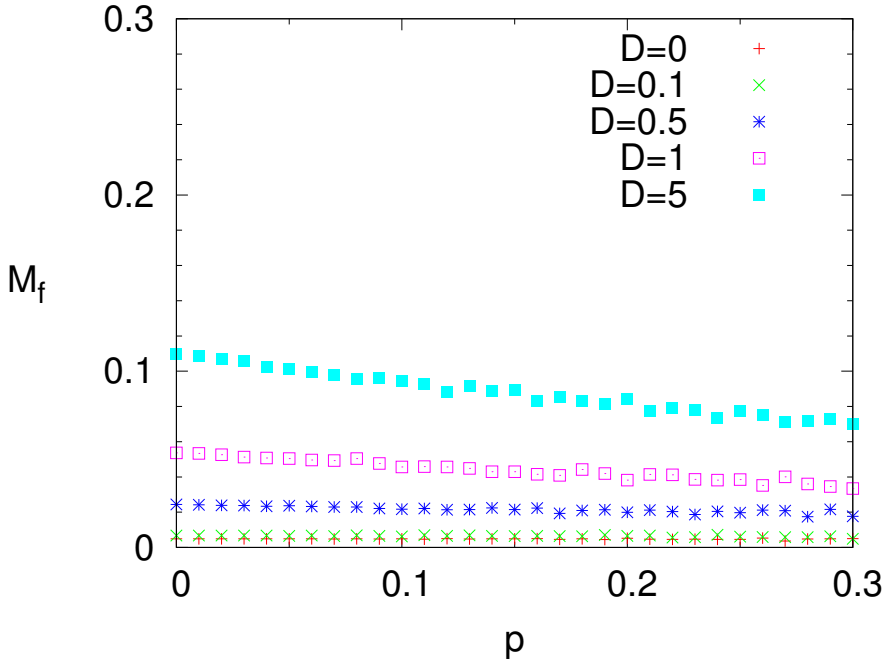

Figure 5.25: Total magnetization of the 6-layer films as a function of p at $T = 0.01$.

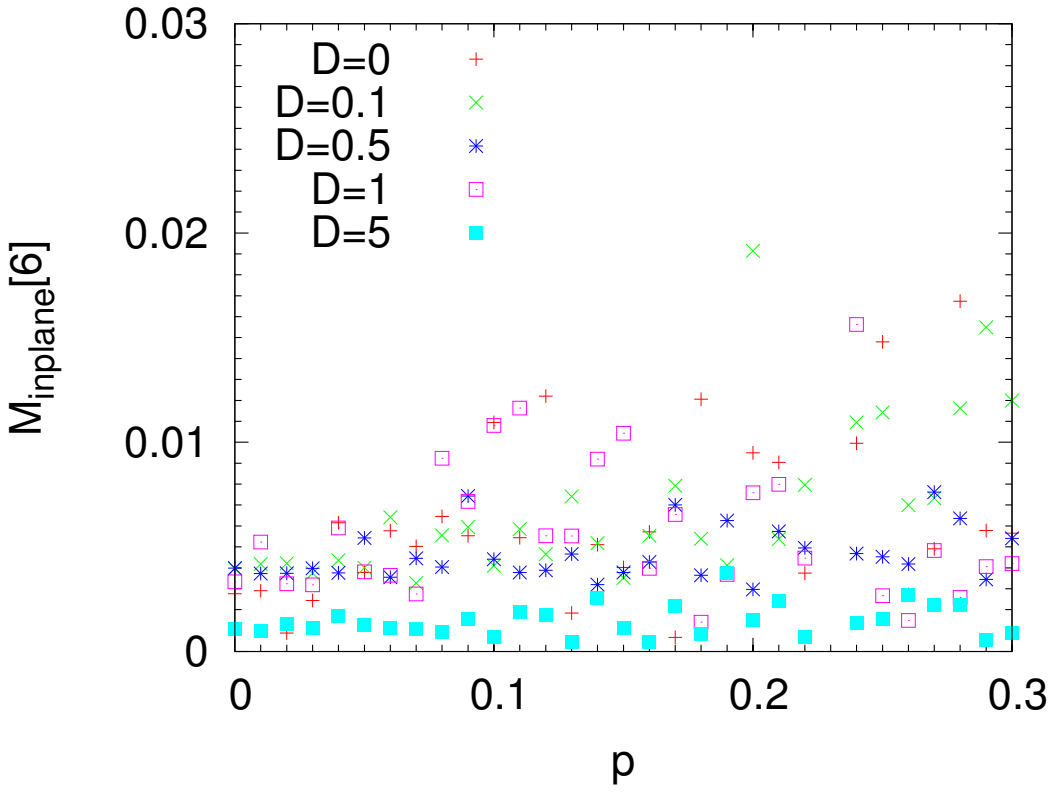

Figure 5.26: In-plane component of the magnetization of the sixth layer (with vacancies) of the 6-layer films as a function of p.

The dependence of the projection of the magnetization of the surface with vacancies onto the plane of the films as a function of vacancy fraction p at $T = 0.01$ (shown in Fig. 5.26) exhibits a possible increasing of its value with increasing p, as in the three-layer case.

To finish this section, a spin structure at $T = 0.01$ for $p = 0.2$ is depicted in Fig. 5.27. Unlike the case of the 3-layer film, the structure of the middle and the bottom surface layer is not significantly influenced by vacancies (at the top surface) and visually is almost the same as in the case without vacancies.

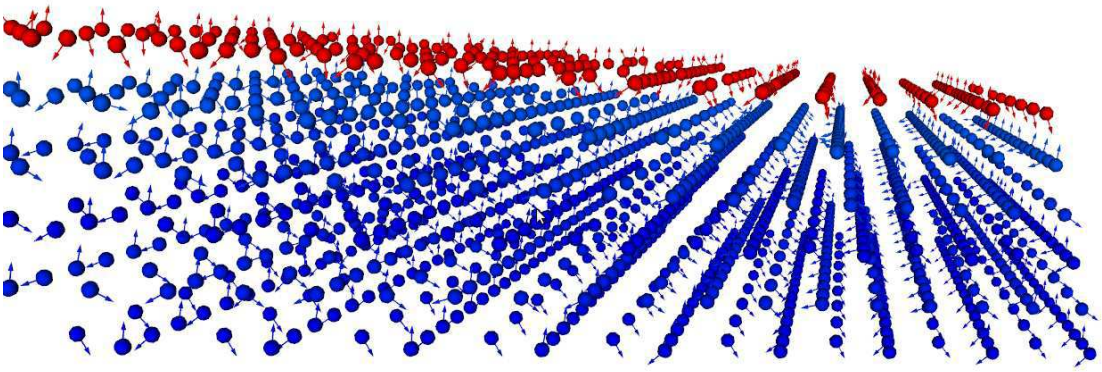

Figure 5.27: Spin structure of the 6-layer film with $p = 0.2$ at $D = 1$ and $T = 0.01$.

Chapter 6

Conclusions and Future Work

6.1 Conclusions

As a prelude to the study of exchange bias phenomena in a model of thin-film $IrMn_3$, classical Metropolis Monte Carlo (MC) simulations have been performed on three and six ABC stacked kagome layers. The spin structure at the surface and in the middle layers was examined as a function of axial surface anisotropy (D) which differs from the cubic anisotropy of the middle layers. The impact of the D surface term on the specific heat, susceptibility, magnetization and order parameter, for both surface and middle layers, was calculated. In addition, non-magnetic vacancies were introduced on the surface layer and shown to reduce the transition temperature as well as induce a small in-plane magnetization.

The presence of the D term in the Hamiltonian leads to a lifting of degeneracy from eight-fold cubic (in the case of the bulk material) to six-fold axial. The ground state spin configurations can be classified based on three (111) planes: $(11\bar{1})$, $(1\bar{1}1)$,

and $(\bar{1}11)$; where spins tend to lie when $D \to 0$. Opposite to the bulk case, spins in the plane (111) do not occur as there would be a large angle between surface spins and D easy axis, which is energetically unfavorable. Spin configurations in the middle layers are close to the bulk $q = 0$ state for all values of D, while on the surfaces the spin configuration becomes closer to Ising type as D increases.

A C++ MC code (see App. A) was constructed and checked by reproducing the previously obtained results for the bulk case. Additionally, the low temperature spin configuration given by MC simulations is very close to the ground state obtained from the $T = 0$ effective field method. As expected, the transition temperature is reduced compared to the bulk case. For $D = 0$, the transition temperatures for 3-layer films and 6-layer films, and bulk $IrMn_3$, are about 0.25, 0.41, and 0.52, respectively. There is a peak in transition temperature at about $D = 1$, which is well pronounced for very thin films. In the case of the film with 3 layers the surface anisotropy for large D ($\gtrsim 1$) leads also to a broad high T shoulder, which is considered as the Schottky anomaly effect.

It is shown that for the six layer case, as distinct from the three layer case, the presence of the surface and the variation in the strength of the surface anisotropy leads to a relatively small change in the value of T_N from the bulk and is relatively insensitive to value of D. In addition, the magnetic structure of the interior layers is qualitatively very similar to the of the bulk material described in [3]. This leads us to suppose that magnetic structure of thicker films would lead to qualitatively similar results, with a spin structure in the interior layers and a value for T_N close to that of the bulk material combined with a surface magnetization similar to that obtained in the current calculation and exhibiting the same dependence on the value of D.

One of the most striking features of the six layer MC calculations presented in Ch.4 is that a moderate to large value of the surface anisotropy parameter D induces a ferrimagnetic arrangement of the spins on the surface of the film with a net magnetization directed perpendicular to the film. The results of these simulations therefore imply that a perpendicular surface single ion anisotropy on $IrMn_3$ would induce a robust surface magnetization, that persists up to T_N, while the interior of the film remains antiferromagnetic with no net magnetization. This suggests a new mechanism for EB that is unique to the fcc kagome structure of $IrMn_3$. To what extent this is relevant to the pinning mechanism in current spin valves is not all obvious. For example, the fact that the surface magnetization is perpendicular to the surface means that a simple exchange coupling between the $IrMn_3$ and the planar ferromagnetic Co layer would not produce exchange bias in the parallel field. However, the more complex coupling (e.g. Dzyaloshinskii-Moriya [31, 32]) could result in a coupling between an fcc kagome lattice and a planar ferromagnet. There is a study [33] which shows that Dzyaloshinskii-Moriya interactions may lead to the exchange bias in the $IrMn_3$/Co heterostructure in the magnetic field perpendicular to the interface. In this work it was assumed that the spins in AF lie parallel to the interface, and spins in Co are perpendicular to it.

MC simulations of the thin films with vacancies at the top layer were also performed. It is noted that the model for these simulations may be considered only as a zeroth order approximation to real films and may be quite crude. As expected, for thinner films the influence of vacancies is more significant. In the case of the 3-layer films, the presence of vacancies leads to substantial changes of the spin structure in all layers, while in the case of the 6-layer films this is not the case. The transition

temperature and the total magnetization decreases as the number of vacancies increases. However, in the case of 3-layer films there are significant deviations from this general trend. This is supposed to be due to different random arrangements of vacancies. Unexpectedly, the magnetization projection onto the plane of the film may increase several fold, but remains small. The study of the vacancies effect requires further simulations in order to more accurately determine their impact on these thin films.

6.2 Future Work

The model utilized in this project does not include dipole-dipole interactions, and the two-site anisotropic exchange interactions are merged with the bulk MCA (K-term) into the effective Hamiltonian. Studying a more rigorous model with distinct two-site and on-site cubic MCA terms, and including dipole-dipole and next nearest neighbours exchange interactions may be a matter of interest. A more thorough study and analysis for the case with vacancies on the surface is needed: MC simulations of films with larger lateral size supplemented with the effective field method calculations will be more convincing, and studying the effect of different vacancies arrangement is desirable. Vacancies in the middle layer also may be considered.

Finally, and most importantly, simulations of FM/AF coupling is required to examine exchange biasing.

Bibliography

[1] R.Moessner and A.P. Ramirez. *Physics Today*, 59(2):24, 2006.

[2] V. Hemmati, M. L. Plumer, J. P. Whitehead, and B. W. Southern. *Phys. Rev. B*, 86:104419, 2012.

[3] M. D. LeBlanc, M. L. Plumer, J. P. Whitehead, and B. W. Southern. *Phys. Rev. B*, 88:094406, 2013.

[4] Stephen Blundell. *Magnetism in Condensed Matter*. Oxford University Press, first edition, 2009.

[5] N.W. Ashcroft and N.D. Mermin. *Solid State Physics*. Thomson Learning, first edition, 1976.

[6] L.D. Landau and E.M. Lifshitz. *Electrodynamics of Continuous Media*. Pergamon, first edition, 1960.

[7] P.Bruno. *Physical origins and theoretical models of magnetic anisotropy, in "Magnetismus von Festkörpern und grenzflächen"*. edited by P.H. Dederichs, P. Grnberg, and W. Zinn, 24. IFF-Ferienkurs, pp. 24.1-24.28, Forschungszentrum Jlich, 1993.

[8] S.T. Bramwell. *J. Phys.:Condens. Matter*, 2:7527, 1990.

[9] A. P. Ramirez, A. Hayashi, R. J. Cava, R. Siddharthan, and B. S. Shastry. *Nature*, 399:333, 1999.

[10] R.K. Pathria. *Statistical Mechanics*. Butterworth-Heinemann, second edition, 1996.

[11] W.H. Meiklejohn and C.P. Bean. *Phys. Rev.*, 105(3):904, 1957.

[12] M. Kiwi. *Journal of Magnetism and Magnetic Materials*, 234:584, 2001.

[13] J. Nogués and Ivan K. Schuller. *Journal of Magnetism and Magnetic Materials*, 192:203, 1999.

[14] D. Mauri, H. C. Siegmann, P. S. Bagus, and E. Kay. *J. Appl. Phys.*, 62:3047, 1987.

[15] A. P. Malozemoff. *Phys. Rev. B*, 35:3679, 1987.

[16] N. C. Koon. *Phys. Rev. Lett.*, 78:4865, 1997.

[17] T. C. Schulthess and W. H. Butler. *Phys. Rev. Lett.*, 81(20):4516, 1998.

[18] M.E.J. Newman and G.T. Barkema. *Monte Carlo Methods in Statistical Physics*. Oxford University Press, first edition, 2001.

[19] N.Metropolis, A.W. Rosenbluth, M.N. Rosenbluth, A.H. Teller, and E.Teller. *J. Chem. Phys.*, 21(6):1087, 1953.

[20] A.B. Harris, C. Kallin, and A.J. Berlinsky. *Phys. Rev. B*, 45(6):2899, 1992.

[21] J.T. Chalker. *Geometrically Frustrated Antiferromagnets: Statistical Mechanics and Dynamics in Introduction to Frustrated Magnetism*. Springer, 2011.

[22] J. T. Chalker, P. C. W. Holdsworth, and E. F. Shender. *Phys. Rev. Lett.*, 68:855, 1992.

[23] Chen Zeng and Veit Elser. *Phys. Rev. B*, 42(13):8436, 1990.

[24] J. B. Marston and C. Zeng. *J. Appl. Phys.*, 69(8):5962, 1991.

[25] D. A. Garanin and Benjamin Canals. *Phys. Rev. B*, 59(1):5962, 1999.

[26] A. Kohn, A. Kova, R. Fan, G. J. McIntyre, R. C. C. Ward, and J. P. Goff. *Scientific Reports*, 45(6):2899, 2013.

[27] L. Szunyogh, B. Lazarovits, L. Udvardi, J. Jackson, and U. Nowak. *Phys. Rev. B*, 79(2):020403, 2009.

[28] I. Tomeno, H.N. Fuke, H. Iwasaki, M. Sahashi, and Y. Tsunoda. *J. Appl. Phys.*, 86(7):3853, 1999.

[29] L. R. Walker and R. E. Walstedt. *Phys. Rev. B*, 22(8):3816, 1980.

[30] P. J. Jensen and K. H. Bennemann. *Surface Science Reports*, 61:129, 2006.

[31] I. Dzyaloshinskii. *J. Phys. Chem. Solids*, 4:241, 1958.

[32] T. Moriya. *Phys. Rev.*, 120:91, 1960.

[33] R. Yanes, J. Jackson, L. Udvardi, L. Szunyogh, and U. Nowak. *Phys. Rev. Lett.*, 111:217202, 2013.

Appendix A

C++ Code for Monte Carlo Simulations

```
//Heisenberg Model for ABC stacked kagome layers (thin film) with vacancies on the top surface
#include <iostream>
#include <math.h>
#include <stdlib.h>
#include <time.h>
#include <stdio.h>
#include <fstream>
#include <string>
#include <sstream>
#include <ctime>
#include "MersenneTwister.h" //contains Mersenne-Twister random generator
#define SQ3 sqrt(3)
#define SQ2 sqrt(2)
#define SQ6 sqrt(6)
using namespace std;
int row,col,hei; // number of rows, columns in a layer, and layers
int t=0;
int N_dots; // number of spins
int j;
int N_uneq; //number of MCS discarded for equilibration
double ***Sx,***Sy,***Sz; //these array contain coordinates of spins
// MAx means x component of the magnetization of the sublattice A, Mx - x component of the total magnetization, etc.
double *MAx,*MAy,*MAz, *MBx,*MBy,*MBz, *MCx,*MCy,*MCz, *Mx,*My,*Mz, *M, *average_M;
double T0=0,T, fi_new, Sx_new, Sy_new, Sz_new;//T0 - initial temperature,
double En,Ma,average_E,average_E2,average_MT,average_MT2, average_MA,average_MA2, average_MB,average_MB2, average_MC,average_MC2, average_MOp,average_MOp2;
string outfile;
```

```
double average_MOp_2,average_MOp2_2; // MOp - order parameter
ofstream Res1_file, StructureHT, StructureT0;
MTRand r; //declaration of the random number r
double J,D,K,B;//J - exchange interaction constant; D - surface anisotropy constant; K - cubic anisotropy constant;  B - magnetic induction
const double k_B=1;//Boltzman constant is taken to be 1
const double dT=0.01,Pi=3.14159265359;//dT - temperature step; Pi is Pi
//MOp_2 - order parameter for the thin film, MOp - order parameter for the 3D case, T in MAxt (and etc.) stands for total
double MAxT,MAyT,MAzT, MBxT,MByT,MBzT, MCxT,MCyT,MCzT, MxT,MyT,MzT, MAT,MBT,MCT, MT, MOp, MOp_2;
double MBulk, MSurf; //M of the interior and the surface, respectively
double average_EBulk,average_EBulk2,average_ESurf,average_ESurf2,average_MBulk,average_MBulk2,average_MSurf,average_MSurf2;
double average_Mx[30],average_My[30],average_Mz[30],MxBulk,MyBulk,MzBulk,MxSurf,MySurf,MzSurf;
double EBulkn,ESurfn;
double average_MTz,average_MBulkz,average_MSurfz; //z component of magnetizations
double MOpLayer[10], MA[10], MB[10], MC[10], average_MOpLayer[10];
double average_MOpLayer2[10], average_ELayer[10], average_E2Layer[10];
double ***avSx,***avSy,***avSz;
double p;
double *MxTl, *MyTl, *MzTl;
ostringstream oss;
string s;
int Nvac1;
double MTinplane;
double *Minplane;// inplane component of M
double newaverage_MOp_2, newaverage_MOpLayer[10], av_MA[10],av_MB[10], av_MC[10];
double average_MAx[10],average_MAy[10],average_MAz[10], average_MBx[10],average_MBy[10],average_MBz[10], average_MCx[10],average_MCy[10],average_MCz[10];

void Init_str(int row, int col, int hei)  // initializing spin configuration at high T
{
double r1,r2,fi0=Pi/6.,fi;
int i1,j1;
    for (int k=1;k!=hei+1;++k)
  for (int i=1;i!=row+1;++i)
  for (int j=1;j!=col+1;++j)
      {
r1=r.rand();r2=r.randExc();

Sz[i][j][k]=2.0*r1-1.0;
Sx[i][j][k]=sqrt(1-Sz[i][j][k]*Sz[i][j][k])*cos(2*Pi*r2);
Sy[i][j][k]=sqrt(1-Sz[i][j][k]*Sz[i][j][k])*sin(2*Pi*r2);

if ( (((i%2)==0)&&((j%2)==0)&&((k%2)==1)) || (((i%2)==1)&&((j%2)==1)&&((k%2)==0)) )
          {Sx[i][j][k]=0; Sy[i][j][k]=0; Sz[i][j][k]=0;}
       }
        for (int i=1;i!=row+1;++i)  // 0th layer consist of 0-length spins, it is used for 0 boundary conditions
  for (int j=1;j!=col+1;++j)
      {
Sz[i][j][0]=0;
Sx[i][j][0]=0;
```

```
Sy[i][j][0]=0;
       }
}
void Vacancies(double p) // setting vacancies on the top layer
{
    int NinL=row*col;   //number of nodes in the kagome layer
    int Nvac;
    Nvac=floor(3.0/4.0*NinL*p+0.5); //number of vacancies
    int V[Nvac+1];
    int f;
    int nr,nc;

    ofstream VacOutfile; // creating a file with vancancy positions
    string VacFile;
    VacFile="VacPositions"+s+".txt";
    VacOutfile.open(VacFile.c_str());
    VacOutfile<<"Vacancies Positions"<<"\n"<<"row"<<"\t"<<"col"<<endl;
    cout<<"Nvac="<<Nvac<<endl;
    V[0]=-1;
    for (int i=1;i<=Nvac;i++)  //choosing vacancy positions randomly
        {
         f=1; // flag, if in the end of the next cycle it is 0 this mean that the picked position was already occupied with zero spin
         while (f) {V[i]=r.randInt(NinL-1)+1;f=0; cout<<i<<"\t"<<V[i]<<endl;
             nc=V[i]%row; nr=V[i]/row+1; if (nc==0) {nc=col;nr=nr-1;}
         VacOutfile<<"nr="<<nr<<"\t"<<"nc="<<nc<<endl;
         if ( (Sx[nr][nc][hei]==0)&&(Sy[nr][nc][hei]==0)&&(Sz[nr][nc][hei]==0)) {f=1;} {Sx[nr][nc][hei]=0; Sy[nr][nc][hei]=0; Sz[nr][nc][hei]=0;}
         }
         cout<<"nr="<<nr<<"\t"<<"nc="<<nc<<endl;
        }
    VacOutfile.close();
}
void show_str() // may be used to show a spin configuration
{
for (int k=1;k!=hei+1;++k)
{for (int i=1;i!=row+1;++i)
   {
for (int j=1;j!=col+1;++j)
{ //cout<<Sx[i][j]<<","<<Sz[i][j]<<"\t";
  cout<<floor(Sz[i][j][k]*1000)/1000.0<<"\t";
}
cout<<endl;
   }
cout<<endl;
}
}
inline double loc_Energy0(int nr, int nc, int nh)//Energy of interaction of a spin in row=nr, column=nc, and layer=nh
{double Eij,Emca;
 int il,ir,jl,jr,kd,ku;
```

```
il=nr-1;ir=nr+1;// il reads as i_left, ir as i_right
jl=nc-1;jr=nc+1;
kd=nh-1;ku=nh+1;// k_down, k_up

// imposing boundary conditions
if (nr==1) {il=row;}  //periodical
if (nr==row) {ir=1;}  //periodical
if (nc==1)  {jl=col;}  //periodical
if (nc==col) {jr=1;}  //periodical
     if (nh==1) {kd=0;}  //free
     if (nh==hei) {ku=0;}  //free

Eij=   (Sx[nr][jr][nh]+Sx[ir][nc][nh]+Sx[ir][jl][nh]+Sx[nr][jl][nh]+Sx[il][nc][nh]+Sx[il][jr][nh])*Sx[nr][nc][nh]+
   (Sy[nr][jr][nh]+Sy[ir][nc][nh]+Sy[ir][jl][nh]+Sy[nr][jl][nh]+Sy[il][nc][nh]+Sy[il][jr][nh])*Sy[nr][nc][nh]+//energy of in-plane interaction
   (Sz[nr][jr][nh]+Sz[ir][nc][nh]+Sz[ir][jl][nh]+Sz[nr][jl][nh]+Sz[il][nc][nh]+Sz[il][jr][nh])*Sz[nr][nc][nh]+

   (Sx[nr][nc][kd]+Sx[ir][nc][kd]+Sx[nr][jr][kd])*Sx[nr][nc][nh]+//interaction with down-plane
   (Sy[nr][nc][kd]+Sy[ir][nc][kd]+Sy[nr][jr][kd])*Sy[nr][nc][nh]+
   (Sz[nr][nc][kd]+Sz[ir][nc][kd]+Sz[nr][jr][kd])*Sz[nr][nc][nh]+

   (Sx[nr][nc][ku]+Sx[nr][jl][ku]+Sx[il][nc][ku])*Sx[nr][nc][nh]+//interaction with up-plane
   (Sy[nr][nc][ku]+Sy[nr][jl][ku]+Sy[il][nc][ku])*Sy[nr][nc][nh]+
   (Sz[nr][nc][ku]+Sz[nr][jl][ku]+Sz[il][nc][ku])*Sz[nr][nc][nh];

        //anisotropy term is calculated in Cartesian coordinates of conventional unit cell
        //magnetic crystal anisotropy energy
        if ( (nh!=1) && (nh!=hei) ) { // in the middle
            if (nh%2==1) {
                if ( (nr&1) && (nc&1) ) {Emca=K*Sz[nr][nc][nh]*Sz[nr][nc][nh];}
                if ( (!(nr&1)) && (nc&1) ) {Emca=K*Sx[nr][nc][nh]*Sx[nr][nc][nh];}
                if ( (nr&1) && (!(nc&1)) ) {Emca=K*Sy[nr][nc][nh]*Sy[nr][nc][nh];}
                if ( (!(nr&1)) && (!(nc&1)) ) {Emca=0;}
            } else {
                if ( (nr&1) && (nc&1) ) {Emca=0;}
                if ( (!(nr&1)) && (nc&1) ) {Emca=K*Sy[nr][nc][nh]*Sy[nr][nc][nh];}
                if ( (nr&1) && (!(nc&1)) ) {Emca=K*Sx[nr][nc][nh]*Sx[nr][nc][nh];}
                if ( (!(nr&1)) && (!(nc&1)) ) {Emca=K*Sz[nr][nc][nh]*Sz[nr][nc][nh];}
            }
         }
        else { // on the surface
            Emca=D/3.*(Sx[nr][nc][nh]+Sy[nr][nc][nh]+Sz[nr][nc][nh])*(Sx[nr][nc][nh]+Sy[nr][nc][nh]+Sz[nr][nc][nh]);
        }
        return -J*Eij-Emca;
}

//Energy of interaction of a changed spin in row=nr, column=nc, and layer=nh
inline double loc_Energy1(int nr, int nc, int nh, double Sx_new, double Sy_new, double Sz_new)
```

```
{double Eij,Emca;
 int il,ir,jl,jr,kd,ku;

il=nr-1;ir=nr+1;
jl=nc-1;jr=nc+1;
kd=nh-1;ku=nh+1;

if (nr==1) {il=row;}
if (nr==row) {ir=1;}
if (nc==1)  {jl=col;}
if (nc==col) {jr=1;}
    if (nh==1) {kd=0;}
     if (nh==hei) {ku=0;}

Eij=   (Sx[nr][jr][nh]+Sx[ir][nc][nh]+Sx[ir][jl][nh]+Sx[nr][jl][nh]+Sx[il][nc][nh]+Sx[il][jr][nh])*Sx_new+
   (Sy[nr][jr][nh]+Sy[ir][nc][nh]+Sy[ir][jl][nh]+Sy[nr][jl][nh]+Sy[il][nc][nh]+Sy[il][jr][nh])*Sy_new+//in-plane interaction
   (Sz[nr][jr][nh]+Sz[ir][nc][nh]+Sz[ir][jl][nh]+Sz[nr][jl][nh]+Sz[il][nc][nh]+Sz[il][jr][nh])*Sz_new+

   (Sx[nr][nc][kd]+Sx[ir][nc][kd]+Sx[nr][jr][kd])*Sx_new+//interaction with down-plane
   (Sy[nr][nc][kd]+Sy[ir][nc][kd]+Sy[nr][jr][kd])*Sy_new+
   (Sz[nr][nc][kd]+Sz[ir][nc][kd]+Sz[nr][jr][kd])*Sz_new+

   (Sx[nr][nc][ku]+Sx[nr][jl][ku]+Sx[il][nc][ku])*Sx_new+//interaction with up-plane
   (Sy[nr][nc][ku]+Sy[nr][jl][ku]+Sy[il][nc][ku])*Sy_new+
   (Sz[nr][nc][ku]+Sz[nr][jl][ku]+Sz[il][nc][ku])*Sz_new;

        if ( (nh!=1) && (nh!=hei) ) {
            if (nh%2==1) {
                if ( (nr&1) && (nc&1) ) {Emca=K*Sz_new*Sz_new;}
                if ( (!(nr&1)) && (nc&1) ) {Emca=K*Sx_new*Sx_new;}
                if ( (nr&1) && (!(nc&1)) ) {Emca=K*Sy_new*Sy_new;}
                if ( (!(nr&1)) && (!(nc&1)) ) {Emca=0;}
            } else {
                if ( (nr&1) && (nc&1) ) {Emca=0;}
                if ( (!(nr&1)) && (nc&1) ) {Emca=K*Sy_new*Sy_new;}
                if ( (nr&1) && (!(nc&1)) ) {Emca=K*Sx_new*Sx_new;}
                if ( (!(nr&1)) && (!(nc&1)) ) {Emca=K*Sz_new*Sz_new;}
            }
        } else {
            Emca=D/3.*(Sx_new+Sy_new+Sz_new)*(Sx_new+Sy_new+Sz_new);
        }
        return -J*Eij-Emca;
}
inline void choose_new_dir()//choosing new direction of spin, uniform distribution on the surface of the sphere
{double r1,r2;
r1=r.rand();r2=r.randExc();
Sz_new=2.0*(r1-0.5);
Sx_new=sqrt(1-Sz_new*Sz_new)*cos(2.0*Pi*r2);
```

```
Sy_new=sqrt(1-Sz_new*Sz_new)*sin(2.0*Pi*r2);
}
void loc_Interact(int nr,int nc, int nh)//make a Monte-Carlo step for spin at nr, nc, nh
{double r0,Eflip;
 int i1,j1,k1;
choose_new_dir();
Eflip=loc_Energy1(nr,nc,nh, Sx_new,Sy_new,Sz_new)-loc_Energy0(nr,nc,nh); //changing of the local energy due to changing the spin direction
if (Eflip<0) {Sx[nr][nc][nh]=Sx_new; Sy[nr][nc][nh]=Sy_new; Sz[nr][nc][nh]=Sz_new;}
else
{
 r0=r.rand();
 if (r0<=exp(-Eflip/k_B/T))
 {Sx[nr][nc][nh]=Sx_new; Sy[nr][nc][nh]=Sy_new; Sz[nr][nc][nh]=Sz_new;}
}
}
inline void Interact_cycle() // Monte-Carlo step for system
{
for (int k=1;k!=hei+1;++k)
  for (int i=1;i!=row+1;++i)
for (int j=1;j!=col+1;++j)
{
if ( !( (((i%2)==0)&&((j%2)==0)&&((k%2)==1)) || (((i%2)==1)&&((j%2)==1)&&((k%2)==0)) ) )  // skipping nodes of ideal kagome layers occupied with zero spins
{if (Sx[i][j][k]*Sx[i][j][k]+Sy[i][j][k]*Sy[i][j][k]+Sz[i][j][k]*Sz[i][j][k]>0.1) {loc_Interact(i,j,k);}}
}
}
double Energy() //Energy of the system
{double E=0,E_mag=0, Emca;
for (int k=1;k<=hei;k++)
 for (int i=1;i<=row;i++)
 {
  for (int j=1;j<=col;j++) {
          if ( (k!=1) && (k!=hei) ) {
          if (k%2==1) {
              if ( (i&1) && (j&1) ) {Emca=K*Sz[i][j][k]*Sz[i][j][k];}
              if ( (!(i&1)) && (j&1) ) {Emca=K*Sx[i][j][k]*Sx[i][j][k];}
              if ( (i&1) && (!(j&1)) ) {Emca=K*Sy[i][j][k]*Sy[i][j][k];}
              if ( (!(i&1)) && (!(j&1)) ) {Emca=0;}
          } else {
              if ( (i&1) && (j&1) ) {Emca=0;}
              if ( (!(i&1)) && (j&1) ) {Emca=K*Sy[i][j][k]*Sy[i][j][k];}
              if ( (i&1) && (!(j&1)) ) {Emca=K*Sx[i][j][k]*Sx[i][j][k];}
              if ( (!(i&1)) && (!(j&1)) ) {Emca=K*Sz[i][j][k]*Sz[i][j][k];}
          }
   } else {
       Emca=D/3.*(Sx[i][j][k]+Sy[i][j][k]+Sz[i][j][k])*(Sx[i][j][k]+Sy[i][j][k]+Sz[i][j][k]);
   }
if ( !( (((i%2)==0)&&((j%2)==0)&&((k%2)==1))||(((i%2)==1)&&((j%2)==1)&&((k%2)==0)) ) )
    {E=E+loc_Energy0(i,j,k)-Emca;}
```

```
}
 }
return E/2.0;
}
double EnergyBulk() //Energy of the middle of the system
{double E=0,E_mag=0, Emca;
for (int k=2;k<=hei-1;k++)
 for (int i=1;i<=row;i++)
 {
  for (int j=1;j<=col;j++) {
  if ( (k!=1) && (k!=hei) ) {
          if (k%2==1) {
              if ( (i&1) && (j&1) ) {Emca=K*Sz[i][j][k]*Sz[i][j][k];}
              if ( (!(i&1)) && (j&1) ) {Emca=K*Sx[i][j][k]*Sx[i][j][k];}
              if ( (i&1) && (!(j&1)) ) {Emca=K*Sy[i][j][k]*Sy[i][j][k];}
              if ( (!(i&1)) && (!(j&1)) ) {Emca=0;}
          } else {
              if ( (i&1) && (j&1) ) {Emca=0;}
              if ( (!(i&1)) && (j&1) ) {Emca=K*Sy[i][j][k]*Sy[i][j][k];}
              if ( (i&1) && (!(j&1)) ) {Emca=K*Sx[i][j][k]*Sx[i][j][k];}
              if ( (!(i&1)) && (!(j&1)) ) {Emca=K*Sz[i][j][k]*Sz[i][j][k];}
          }
   } else {
       Emca=D/3.*(Sx[i][j][k]+Sy[i][j][k]+Sz[i][j][k])*(Sx[i][j][k]+Sy[i][j][k]+Sz[i][j][k]);
   }
if ( !( (((i%2)==0)&&((j%2)==0)&&((k%2)==1))||(((i%2)==1)&&((j%2)==1)&&((k%2)==0)) ) )
    {E=E+loc_Energy0(i,j,k)-Emca;}
}
 }
return E/2.0;
}
double EnergySurf() //Surface energy of the system
{double E=0,E_mag=0, Emca;
for (int k=1;k<=hei;k=k+hei-1)
 for (int i=1;i<=row;i++)
 {
  for (int j=1;j<=col;j++) {
     if ( (k!=1) && (k!=hei) ) {
          if (k%2==1) {
              if ( (i&1) && (j&1) ) {Emca=K*Sz[i][j][k]*Sz[i][j][k];}
              if ( (!(i&1)) && (j&1) ) {Emca=K*Sx[i][j][k]*Sx[i][j][k];}
              if ( (i&1) && (!(j&1)) ) {Emca=K*Sy[i][j][k]*Sy[i][j][k];}
              if ( (!(i&1)) && (!(j&1)) ) {Emca=0;}
          } else {
              if ( (i&1) && (j&1) ) {Emca=0;}
              if ( (!(i&1)) && (j&1) ) {Emca=K*Sy[i][j][k]*Sy[i][j][k];}
              if ( (i&1) && (!(j&1)) ) {Emca=K*Sx[i][j][k]*Sx[i][j][k];}
              if ( (!(i&1)) && (!(j&1)) ) {Emca=K*Sz[i][j][k]*Sz[i][j][k];}
```

```
          }
   } else {
       Emca=D/3.*(Sx[i][j][k]+Sy[i][j][k]+Sz[i][j][k])*(Sx[i][j][k]+Sy[i][j][k]+Sz[i][j][k]);
   }
if ( !( (((i%2)==0)&&((j%2)==0)&&((k%2)==1))||(((i%2)==1)&&((j%2)==1)&&((k%2)==0)) ) )
    {E=E+loc_Energy0(i,j,k)-Emca;}
}
 }
return E/2.0;
}
double EnergyLayer(int nl) //Energy of the nl layer of the system
{double E=0,E_mag=0, Emca;
        for (int k=nl;k<=nl;k++)
         for (int i=1;i<=row;i++)
         {
          for (int j=1;j<=col;j++)   {
                  if ( (k!=1) && (k!=hei) ) {
                  if (k%2==1) {
                      if ( (i&1) && (j&1) ) {Emca=K*Sz[i][j][k]*Sz[i][j][k];}
                      if ( (!(i&1)) && (j&1) ) {Emca=K*Sx[i][j][k]*Sx[i][j][k];}
                      if ( (i&1) && (!(j&1)) ) {Emca=K*Sy[i][j][k]*Sy[i][j][k];}
                      if ( (!(i&1)) && (!(j&1)) ) {Emca=0;}
                  } else {
                      if ( (i&1) && (j&1) ) {Emca=0;}
                      if ( (!(i&1)) && (j&1) ) {Emca=K*Sy[i][j][k]*Sy[i][j][k];}
                      if ( (i&1) && (!(j&1)) ) {Emca=K*Sx[i][j][k]*Sx[i][j][k];}
                      if ( (!(i&1)) && (!(j&1)) ) {Emca=K*Sz[i][j][k]*Sz[i][j][k];}
                  }
            } else {
                Emca=D/3.*(Sx[i][j][k]+Sy[i][j][k]+Sz[i][j][k])*(Sx[i][j][k]+Sy[i][j][k]+Sz[i][j][k]);
            }
             if ( !( (((i%2)==0)&&((j%2)==0)&&((k%2)==1))||(((i%2)==1)&&((j%2)==1)&&((k%2)==0)) ) )
             {E=E+loc_Energy0(i,j,k)-Emca;}
        }
         }
        return E/2.0;
}
inline void Magnet_proj()//calculates component of Magnetizations
{
 for (int k=1;k<=hei;k++)  //these calculationa are carrying on in the conventional cubic coordinate system
{MAx[k]=0;MAy[k]=0;MAz[k]=0;  MBx[k]=0;MBy[k]=0;MBz[k]=0;  MCx[k]=0;MCy[k]=0;MCz[k]=0; Mx[k]=0;My[k]=0;Mz[k]=0;}

for (int k=1;k<=hei;k++)
  for (int i=0;i<=row-2;i=i+2)
for (int j=0;j<=col-2;j=j+2)
{
 if (k%2==1)
  {MAx[k]=MAx[k]+Sx[1+i][1+j][k]; // x component of the magnetization of the sublattice A in the layer k
```

```
   MBx[k]=MBx[k]+Sx[2+i][1+j][k];
   MCx[k]=MCx[k]+Sx[1+i][2+j][k];

   MAy[k]=MAy[k]+Sy[1+i][1+j][k];
   MBy[k]=MBy[k]+Sy[2+i][1+j][k];
   MCy[k]=MCy[k]+Sy[1+i][2+j][k];

        MAz[k]=MAz[k]+Sz[1+i][1+j][k];
   MBz[k]=MBz[k]+Sz[2+i][1+j][k];
   MCz[k]=MCz[k]+Sz[1+i][2+j][k];} else

 { MAx[k]=MAx[k]+Sx[2+i][2+j][k];
   MBx[k]=MBx[k]+Sx[1+i][2+j][k];
   MCx[k]=MCx[k]+Sx[2+i][1+j][k];

   MAy[k]=MAy[k]+Sy[2+i][2+j][k];
   MBy[k]=MBy[k]+Sy[1+i][2+j][k];
   MCy[k]=MCy[k]+Sy[2+i][1+j][k];

   MAz[k]=MAz[k]+Sz[2+i][2+j][k];
   MBz[k]=MBz[k]+Sz[1+i][2+j][k];
   MCz[k]=MCz[k]+Sz[2+i][1+j][k];}
}
MAxT=0;MAyT=0;MAzT=0;  MBxT=0;MByT=0;MBzT=0;  MCxT=0;MCyT=0;MCzT=0;
for (int k=1;k<=hei;k++)
{MAxT=MAxT+MAx[k]; MAyT=MAyT+MAy[k]; MAzT=MAzT+MAz[k];  //total sublattice magnetization, components
 MBxT=MBxT+MBx[k]; MByT=MByT+MBy[k]; MBzT=MBzT+MBz[k];
    MCxT=MCxT+MCx[k]; MCyT=MCyT+MCy[k]; MCzT=MCzT+MCz[k];
 Mx[k]=MAx[k]+MBx[k]+MCx[k];  //full magnetization in each layer
 My[k]=MAy[k]+MBy[k]+MCy[k];
 Mz[k]=MAz[k]+MBz[k]+MCz[k];}
MxT=MxT+MAxT+MBxT+MCxT; MyT=MyT+MAyT+MByT+MCyT; MzT=MzT+MAzT+MBzT+MCzT;  //total magnetization, in conventional cubic coordinate system
}
inline void MagnetLength()// module of Magnetizations
{
MAT=sqrt(MAxT*MAxT+MAyT*MAyT+MAzT*MAzT);  //module of total sublattice magnetization
MBT=sqrt(MBxT*MBxT+MByT*MByT+MBzT*MBzT);
MCT=sqrt(MCxT*MCxT+MCyT*MCyT+MCzT*MCzT);
MOp=MAT+MBT+MCT;  //3D Order parameter through total magnetization
MOp_2=0;
for (int k=1;k<=hei;k++)
{
 MA[k]=sqrt(MAx[k]*MAx[k]+MAy[k]*MAy[k]+MAz[k]*MAz[k]);
 MB[k]=sqrt(MBx[k]*MBx[k]+MBy[k]*MBy[k]+MBz[k]*MBz[k]);
 MC[k]=sqrt(MCx[k]*MCx[k]+MCy[k]*MCy[k]+MCz[k]*MCz[k]);
 MOpLayer[k]=MA[k]+MB[k]+MC[k];
 MOp_2=MOp_2+MOpLayer[k]; // OP for the thin film
}
```

```
}
inline double C(int j)// calculate specific heat
{
return (average_E2-average_E*average_E)/k_B/T/T/N_dots;
}
inline double CBulk(int j)// calculate specific heat of the interior
{
return (average_EBulk2-average_EBulk*average_EBulk)/k_B/T/T/( 3/4.*row*col*(hei-2) );
}
inline double CSurf(int j)// calculate specific heat of the surface
{
return (average_ESurf2-average_ESurf*average_ESurf)/k_B/T/T/(3/4.*row*col*2-Nvac1);
}
inline double CLayer(int j, int k, int Nspins)// calculate specific heat of the layer
{
    return (average_E2Layer[k]-average_ELayer[k]*average_ELayer[k])/k_B/T/T/Nspins;
}
inline double hi(int j)//Susceptibility per spin
{
return (average_MT2-average_MT*average_MT)/k_B/T/N_dots;
}
inline double hiOp(int j)//Susceptibility per spin
{
return (average_MOp2-average_MOp*average_MOp)/k_B/T/N_dots;
}
inline double hiOp_2(int j)//Susceptibility per spin
{
return (average_MOp2_2-average_MOp_2*average_MOp_2)/k_B/T/(N_dots);
}
inline double hiOp2Layer(int j, int k, int Nspins)//Susceptibility per spin
{
    return (average_MOpLayer2[k]-average_MOpLayer[k]*average_MOpLayer[k])/k_B/T/Nspins;
}


void save_StrT(double T, string s)  // writing a spin structure into a file
{
ostringstream oss2;
oss2<<T;
ofstream StructureT;
outfile="Structure"+s+"T"+oss2.str()+".txt";
StructureT.open(outfile.c_str());
StructureT<<N_dots<<"\n";
for (int k=1;k!=hei+1;++k)
{for (int i=1;i!=row+1;++i)
   {
for (int j=1;j!=col+1;++j)
{
  StructureT<<Sx[i][j][k]<<" "<<Sy[i][j][k]<<" "<<Sz[i][j][k]<<"\t";
```

```
}
StructureT<<"\n";
   }
StructureT<<"\n\n\n";
}
StructureT.close();
}

int main(int argc, char *argv[]) //arguments should be input in the following sequenve: row col hei N_steps J D K p
{
ostringstream arg;  //example of an argument line: "18 18 18 1000000 -1 0.5 0.1 0"
for (int i=1;i<=argc-1;++i)
{arg<<argv[i]<<" ";}
istringstream iss(arg.str());
cout<<arg.str()<<endl;
int v;
iss>>row;
cout<<"row="<<row<<endl;
iss>>col;
cout<<"col="<<col<<endl;
iss>>hei;
cout<<"hei="<<hei<<endl;
iss>>v;
const int N_steps=v;
cout<<"N="<<N_steps<<endl;
iss>>J;
cout<<"J="<<J<<endl;
iss>>D;
cout<<"D="<<D<<endl;
iss>>K;
cout<<"K="<<K<<endl;
iss>>p;
cout<<"p="<<p<<endl;

Mx=new double [hei+1]; My=new double [hei+1]; Mz=new double [hei+1]; //allocation memory for the listed arrays
MxTl=new double [hei+1]; MyTl=new double [hei+1]; MzTl=new double [hei+1];
MAx=new double [hei+1]; MAy=new double [hei+1]; MAz=new double [hei+1];
MBx=new double [hei+1]; MBy=new double [hei+1]; MBz=new double [hei+1];
MCx=new double [hei+1]; MCy=new double [hei+1]; MCz=new double [hei+1];

M=new double [hei+1];
average_M=new double [hei+1];
Minplane=new double [hei+1];
N_uneq=N_steps/10;cout<<"N_uneq="<<N_uneq<<endl; //Number of discared MCS for the equilibration is taken as 10% of overall number of MCS
int NinL=row*col; //number of nodes in a layer
Nvac1=floor(3.0/4.0*NinL*p+0.5);  //number of vacancies
N_dots=3.0/4.0*row*col*hei-Nvac1;  //number of spins in the system
cout<<"Nvac1="<<Nvac1<<endl;
```

```
Sx=new double** [row+2];  //allocation memory for the corresponding arrays
Sy=new double** [row+2];
Sz=new double** [row+2];
for (int i=0;i<=row+1;++i)
{
Sx[i]=new double* [col+2];
Sy[i]=new double* [col+2];
Sz[i]=new double* [col+2];
}
for (int i=0;i<=row+1;++i)
for (int j=0;j<=col+1;++j)
{
Sx[i][j]=new double[hei+2];
Sy[i][j]=new double[hei+2];
Sz[i][j]=new double[hei+2];
}
double start,stop;
start=clock();//start "time"
ostringstream oss;
oss<<row;oss<<" ";oss<<col;oss<<" ";oss<<hei;oss<<" ";oss<<N_steps;oss<<" ";oss<<J;oss<<" ";oss<<D;oss<<" ";oss<<K;oss<<"p";oss<<p;
s=oss.str();  //s is a string containing arguments of the job
Init_str(row,col,hei);  //initializing structure
Vacancies(p);    //creating vacancies
cout<<"E="<<Energy()<<"\t"<<endl;
outfile="NOPKiRes="+s+".txt";
Res1_file.open(outfile.c_str());
Res1_file<<"percent of vacancies is "<<p<<endl;
Res1_file<<"T"<<"\t"<<"Energy    "<<"\t"<<"Spec_heat"<<"\t"<<"Mag_Tot"<<"\t"<<"Mag_Op"<<"\t"<<"hiOp"<<"\t"<<"MOp_2"<<"\t"<<"hiOp_2"<<"\t"<<"Cbulk"<<"\t"<<
"Csurf"<<"\t"<<"Mag_BulkT"<<"\t"<<"Mag_SurfT"<<"\t"<<"MTz"<<"\t"<<"MBulkz"<<"\t"<<"MSurfz";
for (int k=1;k<=hei;k++)
    {Res1_file<<"\t"<<"Mz["<<k<<"]"<<"\t"<<"M["<<k<<"]";}
for (int k=1;k<=hei;k++)
{Res1_file<<"\t"<<"MOPLayer["<<k<<"]";}
for (int k=1;k<=hei;k++)
    {Res1_file<<"\t"<<"CLayer["<<k<<"]";}
for (int k=1;k<=hei;k++)
    {Res1_file<<"\t"<<"hiOp2Layer["<<k<<"]";}
Res1_file<<endl;
Res1_file<<"\t"<<"MTinpl_per_spin";
for (int k=1;k<=hei;k++)
    {Res1_file<<"\t"<<"Minplane_per_sp["<<k<<"]";}
Res1_file<<"\t"<<"MTinpl_per_node"; //per node = all kagome lattice nodes are included
for (int k=1;k<=hei;k++)
    {Res1_file<<"\t"<<"Minplane_per_node["<<k<<"]";}
Res1_file<<endl;
int Nspins;
T=0.51;
```

```
while (T>=0)
{
if ( (T>0.32)||(T<0.13) ) {T=T-0.01;} else {T=T-0.005;}
average_E=0;average_E2=0;
    for (int k=1; k<=hei; k++)
    {
        average_ELayer[k]=0;average_E2Layer[k]=0;
        average_MOpLayer2[k]=0;
newaverage_MOpLayer[k]=0;
average_MAx[k]=0;average_MAy[k]=0;average_MAz[k]=0;
average_MBx[k]=0;average_MBy[k]=0;average_MBz[k]=0;
average_MCx[k]=0;average_MCy[k]=0;average_MCz[k]=0;
    }
average_MT=0;average_MT2=0; average_MA=0;average_MA2=0; average_MB=0;average_MB2=0;
average_MC=0;average_MC2=0; average_MOp=0;average_MOp2=0;
average_MOp_2=0;average_MOp2_2=0;
MxT=0;MyT=0;MzT=0;
newaverage_MOp_2=0;
for (int k=1;k<=hei;k++)
{average_MOpLayer[k]=0;}
for (int k=1; k<=hei; k++)
{Mx[k]=0;My[k]=0;Mz[k]=0;}
for (int k=1; k<=hei; k++)
                {
                MxTl[k]=0;
                MyTl[k]=0;
                MzTl[k]=0;
            }
average_EBulk=0;average_EBulk2=0;
average_ESurf=0;average_ESurf2=0;
average_MBulk=0;average_MBulk2=0;
MxBulk=0;MyBulk=0;MzBulk=0;
for (int k=2; k<=hei-1; k++)//for bulk
{
 average_Mz[k]=0;
 average_Mx[k]=0;
 average_My[k]=0;
}
average_MSurf=0;average_MSurf2=0;
MxSurf=0;MySurf=0;MzSurf=0;
for (int k=1; k<=hei; k=k+hei-1)//for surface
{
 average_Mz[k]=0;
 average_Mx[k]=0;
 average_My[k]=0;
}
for (int i=0;i<=N_steps-1;++i)
{
```

```
Interact_cycle();
if (i>N_uneq-1) {
En=Energy(); EBulkn=EnergyBulk(); ESurfn=EnergySurf();
average_E=average_E+En;average_E2=average_E2+En*En;
average_EBulk=average_EBulk+EBulkn;average_EBulk2=average_EBulk2+EBulkn*EBulkn;
average_ESurf=average_ESurf+ESurfn;average_ESurf2=average_ESurf2+ESurfn*ESurfn;
            Magnet_proj();MagnetLength();
    for (int k=1;k<=hei;k++)
{
 average_MAx[k]=average_MAx[k]+MAx[k];
 average_MAy[k]=average_MAy[k]+MAy[k];
 average_MAz[k]=average_MAz[k]+MAz[k];

 average_MAx[k]=average_MAx[k]+MAx[k];
 average_MAy[k]=average_MAy[k]+MAy[k];
 average_MAz[k]=average_MAz[k]+MAz[k];

 average_MAx[k]=average_MAx[k]+MAx[k];
 average_MAy[k]=average_MAy[k]+MAy[k];
 average_MAz[k]=average_MAz[k]+MAz[k];
}
    for (int k=1; k<=hei; k++)
            {
                average_ELayer[k]=average_ELayer[k]+EnergyLayer(k); average_E2Layer[k]=average_E2Layer[k]+EnergyLayer(k)*EnergyLayer(k);
            }
            for (int k=1; k<=hei; k++)
                {
                MxTl[k]=MxTl[k]+Mx[k];
                MyTl[k]=MyTl[k]+My[k];
                MzTl[k]=MzTl[k]+Mz[k];
            }
for (int k=2; k<=hei-1; k++)//for bulk
{
 average_Mz[k]=average_Mz[k]+(Mx[k]+My[k]+Mz[k])/SQ3;
 MxBulk=MxBulk+Mx[k];
 MyBulk=MyBulk+My[k];
 MzBulk=MzBulk+Mz[k];
}
for (int k=1; k<=hei; k=k+hei-1)//for surface
{
 average_Mz[k]=average_Mz[k]+(Mx[k]+My[k]+Mz[k])/SQ3;
                  MxSurf=MxSurf+Mx[k];
 MySurf=MySurf+My[k];
 MzSurf=MzSurf+Mz[k];
}
average_MOp=average_MOp+MOp;average_MOp2=average_MOp2+MOp*MOp;
average_MOp_2=average_MOp_2+MOp_2;average_MOp2_2=average_MOp2_2+MOp_2*MOp_2;
for (int k=1;k<=hei;k++)
```

```
                {average_MOpLayer[k]=average_MOpLayer[k]+MOpLayer[k];
                 average_MOpLayer2[k]=average_MOpLayer2[k]+MOpLayer[k]*MOpLayer[k];}
}
}
newaverage_MOp_2=0;
for (int k=1;k<=hei;k++)
{
 av_MA[k]=sqrt(average_MAx[k]*average_MAx[k]+average_MAy[k]*average_MAy[k]+average_MAz[k]*average_MAz[k]);
 av_MB[k]=sqrt(average_MBx[k]*average_MBx[k]+average_MBy[k]*average_MBy[k]+average_MBz[k]*average_MBz[k]);
 av_MC[k]=sqrt(average_MCx[k]*average_MCx[k]+average_MCy[k]*average_MCy[k]+average_MCz[k]*average_MCz[k]);
 newaverage_MOpLayer[k]=(av_MA[k]+av_MB[k]+av_MC[k])/(N_steps-N_uneq);
 newaverage_MOp_2=newaverage_MOp_2+newaverage_MOpLayer[k];
}
newaverage_MOp_2=newaverage_MOp_2/N_dots;
save_StrT(T, s);
MT=sqrt(MxT*MxT+MyT*MyT+MzT*MzT);
    for (int k=1; k<=hei; k++)
        {
        MxTl[k]=MxTl[k]/(N_steps-N_uneq);
        MyTl[k]=MyTl[k]/(N_steps-N_uneq);
        MzTl[k]=MzTl[k]/(N_steps-N_uneq);
if (k==hei) {Nspins=3./4.*row*col-Nvac1;} else {Nspins=3./4.*row*col;}
        M[k]=sqrt(MxTl[k]*MxTl[k]+MyTl[k]*MyTl[k]+MzTl[k]*MzTl[k])/Nspins; //per spin
    }
for (int k=1; k<=hei; k++)
{
if (k==hei) {Nspins=3./4.*row*col-Nvac1;} else {Nspins=3./4.*row*col;}
 average_Mz[k]=average_Mz[k]/(N_steps-N_uneq)/Nspins; //per spin
}
for (int k=1; k<=hei; k++)
{
 if (k==hei) {Nspins=3./4.*row*col-Nvac1;} else {Nspins=3./4.*row*col;}
 Minplane[k]=sqrt(M[k]*M[k]-average_Mz[k]*average_Mz[k]); //per spin
}
average_MTz=0;average_MSurfz=0;average_MBulkz=0;
for (int k=2; k<=hei-1; k++)
{
 average_MBulkz=average_MBulkz+average_Mz[k];
}
average_MSurfz=(3./4.*row*col)/(3./2.*row*col-Nvac1)*average_Mz[1]+(3./4.*row*col-Nvac1)/(3./2.*row*col-Nvac1)*average_Mz[hei];  //per spin
average_MTz=(average_MBulkz*(3./4.*row*col)+average_MSurfz*(3./2.*row*col-Nvac1))/N_dots; //per spin
MBulk=sqrt(MxBulk*MxBulk+MyBulk*MyBulk+MzBulk*MzBulk);
   MSurf=sqrt(MxSurf*MxSurf+MySurf*MySurf+MzSurf*MzSurf);
average_E=average_E/(N_steps-N_uneq);average_E2=average_E2/(N_steps-N_uneq);
average_EBulk=average_EBulk/(N_steps-N_uneq);average_EBulk2=average_EBulk2/(N_steps-N_uneq);
average_ESurf=average_ESurf/(N_steps-N_uneq);average_ESurf2=average_ESurf2/(N_steps-N_uneq);
average_MT=MT/(N_steps-N_uneq);
average_MOp=average_MOp/(N_steps-N_uneq);average_MOp2=average_MOp2/(N_steps-N_uneq);
```

```
average_MOp_2=average_MOp_2/(N_steps-N_uneq);average_MOp2_2=average_MOp2_2/(N_steps-N_uneq);
average_MBulk=MBulk/(N_steps-N_uneq);average_MBulk2=average_MBulk2/(N_steps-N_uneq);
average_MSurf=MSurf/(N_steps-N_uneq);average_MSurf2=average_MSurf2/(N_steps-N_uneq);
    for (int k=1; k<=hei; k++)
    {
        average_ELayer[k]=average_ELayer[k]/(N_steps-N_uneq); average_E2Layer[k]=average_E2Layer[k]/(N_steps-N_uneq);
    }
    for (int k=1;k<=hei;k++)
        {average_MOpLayer[k]=average_MOpLayer[k]/(N_steps-N_uneq);
         average_MOpLayer2[k]=average_MOpLayer2[k]/(N_steps-N_uneq);
    }
cout<<T<<"\t"<<average_E/N_dots<<"\t"<<average_MOp_2/N_dots<<endl;
    Res1_file<<T<<"\t"<<average_E/N_dots<<"\t"<<C(j)<<"\t"<<average_MT/N_dots<<"\t"<<average_MOp/N_dots<<"\t"<<hiOp(j)<<"\t"<<newaverage_MOp_2<<"\t"<<
hiOp_2(j)<<"\t"<<CBulk(j)<<"\t"<<CSurf(j)<<"\t"<<average_MBulk/(3./4.*row*col*(hei-2))<<"\t"<<average_MSurf/(3./2.*row*col-Nvac1)<<"\t"<<average_MTz
<<"\t"<<average_MBulkz/(hei-2)<<"\t"<<average_MSurfz;  //everything is calculated per spin
for (int k=1;k<=hei;k++)
    {Res1_file<<"\t"<<average_Mz[k]<<"\t"<<M[k];}   //per spin
for (int k=1;k<=hei;k++)
    {
if (k==hei) {Nspins=3./4.*row*col-Nvac1;} else {Nspins=3./4.*row*col;}
Res1_file<<"\t"<<newaverage_MOpLayer[k]/(Nspins);}  //per spin
    for (int k=1;k<=hei;k++)
        {
if (k==hei) {Nspins=3./4.*row*col-Nvac1;} else {Nspins=3./4.*row*col;}
Res1_file<<"\t"<<CLayer(j, k, Nspins);}    //per spin
for (int k=1;k<=hei;k++)
    {
if (k==hei) {Nspins=3./4.*row*col-Nvac1;} else {Nspins=3./4.*row*col;}
Res1_file<<"\t"<<hiOp2Layer(j, k, Nspins);}      //per spin
MTinplane=sqrt(average_MT*average_MT-average_MTz*average_MTz*N_dots*N_dots);
Res1_file<<"\t"<<MTinplane/N_dots;  // per spin
for (int k=1;k<=hei;k++)
    {Res1_file<<"\t"<<Minplane[k];}
Res1_file<<"\t"<<MTinplane/(3./4.*row*col*hei);  //per node
for (int k=1;k<=hei;k++)
    {
if (k==hei) {Nspins=3./4.*row*col-Nvac1;} else {Nspins=3./4.*row*col;}
Res1_file<<"\t"<<Minplane[k]*Nspins/(3./4.*row*col);}
Res1_file<<endl;
}
stop=clock();//end "time"
cout<<"time="<<(stop-start)/CLOCKS_PER_SEC<<endl;//time in sec
Res1_file<<"time"<<"\t"<<(stop-start)/CLOCKS_PER_SEC<<endl;
return 0;
}
```